ABSTRACT

Title of Dissertation: DYNAMICS OF A LARGE SUBMERSED PLANT BED IN UPPER CHESAPEAKE BAY

Cassie Gurbisz, Doctor of Philosophy, 2016

Dissertation directed by: Professor W. Michael Kemp, Marine Estuarine Environmental Sciences

A large SAV bed in upper Chesapeake Bay has experienced several abrupt shifts over the past half-century, beginning with near-complete loss after a record-breaking flood in 1972, followed by an unexpected, rapid resurgence in the early 2000's, then partial decline in 2011 following another major flood event. Together, these trends and events provide a unique opportunity to study a recovering SAV ecosystem from several different perspectives. First, I analyzed and synthesized existing time series datasets to make inferences about what factors prompted the recovery. Next, I analyzed existing datasets, together with field samples and a simple hydrodynamic model to investigate mechanisms of SAV bed loss and resilience to storm events. Finally, I conducted field deployments and experiments to explore how the bed affects internal physical and biogeochemical processes and what implications those effects have for the dynamics of the system.

I found that modest reductions in nutrient loading, coupled with several consecutive dry years likely facilitated the SAV resurgence. Furthermore, positive

feedback processes may have played a role in the sudden nature of the recovery because they could have reinforced the state of the bed before and after the abrupt shift. I also found that scour and poor water clarity associated with sediment deposition during the 2011 flood event were mechanisms of plant loss. However, interactions between the bed, water flow, and waves served as mechanisms of resilience because these processes created favorable growing conditions (i.e., clear water, low flow velocities) in the inner core of the bed. Finally, I found that that interactions between physical and biogeochemical processes led to low nutrient concentrations inside the bed relative to outside the bed, which created conditions that precluded algal growth and reinforced vascular plant dominance. This work demonstrates that positive feedbacks play a central role in SAV resilience to both chronic eutrophication as well as acute storm events. Furthermore, I show that analysis of long-term ecological monitoring data, together with field measurements and experiments, can be an effective approach for understanding the mechanisms underlying ecosystem dynamics.

DYNAMICS OF A LARGE SUBMERSED PLANT BED IN UPPER CHESAPEAKE BAY

by

Cassie Gurbisz

Dissertation submitted to the Faculty of the Graduate School of the
University of Maryland, College Park, in partial fulfillment
of the requirements for the degree of
Doctor of Philosophy
2016

Advisory Committee:
Professor W. Michael Kemp, Chair
Jeffrey Cornwell
Lora Harris
Laura Murray
Lawrence Sanford

Dedication

For Mom and Dad, who joked, I'd be a student forever but have always provided unyielding love and support.

Acknowledgements

First, I must thank those who directly shaped the outcome of this work. My co-authors on the manuscript versions of Chapters 2 and 3, Michael Kemp, Larry Sanford, and Bob Orth were instrumental in providing guidance on study design, data analysis, and interpretation of results. Larry Sanford additionally developed the hydrodynamic model used in Chapter 3 and led efforts to collect hydrodynamic data used in Chapter 4. I would also like to thank Jeff Cornwell and Mike Owens for collecting denitrification data and teaching me the science (and art) of making sediment-water flux measurements, Lora Harris and Laura Murray for offering helpful feedback on earlier versions of my manuscripts and on my research, in general, and Slava Lyubchich for providing statistical guidance. Tjisse van der Heide and 3 anonymous reviewers provided constructive suggestions for improving earlier versions of Chapters 2 and 3. Eva Koch also deserves a big "thank you" for her advice on issues related to fluid dynamics; I'm saddened that our time working together was cut short by her passing.

Many thanks to everyone who provided assistance with data collection, especially Debbie Hinkle, whose infinite strength and energy were pivotal to our field efforts. Alex Fisher, Emily Russ, Cindy Palinkas, Connor Reyer, Alex Myrie, Angela Cole, Jonathan Garing, Steven DiFalco, Dale Booth, Mike Malpezzi, Ginger Durkin, Cheryl Campbell, Laura Hofherr, Ralph Kimes, Nancy Rybicki, Stan Kollar, Maureen Brooks, and Jeremy Testa were also incredibly helpful. I heartily thank all who pulled the boat when the tide got too low. Keith Williams, Bob Burkhardt, and staff at "NorthBay Adventure" generously provided support and facilities, without which our field work would have been extremely cumbersome, if not impossible. Thanks also go to Lee Karrh, Becky Golden, and Brooke Landry for assistance with biomass sampling and overall enthusiastic support of our research.

Thank you also to the agencies and organizations that made this work possible. Maryland Sea Grant, Horn Point Laboratory, and the Concordia Foundation provided funding for the research and my graduate education. The Maryland Department of Natural Resources, United States Geological Survey, National Oceanic and Atmospheric Administration, and Virginia Institute of Marine Science collected and made publically available the environmental monitoring data that played a key role in in many of my analyses. I am particularly indebted to Bruce Michael, Peter Tango, Lee Karrh, Robert Orth, David Wilcox, Peter Bergstrom, Grace Brush, and Qian Zhang, who were pivotal in helping me obtain and interpret data.

Thanks to Shawn Ridgley and Jessie Marsh for teaching me how to drive boats and read the water, and for helping to kindle my "Bay love." Thanks also to Laura Burrell Baxter, Pat and Nancy Noonan, and the Chesapeake Bay Foundation for offering me the opportunity to live and work on the Bay during what turned out to be several very formative years in my life. That experience shaped who I am and my ultimate career path.

I am immensely thankful for my advisor, Michael Kemp, who helped mold me into a confident, productive ecologist. It has been an honor working with him and words cannot express my gratitude for all he has done to enrich my professional pursuits. I am also forever indebted to Laura Murray for bringing me into the world of science and being my champion and mentor for many years, both professionally and personally.

Finally, I acknowledge all of my friends and family for providing support, inspiration, encouragement, and stress relief. And, of course, thank you many times over to my partner in life, Todd Lester, for everything.

Table of Contents

List of Tables

List of Figures

Chapter 1: Introduction and overview

Seagrasses and associated submersed aquatic vegetation (SAV) are rooted angiosperms that inhabit shallow coastal, estuarine, and inland waters throughout the world. SAV are highly productive and carry out important functions in aquatic ecosystems. For example, they provide habitat structure to invertebrates and juvenile fish and food for waterfowl, manatees, and other organisms (Lubbers et al. 1990; Ralph et al. 2013). They can also enhance nutrient cycling (Caffrey and Kemp 1990; Risgaard-Petersen et al. 2000; Lawson et al. 2012) and attenuate waves and currents (Fonseca and Fisher 1986; Infantes et al. 2012). These functions provide valuable ecological services to society, including support for commercial and recreational fisheries, eutrophication control, and water clarity improvement, among others (Costanza et al. 1997).

Shallow aquatic ecosystems in which submersed plants dominate primary production are considered "pristine" (Valiela et al. 1997). However, systems may transition from vascular plant to algal dominance as a function of nutrient loading and light availability (Sand-Jensen and Borum 1991; Flindt et al. 1999; Havens et al. 2001). For instance, at lower nutrient loading rates, phytoplankton growth tends to be nutrient limited, and SAV thrive because they can obtain nutrients from sediment pore water through root uptake. At higher nutrient loading rates, phytoplankton dominate primary production because they have higher nutrient uptake rates than SAV and can, therefore, out-compete benthic plants for water column nutrients.

Furthermore, phytoplankton attenuate light penetration through the water column when in high abundance, thus limiting submersed plant production due to light limitation. Systems in which SAV abundance has decreased are often considered to be degraded because of the loss of ecosystem services.

Storm events also play a role in structuring shallow aquatic systems. For example, extreme waves and currents generated by high winds and flooding can break or uproot SAV, and huge loads of sediment delivered by floodwaters can bury plants (Preen et al. 1995; Cabaço et al. 2008). In addition, pulses of suspended sediments or nutrients and subsequent algal blooms can degrade water clarity, thereby decreasing the amount of light available for SAV production (Moore et al. 1997; Longstaff and Dennison 1999). Consequently, extreme weather events can result in major SAV losses over a short period of time (e.g., Campbell & McKenzie 2004, Cardoso et al. 2008, Grilo et al. 2011, Hanington et al. 2014).

Although chronic nutrient (nitrogen and phosphorous) loading and acute disturbance events are both important external drivers of change in ecosystems containing SAV, internal biophysical and biogeochemical processes also play a role in the dynamics of these systems. For example, SAV attenuate wave energy and current velocity, which causes suspended particles to sink, improves ambient water clarity and, thus, enhances plant growth (Ward et al. 1984; De Boer 2007; Gruber and Kemp 2010; Carr et al. 2010). SAV also assimilate nutrients and, in some cases, enhance nutrient loss through coupled nitrification-denitrification, thereby decreasing water column nutrient concentrations (Caffrey and Kemp 1992; McGlathery et al. 2007). As a result, growth of phytoplankton in the water column and epiphytes on

SAV leaves becomes nutrient limited and water clarity improves. One consequence of these positive feedback processes is that SAV ecosystems tend to respond nonlinearly to external drivers because they help maintain a suitable growing environment despite changes in external conditions (Scheffer et al. 1993; Viaroli et al. 2008). However, beyond a critical threshold (e.g., a minimum light level needed for plant growth), feedback processes no longer act as a buffer and the system suddenly shifts to a degraded state. Abrupt ecological changes are often unexpected or surprising because there is little change preceding the shift to serve as warning (Scheffer et al. 2012).

Over the past several decades, most studies documenting SAV dynamics have reported global declines, primarily in association with cultural eutrophication (Waycott et al. 2009) or extreme weather events such as hurricanes, floods, and heat waves (Preen et al. 1995; Rasheed and Unsworth 2011). In an effort to bring back lost ecosystem services, management agencies in the United States and throughout the world have committed to SAV and seagrass restoration largely through reduction of nutrient and sediment loading from anthropogenic sources. Accordingly, a small but increasing number of studies have reported SAV recovery in relation to improved water clarity resulting from management actions, such as sewage treatment plant upgrades (Tomasko et al. 2005; Ruhl and Rybicki 2010; Cardoso et al. 2010). Climate-related factors, such as decreased storm intensity and frequency have also been cited (Reise and Kohlus 2007).

An impressive example of SAV recovery recently occurred in a broad shallow region of upper Chesapeake Bay known as Susquehanna Flats. SAV at “the flats,” historically renowned to fishermen and waterfowl enthusiasts as exceptional wildlife

habitat, began to decline when nutrient loading and eutrophication intensified in the 1960's (Bayley et al. 1978; Kemp et al. 2005). Following a major flood during Tropical Storm Agnes in 1972, submersed plants at Susquehanna Flats virtually disappeared for nearly three decades until the early 2000's, when they rapidly recolonized nearly the entire region (>50 km^2). Similar to unanticipated ecosystem collapses, this sudden recovery was also quite unexpected; however, in this case, the trajectory of the rapid change was in the positive direction. Then, in 2011, the region experienced another major flood event. However, in contrast to the widespread SAV loss that occurred during Tropical Storm Agnes, only half the bed was lost. Together, these trends and events provide a unique opportunity to study a recovering SAV ecosystem from several different perspectives.

First, the factors driving the abrupt SAV resurgence are unclear. For example, the extended lack of plant recovery after Tropical Storm Agnes is puzzling because it appears that environmental conditions at a nearby monitoring station had generally satisfied the habitat requirements for SAV in oligohaline regions of Chesapeake Bay since water quality monitoring began in 1984 (i.e., April-October median light attenuation coefficient <2.0 m^{-1}, total suspended solid and dissolved inorganic phosphorous concentrations <15 mg L^{-1} and 0.67μmol l^{-1}, respectively) (Dennison et al. 1993; Kemp et al. 2004). Furthermore, there were also no immediately obvious changes in environmental conditions that could be easily linked to the recovery. Therefore, in Chapter 2 of this dissertation, I analyze and synthesize existing time series datasets to address the questions:

1) *How do patterns and trends in anthropogenic and climatic variables relate to SAV abundance?*
2) *Could the sudden resurgence reflect a threshold response to change in environmental conditions?*
3) *Could feedback processes have played a role in this resurgence?*

Next, the 2011 flood clearly damaged the SAV bed; however the large remaining stand of plants suggests that the system was also apparently resilient, or able to resist and possibly recover quickly from the disturbance. In Chapter 3, I analyze existing datasets, together with field samples and a simple hydrodynamic model, to address the questions:

1) *What mechanisms drove SAV loss in response to the flood event?*
2) *What mechanisms control SAV ecosystem resilience?*

Finally, preliminary examination of water quality monitoring data shows large seasonal differences in nutrient and suspended sediment concentrations between sample sites located inside and outside the SAV bed. These differences imply that the bed may be affecting flow and, thus, sediment dynamics, as well as nutrient cycling and, thus, local nutrient concentrations. In Chapter 4, I address the questions:

1) *What underlying mechanisms drive these biophysical and biogeochemical feedbacks?*
2) *Do physical and biogeochemical processes interact to affect internal nutrient cycling?*
3) *What effect do these processes have on the relative composition of primary producers in the system?*

My goal for carrying out this research is to contribute to our understanding of the factors controlling the recovery and resilience of SAV populations. Empirical insights into feedbacks, resilience, and nonlinear ecosystem dynamics will be broadly relevant to the field of ecology as well as to regional and global SAV conservation and management applications.

Chapter 2: Unexpected resurgence of a large submersed plant bed in Chesapeake Bay: Analysis of time series data

Abstract

An historically large (>50 km^2) submersed plant bed in upper Chesapeake Bay virtually disappeared in 1972 following Tropical Storm Agnes. The bed experienced little regrowth until the early 2000s, when plant abundance rapidly increased. Here, we analyze a suite of recent (1984-2010) and historical (1958-1983) time series datasets to assess alternative explanations for the submersed plant resurgence. Change-point analysis showed that spring nitrogen loading increased from 1945-1988 and decreased from 1988-2010. Analysis of variance on recent time series showed a significant difference in submersed aquatic vegetation (SAV) abundance percent change during wet years (-7±11%) and dry years (53±20%), indicating that floods and droughts likely contributed to SAV loss and growth, respectively. In the historic dataset, however, increasingly poor water quality led to SAV loss despite an extended drought period, indicating that underlying water quality trends were also important in driving change in SAV abundance. Several water quality variables, including nitrogen concentration and turbidity, were lower inside the SAV bed than outside the SAV bed, implying the presence of feedback processes whereby the bed improves its own growing conditions by enhancing bio-physical processes such as sediment deposition and nutrient cycling. Together, these analyses suggest that stochastic extremes in river discharge and long-term water quality trends synergistically facilitated sudden

shifts in SAV abundance and that feedback processes likely reinforced the state of the bed before and after the shifts. Management efforts should consider these dynamic interactions and minimize chronic underlying stressors, which are often anthropogenic in origin.

Introduction

Change is ubiquitous in natural systems because the environmental conditions that affect biota are also inherently variable. Seagrass and associated submersed aquatic vegetation (SAV) communities in particular undergo episodes of decline and recovery that span seasons to multiple decades. Reports of decline dominate the literature, with many examples of SAV loss attributed to chronically degraded water quality associated with eutrophication (Kemp et al. 1983) or extreme weather events such as hurricanes, flooding, and temperature stress (Preen et al. 1995). Recent studies, however, have also reported instances of SAV recovery. Most relate expanded plant cover to improved water clarity resulting from management actions, such as sewage treatment plant upgrades (Burkholder et al. 2007; Rybicki and Landwehr 2007). Climate-related factors, such as decreased storminess (Reise and Kohlus 2007) have also been cited. The rate of both negative and positive trends can be substantially modified by the combined effects of short-term climatic drivers and long-term trends in anthropogenic stressors (Cardoso et al. 2004).

Change in SAV abundance can be abrupt, either as a linear response to an acute event or as a non-linear threshold effect in which a sudden shift occurs after gradually changing environmental conditions cross some critical threshold (Scheffer

et al. 2001; van der Heide et al. 2007). Theory suggests that feedback processes, through which a plant bed modifies its environment in ways that enhance its own growth, may facilitate threshold responses. For example, SAV attenuate wave energy and current velocity, which causes suspended particles to sink, improves ambient water clarity and, thus, enhances plant growth (Ward et al. 1984; Gruber and Kemp 2010). SAV beds also decrease water column nutrient concentrations, thereby precluding the growth of phytoplankton and epiphytes and allowing more light to reach the leaf surface (Moore 2004). Positive feedbacks help maintain a suitable growing environment despite changes in external conditions. However, beyond a critical threshold (e.g., a minimum light level needed for plant growth), feedback processes no longer buffer against disturbance and the system suddenly shifts to a degraded state (Scheffer et al. 1993). As conditions approach this threshold, resilience decreases and a small change in environmental conditions can drive the system beyond its 'tipping point'.

In some instances, plant reestablishment in bare sediment requires more stringent conditions than those needed to maintain an already established bed (Scheffer et al. 2001). As a result, restoration of a degraded submersed plant bed can be extremely difficult. The initiation of positive and negative shifts at different critical conditions (a pattern known as hysteresis) also means that different system 'states' (e.g., bare sediment and sediment colonized by SAV) can exist under the same set of environmental conditions (e.g., turbid and clear water).

An abrupt increase in submersed plant abundance recently occurred in a broad shallow region in the upper Chesapeake Bay known as Susquehanna Flats. SAV at

'the flats,' historically extolled by fishermen and waterfowl enthusiasts as prime wildlife habitat, began to decline when nutrient loading and eutrophication intensified in the 1960s (Bayley et al. 1978; Kemp et al. 2005). Following Tropical Storm Agnes in 1972, submersed plants virtually disappeared for nearly three decades until the early 2000s, when they rapidly recolonized nearly the entire region (>50 km^2). While an extreme flood event apparently triggered the historic demise of SAV at Susquehanna Flats, the extended lack of recovery is puzzling because it appears that environmental conditions have generally satisfied the habitat requirements for SAV in oligohaline regions of Chesapeake Bay since water quality monitoring began in 1984 (i.e., April-October median light attenuation coefficient <2.0 m^{-1}, total suspended solid and dissolved inorganic phosphorous concentrations <15 mg L^{-1} and 0.67μmol L^{-1}, respectively) (Dennison et al. 1993; Kemp et al. 2004).

Given the valuable ecological services that submersed plant beds provide, such as nutrient uptake and habitat for economically important fisheries, it is imperative that we refine our understanding of why they disappear and what conditions are required for their return. In the Chesapeake Bay region, monitoring programs have generated a wealth of detailed time series datasets measuring submersed plant abundance since 1958, water quality since 1984, and climate-related variables, such as temperature and river discharge since the late 1800s. Here, we rigorously examine and analyze these diverse time series datasets to develop an explanatory model for the recent rapid recovery of the large SAV bed at Susquehanna Flats. Specifically, we investigate 1) how patterns and trends in anthropogenic and climatic variables relate to SAV abundance, 2) whether the sudden resurgence could

reflect a threshold response to change in environmental conditions, and 3) whether feedback processes could have played a role in this resurgence. While retrospective data analysis is inherently limited because, for example, the data are restricted to what is available and often contain gaps, the inferences developed through such exercises can facilitate interpretation of current ecological dynamics as well as prediction about the future. Our broader motivation lies in the idea that the methods used and explanatory model derived here can be applied elsewhere to explore similar plant bed dynamics worldwide.

Methods

Study site

Susquehanna Flats is a broad, tidal fresh-water region located near the mouth of the Susquehanna River at the head of Chesapeake Bay (Fig. 2.1a). The shallow flats, formed from sand and silt deposited where the Susquehanna River broadens as it flows into the Bay, cover roughly 50 km^2 with a relatively narrow but continuous channel (3-7 m deep) bordering the western side and also relatively deep but discontinuous channels to the east and south of the flats. As of 2010, SAV covered most of Susquehanna Flats with dense stands of as many as 13 plant species, co-dominated by *Vallisneria americana*, *Myriophyllum spicatum*, *Hydrilla verticillata*, and *Heteranthera dubia*.

Data sources

The data described herein were collected by various agencies and organizations at a range of sampling intervals and durations (Table 2.1). Water quality data were

collected at 2-4 week intervals beginning in 1984. We used data from the sampling station CB1.1, which we call 'up-bay,' located at the mouth of the Susquehanna River for most analyses (Fig. 2.1). Because upper Chesapeake Bay hydrology is dominated by Susquehanna River outflow (Schubel and Pritchard 1986), data from this station are likely representative of water flowing into and around the plant bed. This study focuses on chlorophyll *a* (Chl *a*), total suspended solids (TSS), Secchi depth, total nitrogen (TN), dissolved inorganic nitrogen (DIN), particulate nitrogen (PN), total phosphorous (TP), dissolved inorganic phosphorous (DIP), particulate phosphorous (PP), particulate carbon (PC), the diffuse downwelling attenuation coefficient (K_D), and water temperature (temp). We also examined high sampling frequency (4 $hour^{-1}$) water quality data for dissolved oxygen (DO), pH, Chl *a*, turbidity, and temperature measured continuously from April through October since 2007. From 2007-2009, bi-weekly to monthly water quality data were available for several additional locations around Susquehanna Flats, including inside the SAV bed and down-bay from the SAV bed. Salinity was not included in this analysis because values in and around the plant bed were generally < 1.0, well within the tolerance range of the dominant submersed plant species populating the study site (Haller et al. 1974). Susquehanna River flow rates were measured at gauging stations located at Conowingo Dam (1968-present) and at Harrisburg, Pennsylvania (1890-present). Daily mean TN, TP, and TSS (1978-2010) loading rates at Conowingo Dam (Fig. 2.1) were calculated for each month based on streamflow and water quality concentrations using the weighted regressions on time, discharge, and season (WRTDS) method (Hirsch et al. 2010). Mean TN loading rates from 1945-1978 were estimated based on loading rates

calculated for Harrisburg (Hagy et al. 2004; Zhang et al. 2013).

Annual estimates of total SAV cover and crown density from 1984-2010 were based on geo-referenced aerial photographs (Table 2.1). Previous studies using aerial survey data focused on total area occupied by plants, which we call 'bed area' (Orth et al. 2010). However we felt that for this region, using a measure of plant abundance that reflected plant density was particularly important. From 1984-2000, plants were sparsely distributed throughout Susquehanna Flats. While the bed area was large, the actual abundance of plants was low. Therefore, we calculated SAV bed area weighted for density using a multiplier based on crown density categories (1-4) to estimate an index of total plant biomass, which we call 'bed abundance' (Moore et al. 2000; Rybicki and Landwehr 2007). We characterized temporal SAV trends in terms of both bed area and bed abundance, although our statistical analyses focused on the latter. We also determined the mean depth of the bed perimeter, which we call 'perimeter depth,' with geographic information systems (GIS) software (Esri ArcGIS) by overlaying SAV shape-files on bathymetric data and extracting the depth of the SAV shape-file perimeter. Historical SAV data for the period 1958-1975 (Bayley et al. 1978) and 1971-1988 (Maryland Department of Natural Resources unpubl.) were reported as a unitless annual plant abundance rating based on material recovered with a standard rake collected along four transects crisscrossing Susquehanna Flats (Bayley et al. 1978).

Data analyses

While relative SAV abundance, river discharge, and nitrogen loading data were available since 1958 and earlier, regular water quality monitoring did not begin

until the 1980s. Thus, our overall approach was to first rigorously analyze and synthesize the recent time series datasets (1984-2010), which include SAV abundance, water quality, river discharge, and loading, to generate a detailed explanatory model for the recent sudden SAV resurgence. We then conducted limited statistical analysis on the historical datasets (1958-1983) and used the relationships established through analysis of the recent data to make logical assumptions about the underlying mechanisms driving change across the entire time series. We performed all calculations and plotted all figures with the statistical computing and graphics software R with its *base* and *stats* packages unless otherwise noted.

We used change-point analysis to characterize the sudden change in features of the SAV bed. A change-point is defined as the point at which the statistical properties of a time series abruptly change. In this case, we performed segmented regression analysis to test for sudden and sustained changes in trend trajectories for bed area, bed abundance, and perimeter depth. We used the R package *segmented* for this analysis (Muggeo 2008). The sample size (n) was 26 years (aerial SAV surveys were not conducted at Susquehanna Flats in 1988). This method constrains the segments to be continuous; however trends in the historic SAV time series were clearly discontinuous. Therefore, we used a slightly different approach for this dataset, where change-point selection was based on minimizing the mean squared error from iteratively generated two-segment piecewise regression models (Crawley 2007). Although this approach allows for a more accurate characterization of discontinuous breaks in trends, it does not calculate confidence intervals or p-values.

We also characterized patterns and trends in environmental drivers. We calculated seasonal means for river discharge and water quality. Seasons are defined as follows: growing season = June through October; winter = December through February; spring = March through May; summer = June through August; fall = September through November. For variables that were sampled at multiple depths, we calculated the water column mean before calculating seasonal means. We then conducted segmented regression analysis on these growing season means to detect change-points. We also tested for long-term trends using the non-parametric Mann-Kendall trend test, which is often the preferred method of trend analysis for characteristically non-normal and/or skewed time series datasets (Hirsch et al. 1982). Sample sizes ranged from 23 to 26. In addition, because light availability is often a key driver of SAV growth (Dennison 1987), we used the non-parametric Spearman rank-order test to calculate correlations between K_D and the growing season means for parameters with significant long-term trends. To broadly demonstrate how all of the environmental variables included in this study were interrelated, we performed standardized principal component analysis (PCA) on growing season mean values for all surface water quality variables and then tested for correlation between the first principal component and growing season mean river discharge using the Spearman rank-order test.

To show how environmental variables were related to bed abundance, we constructed simple linear regression models using seasonal means and medians for each climatic and water quality parameter as the predictor variable and bed abundance as the response variable. We tested the residuals of each model for

normality, independence, and heteroskedasticity using the Shapiro, Durbin-Watson, and non-constant error variance tests, respectively. We performed data transformations (e.g., log) as necessary. Because the bed abundance data were autocorrelated, we used differencing to obtain a time series reflecting interannual change in bed abundance (i.e., the first difference of y at time t is equal to $y(t)-y(t-1)$), which we call 'bed change.' Even after transformation, the relationship between bed change and environmental time series was clearly non-linear (i.e., the relationship between predictor and response variables changed over time). While environmental variables and bed change appeared to be unrelated when bed change was minimal, linear relationships were apparent when bed change $\neq 0$. Thus, we partitioned the bed change dataset into two time periods: 'stable' (1984-1998 and 2009-2010, characterized by little interannual change) and 'transition' (1999-2008, when bed abundance rapidly increased). We then conducted piecewise regressions on these segments.

The non-linear nature of these relationships may suggest that the change in SAV abundance was related to a threshold response to changes in environmental conditions. Segmented regression, in addition to detecting points in time at which a temporal trend trajectory shifts, can also be used to identify the threshold value at which at the slope of the relationship between predictor and response variables changes. Because, again, light is a critical resource for SAV growth, we used segmented regression to detect a potential threshold response of bed abundance to change in the light environment, as indicated by growing season mean K_D.

In addition, because extreme weather events can modify SAV trends, we also tested for relationships between bed change and extremes in river discharge. We classified years with river discharge values exceeding the 75th percentile of growing season mean river discharge as 'wet years' and those that fell below the 25th percentile as 'dry years' (United States Geological Survey http://md.water.usgs.gov/waterdata/chesinflow/wy/). We classified 'normal' river discharge values as those between the 25th and 75th percentiles. We then used Kruskal-Wallis one-way analysis of variance (ANOVA) by ranks to further investigate how weather-related mechanisms affected bed change by testing for differences in percent change in bed abundance during wet years, dry years, and average years. This test was a better choice than parametric ANOVA because the groups were unequal in size and variance was not homogeneous over time. We then calculated post-hoc individual comparisons using the Mann-Whitney test.

To quantify spatial differences in water quality, which may indicate how the SAV bed affected ambient growing conditions, we calculated the mean difference and a 95% confidence interval between monitoring data collected inside and outside the SAV bed for each month during which data were collected (April-October). Turbidity, Chl *a*, DO, and pH were measured at 15 minute intervals with continuous monitoring data sondes while grab samples analyzed for DIN were collected every 2-4 weeks. Because sample sizes were large (n>2000 for most parameters, with the exception of DIN) we felt that a significance test (e.g., t-test) would be inappropriate because with so many samples, such tests usually yield significant results even if the actual differences are minimal (McBride 1993). Rather, we quantified the magnitude

of differences (effect size) between sample stations, which, in this context, is more ecologically meaningful.

Results

There was a change-point indicating sudden plant loss in 1972, which coincided with Tropical Storm Agnes (Fig. 2.2a). Several change-points were also evident in the recent SAV time series for bed abundance, bed area, and perimeter depth. Bed abundance was near zero with little change from 1984-2000, but it increased gradually between 2001 and 2004, then rapidly increased to >40 km^2 after the 2004 change-point (Fig. 2.2a). Bed area was generally constant from 1984 to ~1998 and then increased to nearly 50 km^2 by 2010 (Fig. 2.2b). Perimeter depth decreased between 1984-1997, and then increased following a change-point around 1997 (Fig. 2.2c). These trends are illustrated in more detail by the series of SAV maps generated through analysis of aerial photographs (Fig. 2.3), which show that submersed plant cover was persistently sparse (<10% cover) through much of the 1980s and 1990s and then rapidly increased in size and density between 2000 and 2006. The bed remained persistently large and dense after 2007.

There were several significant long-term trends in the surface water quality time series data (Table 2.2). Notably, water clarity, indicated by K_D, improved by ~40% between 1984 and 2010. TP, PP, PN, and PC concentrations also significantly decreased and temperature increased. There was also a change-point in spring N loading, which gradually increased prior to 1988 and then began to decrease after 1988 (p<0.01; Fig. 2.4a). Most significant trends for individual seasonal means (winter, spring, summer, fall) were also significant for the entire growing season

(June-August). Therefore, we simply report trend test and change-point results for growing season means. However, one exception was the significant change-point in only spring N-loading, as reported above. Of the trending variables, K_D was correlated with N load (ρ=0.62, p<0.05), TP (ρ=0.65, p<0.001), PP (ρ=0.66, p<0.001), PC (ρ=0.49, p<0.05), and temperature (ρ=-0.86, p<0.001).

Principal component analysis results show that TN, TP, DIN, DIP, PP, TSS, Secchi depth, and K_D were interrelated (Fig. 2.5a). These variables all projected strongly onto the first principal component (PC1), which accounted for 53% of the variance in water quality. PC1 was significantly correlated with river discharge (ρ=0.57, p<0.01) (Fig. 2.5b). Chl *a*, PN, and PC projected strongly onto the second principal component (PC2), which represented 20% of the variance in water quality.

Bed change was related to river flow and several water quality variables during the transition period but not during the stable time period (Fig. 2.6; Table 2.3). Generally, winter and spring environmental conditions were not related to bed change, with the exception of spring TN concentration (R^2 = 0.45, p<0.05) and possibly TN loading (R^2 = 0.47, p<0.07). Relationships between bed change and most environmental variables were stronger during the summer and weaker but often significant in the fall. Summer mean river flow explained the greatest proportion of variance in bed change (R^2=0.88 p<0.001). Bed change was, however, not related to Chl *a*, DIN, PN, or PC during any season. Regression results also indicated several weaker but significant positive relationships during the stable period between bed change and winter and fall TN as well as weak but significant negative relationships with spring water temperature. Regression analyses using historical TN loading and

river discharge as predictors and SAV relative abundance as the response variable yielded no significant results. We used both seasonal mean and median values to construct regression models, and we report results for whichever explained more variance in bed change. Segmented regression on bed abundance and growing season mean K_D indicated that the rapid increase in bed abundance occurred around a threshold K_D value of 1.3 m^{-1} ($p<0.001$) with a 95% confidence interval of 1.1 to 1.5 m^{-1}.

Extremes in river discharge were related to shifts in bed abundance. In 2003, growing season mean river flow was particularly high (1449 $m^3 s^{-1}$; Fig. 2.4b) and bed abundance declined by 45%. Conversely, from 1995-2002, there were no wet years and no daily flow rates exceeded 10,000 $m^3 s^{-1}$. The change-point in SAV total area occurred during this time and bed abundance rapidly increased shortly thereafter (Fig. 2.2). On average, bed abundance increased by 53±20% and 21±10% during dry years and normal flow years, respectively, and decreased by 7±11% during wet years (Fig. 2.7). Kruskal-Wallis ANOVA results indicate that percent change in bed abundance was significantly different depending on growing season flow conditions (wet years, average flow, dry years; $\chi^2=7.63$, $p<0.05$). Post-hoc comparisons indicate a significant difference between bed change during wet years and dry years ($p<0.05$). Although the 1972 demise of SAV was clearly linked to a record river discharge maximum (Figs. 2.2, 2.4), this relationship could not be generalized across the entire historical dataset, as ANOVA resulted in no significant differences in bed change under different flow conditions.

Water quality variables measured in and around the SAV bed varied over space and time. Turbidity and Chl *a* were lower inside the bed than up-bay from the bed while pH and DO were higher inside the bed (Table 2.4; Fig. 2.8). DIN was lower inside the SAV bed compared to both up-bay and down-bay stations and slightly lower down-bay compared to the up-bay station. Generally, the magnitude of these differences was smaller early in the growing season and increased as the SAV growing season progressed. The difference in DIN, which was >30 times lower inside the bed compared to up-bay in July and August during peak biomass, was particularly striking. Monthly mean DIN concentrations inside the bed ranged from 1.6-2.3 μmol L^{-1} during the summer (July-September) while up-bay concentrations ranged from 39-54 μmol L^{-1}.

Discussion

Here, we first examine the results of our analyses separately to explore potential causes and/or effects of each set of observations. We then take a step back and consider these disparate observations together to construct an explanatory model of the SAV resurgence. Our overall line of reasoning begins with the hypothesis that reductions in nutrient loading led to long-term water clarity improvement, and thus, a long-term increase in light availability for plant photosynthesis. Then, during a dry period from 1997-2002, a critical light threshold was crossed, which, together with an absence of storm events, provided ideal conditions for new plant growth. As a result, the bed began to expand and colonize deeper water. Finally, as plant density increased, positive feedback effects between the bed and ambient water quality

facilitated the subsequent rapid SAV resurgence. The following paragraphs provide a detailed explanation of this sequence of logic.

Environmental drivers

It has been well established that light availability is the most important constraint on the growth of submersed plants when other habitat requirements, such as substrate composition, wave exposure, and flow regime, are satisfied (Dennison 1987). Our analyses show that water clarity increased over time and that nitrogen loading has been decreasing over the last several decades. We suggest that these trends may have been a key component in the SAV resurgence. Other instances of SAV restoration have been attributed to decreased nutrient loading and associated declines in phytoplankton abundance (Burkholder et al. 2007). Therefore, we were surprised to find no significant decline in Chl *a* concentration and no significant correlations between Chl *a* and K_D or Secchi depth. There were, however, declines in PN, PC, TP, and PP. Of these trending parameters, PC, TP, and PP were correlated with K_D. In addition, principal component analysis showed that Chl *a*, PN, and PC tended to covary (Fig. 2.5). Thus, decreases in particulates, possibly the result of reduced nutrient loading, may have been responsible for improved water clarity. Furthermore, in tidal freshwater regions of Chesapeake Bay, epiphytes can contribute 20-60% additional shading beyond light attenuation by dissolved and suspended material in the water column (Kemp et al. 2004). Thus, reductions in nutrient loading may have also limited the growth of epiphytes, allowing more light to reach the SAV leaf surface.

Our analyses also suggest that interannual change in bed abundance around the trend of recovery was driven by stochastic weather variability, at least during transition years. Physical and biological processes in estuaries are often directly linked to watershed rainfall and, subsequently, down-stream river discharge into the estuary. In the present study, correlation between PC1 and river discharge demonstrates that Susquehanna River outflow and, thus, rainfall, was a major driver of change for many key water quality parameters, which co-varied as a result of their collective response to river flow. Consequently, bed change was also strongly related to river flow during the transition period. Because water quality variables often co-vary (van der Heide 2009), it is difficult to identify which variables were specifically responsible for bed change. However, significant correlation among TSS, Secchi depth, K_D, and river discharge suggests that flow controlled the concentration of suspended particles, which affected water clarity and, in turn, bed change. TN and TP were also related to river discharge and could have affected epiphyte growth. Because river discharge was related to bed change, it comes as little surprise that extremes in river discharge were related to substantial SAV loss and growth (Fig. 2.7). Interestingly, however, Chl *a*, PN, and PC were not related to bed change or river discharge (Fig. 2.5; Table 2.3). Thus, although these parameters appeared to be related to long-term water clarity improvement, they were unrelated to weather-driven interannual variation in and river discharge and bed change.

The strong relationships between bed change, river discharge, and water quality during June through August in particular demonstrate that the annual change in size and density of the SAV bed is largely a function of summer river discharge.

Because the dominant macrophyte species at Susquehanna Flats do not generally emerge until late spring to early summer (Carter et al. 1985), winter and spring flow has little effect on the SAV bed. On the other hand, summer river discharge explained nearly 90% of the variability in bed change because plants are especially sensitive to turbidity during this critical stage in the growth cycle, when they emerge from the sediment and begin to actively grow. These results support modeling studies, which simulate severe effects on SAV beds by storms that occur during the height of the growing season but muted effects for storms occurring after biomass has peaked (Wang and Linker 2005).

Although summer environmental conditions had the strongest effect on bed change, the relationships between bed change and spring TN concentration and TN loading (Table 2.3) are also worth noting. In estuarine ecosystems, ecological response often lags change in river flow (Hagy et al. 2004). Our analyses suggest that springtime N inputs may have had a similar lagged effect on the SAV bed, possibly because of a delayed response between N loading and phytoplankton and/or epiphyte production.

The absence of significant statistical relationships between bed change and external drivers during stable years as well as the sudden nature of the SAV resurgence implies a non-linear threshold response to improving environmental conditions. It appears that a critical threshold in light availability was crossed during an extended period of low to normal river flow (1995-2002), when the light environment substantially improved. Before the dry period (1984-1994) the average percent of incident light reaching the bottom (*PLB*) was ~17%, which we calculated

by assuming a mean depth (z) of 1 m and inserting growing season mean K_D values into the Lambert-Beer relationship ($I_z/I_o = e^{-K_D z}$), where *PLB* (100 (I_z/I_o)) is irradiance reaching the sediment surface (I_z) as a percentage of that at the water surface (I_o). We estimated that PLB was ~27% during the dry period and ~25% after the dry period (2003-2010). The light threshold for tidal freshwater SAV in Chesapeake Bay is ~13-14% (Dennison et al. 1994; Kemp et al. 2004); however this threshold generally applies to existing SAV beds rather than initiation of a new bed. That our estimated threshold is greater supports the idea that new SAV growth requires more light than an already established bed. Thus, although water quality gradually improved across the entire 1984-2010 time series, the SAV bed only began to expand after this critical threshold was exceeded.

Comparison of trends in river discharge, N loading, and SAV from 1958-1988 implies that the same processes described above occurred in reverse. In the decade prior to the 1972 SAV demise, bed abundance was declining despite an extended drought period (Figs. 2.2, 2.4). N loading was also increasing and, consequently, chronic eutrophication led to poor water quality and widespread SAV loss (Bayley et al. 1978; Kemp et al. 1983, 2005). Tropical Storm Agnes then pushed the already deteriorating SAV system beyond its 'tipping point' into a degraded state in 1972. Thus, it appears that the ultimate response of the SAV bed to precipitation patterns depended on underlying water quality trends. This may explain the lack of statistical differences in percent bed change during wet and dry years for these historical time series. While the bed tended to expand during dry years in recent decades as water

quality improved, deteriorating water quality from the 1950s through the 1980s likely precluded this response.

Internal feedback processes

Differences in water quality inside and outside the SAV bed suggest the presence of strong positive feedback processes (Table 2.4). For example, low turbidity inside the plant bed (Fig. 2.8a) was likely the result of particle trapping or reduced sediment resuspension due to the effects of bed architecture on local hydrodynamics (Ward et al. 1984; Gruber and Kemp 2010). Reduced Chl *a* inside the bed (Fig. 2.8b) could also result from particle trapping or from nutrient limitation within the plant bed. Low DIN within the plant bed during summer months (Fig. 2.8c) is evidence of direct nutrient uptake by plants and/or enhanced denitrification within the plant bed (Caffrey and Kemp 1992). This effect on DIN may extend beyond the SAV bed, as down-bay DIN concentrations were substantially less than those measured up-bay. Elevated pH (Fig. 2.8d) and dissolved oxygen (Fig. 2.8e), which are indicative of plant photosynthesis, further illustrate the strong effects of dense vegetation on water quality. Seasonality in these spatial patterns demonstrates that as plant biomass increased throughout the growing season, so did the magnitude of the feedback effects.

These feedback processes may explain the threshold-type response of the SAV bed to change in environmental conditions. Feedbacks help maintain densely vegetated plant beds; however, in the absence of sediment-stabilizing vegetation, bottom sediments are easily resuspended, leading to elevated turbidity (Scheffer et al. 1993). As a result, the system tends to persist within one of these states (clear water

with SAV or turbid water without SAV) until an externally driven change in water clarity induces a shift into the alternate state. We suggest that exceptional growing conditions during the drought period allowed the system to overcome the turbid water state, serving as a 'kick-start' to facilitate the rapid resurgence.

Alternative explanations

An alternative explanation for sparse plant cover from the 1970s through the 1990s is lack of propagules, possibly the result of scouring or burial during Tropical Storm Agnes. The SAV increase in the early 2000s could, thus, be attributed to reintroduction of new propagules and bed expansion by rapid clonal growth. This occurred in Virginia's coastal bays, where historically abundant eelgrass (*Zostera marina*) disappeared in the 1930s due to a fungal disease and hurricane damage (Orth et al. 2006). When the area was reseeded through restoration efforts in 2001, eelgrass flourished because water quality was already suitable for plant growth. In contrast, SAV restoration efforts in and around Susquehanna Flats in the late 1980s were met with only marginal success, in part due to epiphytic growth on seedlings and transplants (Kollar 1989). If lack of propagules was the only limiting factor for plant growth in this system, then survival rates for transplants and seedlings should have been greater in the absence of other limiting factors, such as light availability. Furthermore, patches of *Myriophyllem spicatum* have persisted on Susquehanna Flats since at least the 1960s and *Vallisneria americana* was always present and often abundant along the area's shoreline (Bayley et al. 1978; Kollar 1989). Presumably, these populations could have served as propagule sources for new plants. Therefore,

we suggest that inadequate growing conditions are a more likely explanation for lack of SAV regeneration following their historic decline.

Another variable that warrants consideration is the trend of increasing growing season mean temperature, which continues to rise at $0.1^{o}C\ year^{-1}$ (Table 2.2). Global warming is already causing temperature stress and diebacks for SAV species that prefer cold water, such as eelgrass, whose optimal temperature ranges from 10-$20^{o}C$ (Nejrup and Pedersen 2008). For many freshwater SAV species, however, elevated water temperatures that are still within physiological tolerance ranges tend to promote increased plant production (Barko and Smart 1981). Because the optimal temperature for the dominant species at Susquehanna Flats exceeds $30^{o}C$ (Van et al. 1976), warmer water could increase production. From 1984-1992, water temperature during the SAV growing season never exceeded $30^{o}C$; yet between 1993-2010, 10-15% of water temperature measurements were greater than $30^{o}C$. Because, however, SAV were historically abundant in the upper Chesapeake Bay before this recent warming trend, we suggest that other factors were more important in driving the sudden SAV resurgence.

Future implications

These processes and patterns are not unique to Susquehanna Flats. Instances of nonlinear temporal trends in submersed plant systems have been suggested for the Dutch Wadden Sea (van der Heide et al. 2007), U.S. mid-Atlantic Coastal Bays (Carr et al. 2010), as well as shallow lakes in the U.S. (Carpenter et al. 2001) and Northern Europe (Scheffer et al. 1993). While the variables affecting SAV systems may differ according to particular geographic features and plant species, the underlying

mechanisms driving system dynamics are broadly relevant to our understanding of ecological change and can help guide SAV management. External perturbations that can shock a system are typically stochastic. However, the controlling variables that affect an ecosystem's resilience, or ability to withstand disturbance, are frequently related to anthropogenic activity (Walker 2004). Management efforts should consider dynamic interactions, which may include threshold effects, between SAV and relevant controlling variables. Particularly in light of predicted future increases in weather extremes, which are often the source of external perturbations, maximizing resilience by minimizing chronic anthropogenic stressors should be a core goal in the conservation of SAV ecosystems.

Tables

Table 2.1 Summary of data sources, sampling intervals, and date ranges.

Data type	Source	Sampling interval	Date range
SAV cover	Virginia Institute of Marine Science http://web.vims.edu/bio/sav/index.html	annual	1984-2011
SAV relative abundance	Bayley et al.1978 study and Maryland Department of Natural Resources (MDDNR)	annual	1958-1988
Water quality	Chesapeake Bay Monitoring Program, http://www.chesapeakebay.net/data/downloads/cbp_water_quality_database_1984_present	2-4 weeks	1984-2011
Water quality	MDDNR Continuous Monitoring Program Calibration Data, http://www.chesapeakebay.net/data/downloads/cbp_water_quality_database_1984_present	2-4 weeks	2007-2010
Water quality	MDDNR Continuous Monitoring Program, http://mddnr.chesapeakebay.net/eyesonthebay/index.cfm	15 minutes	2007-20101 (spring-fall)
Susquehanna River discharge	United States Geological Survey (USGS), http://waterdata.usgs.gov/md/nwis/uv?01578310	daily	1890-2011
Susquehanna River TN, TP, and TSS loading rate	USGS	monthly	1978-2010
Susquehanna River TN loading rate	Zhang et al. 2013	monthly	1945-1978

Table 2.2 Mann-Kendall trend test results for annual loading rates at Conowingo Dam and growing season (June-October) mean water quality variables from 1984-2010. Kendall's τ, associated *p*-values, and trend slopes are listed. Rows in bold are significant at the 0.05 level.

Parameter	τ	*p*	Slope
TN loading	-0.19	0.18	-0.50
TP loading	-0.03	0.82	-0.01
TSS loading	0.19	0.18	1.42
TN	-0.13	0.36	-0.48
DIN	0.07	0.65	0.07
PN	**-0.30**	**0.03**	**-0.10**
TP	**-0.28**	**0.04**	**-0.01**
DIP	-0.01	0.97	0.00
PP	**-0.40**	**0.00**	**-0.01**
PC	**-0.31**	**0.03**	**-0.01**
Chl *a*	-0.19	0.17	-0.09
TSS	-0.04	0.80	-0.02
Secchi	0.14	0.31	0.00
K_D	**-0.44**	**0.00**	**-0.03**
Temp	**0.50**	**0.00**	**0.10**

Table 2.3 Linear regression results for transition (1999-2008) and stable (1984-1998; 2009-2010) time periods. For each regression, bed change was the response variable; seasonal means (or medians, if indicated) for each environmental parameter were the predictor variables. An annual median for predictor variable was used instead of the mean; blog(predictor variable); bold values are significant at the 0.05 level. Tables are presented on the proceeding two pages

Transition period	*June-October*			*Winter*			*Spring*			*Summer*			*Fall*		
Predictor variable	Slope	R^2	*p*	Slope	R^2	*p*	Slope	R^2	*p*	Slope	R^2	*p*	Slope	R^2	*p*
River flow	-	**0.76**[b]	**0.002**	-	0.04[b]	0.739	-	0.04[b]	0.629	-	**0.88**[b]	**0**	-	**0.57**[a]	**0.018**
N load	-	0	0.941	-	0.37	0.108	-	0.47	0.061	-	0.01	0.781	-	0	0.917
TSS load	-	0.03	0.708	-	0.08	0.498	-	0.22	0.24	-	0.09	0.464	-	0.08	0.504
TN	-	0.2	0.223	-	0.41	0.062	-	**0.45**[a]	**0.049**	-	0.18	0.252	-	0.15	0.307
TP	-	**0.67**[a b]	**0.007**	-	0.01	0.767	-	0.04	0.627	-	**0.70**[b]	**0.005**	-	0.32	0.112
DIN	-	0.14	0.313	-	0.3	0.129	-	0.08	0.448	-	0.11	0.386	-	0.17	0.273
DIP	-	**0.71**[b]	**0.004**	-	0.04	0.587	-	0.21	0.214	-	**0.54**[b]	**0.022**	-	0.18	0.249
PN	+	0	0.975	+	0.29	0.138	-	0.02	0.69	+	0.05	0.553	-	0.05	0.566
PP	-	0.4	0.067	+	0.13	0.333	+	0	0.955	-	**0.52**	**0.029**	-	**0.02**	**0.049**
PC	-	0.17	0.264	+	0.39	0.071	-	0	0.933	-	0.02	0.689	-	0.05	0.566
TSS	-	**0.75**[a]	**0.021**	-	0.14	0.32	-	0.05	0.582	-	**0.62**[a]	**0.011**	-	0.1	0.397
Chl *a*	+	0.14	0.33	+	0.04	0.589	+	0.09	0.443	+	0.11	0.384	+	0.05	0.562
K_D	-	**0.61**[a]	**0.013**	-	0.01	0.795	-	0.04	0.623	-	**0.61**[a]	**0.014**	-	**0.50**[a]	**0.049**
Secchi	+	**0.61**	**0.012**	+	0.32	0.13	+	0	0.994	+	**0.62**	**0.011**	+	**0.48**	**0.037**
Temp	+	**0.67**	**0.007**	+	0.21	0.213	+	0.06	0.525	+	0.43	0.056	+	0.19	0.247

Stable period	*June-October*			*Winter*				*Spring*			*Summer*			*Fall*		
Predictor variable	Slope	R^2	*p*	Slope	R^2	*p*	*p*	Slope	R^2	*p*	Slope	R^2	*p*	Slope	R^2	*p*
River flow	0.561	-	0.01	0.77	-	0.06	0.391	+	0	0.817	-	0	0.954	-	0.03	0.561
N load	0.719	+	0	0.884	-	0	0.887	-	0.04	0.514	-	0	0.847	+	0.01	0.719
TSS load	0.904	+	0	0.997	-	0	0.926	-	0.04	0.516	-	0	0.837	+	0	0.904
TN	0.911	-	0	0.845	-	0	0.918	-	0.05	0.424	-	0.01	0.711	-	0	0.911
TP	**0.041**	-	0	0.948	+	**0.27**	**0.047**	+	0.01	0.803	-	0.12	0.217	+	**0.28**	**0.041**
DIN	0.292	+	0.1	0.258	+	0.22	0.077	-	0.03	0.531	+	0.01	0.805	+	0.09	0.292
DIP	0.137	-	0.06	0.378	+	0.22	0.075	+	0	0.941	-	0.26	0.051	+	0.16	0.137
PN	0.198	+	0.06	0.388	+	0.19	0.105	+	0.04	0.456	-	0.02	0.608	+	0.12	0.198
PP	0.986	+	0.07	0.342	+	0.03	0.569	-	0.03	0.567	+	0.18	0.128	-	0	0.986
PC	0.593	+	0.05	0.408	+	0.19	0.102	-	0.02	0.579	+	0.06	0.371	+	0.02	0.593
TSS	0.585	+	0.16	0.145	-	0.07	0.366	-	0.01	0.722	+	0.26	0.062	+	0.02	0.585
Chl *a*	0.453	+	0.15	0.152	+	0.16	0.146	-	0.03	0.571	+	0.02	0.633	+	0.04	0.453
K_D	0.559	+	0.01	0.741	-	0.01	0.7	-	0.06	0.397	+	0.06	0.365	-	0.03	0.559
Secchi	0.14	+	0.08	0.366	-	0.02	0.721	-	0.09	0.313	+	0.03	0.603	+	0.2	0.14
Temp	0.793	-	0.07	0.326	-	0.01	0.797	+	0.1	0.248	-	0.04	0.458	-	0.01	0.793

Table 2.4. Mean water quality differences ± 95% confidence intervals between monitoring sites located inside and outside the SAV bed for Chl *a*, turbidity, dissolved oxygen, pH, and dissolved inorganic nitrogen

	n	Mean difference	95% confidence interval			*n*	Mean difference	95% confidence interval	
Chl *a:* Up-bay, SAV bed					DIN: Up-bay, SAV bed				
Apr	597	2.92	2.65	3.19	Apr	10	13.99	0.70	27.28
May	2189	0.44	0.18	0.70	May	15	11.59	-3.05	26.24
Jun	1847	3.87	3.69	4.06	Jun	13	50.14	34.82	65.46
Jul	1248	3.13	2.99	3.28	Jul	15	70.61	65.57	75.66
Aug	2499	2.78	2.68	2.89	Aug	13	65.15	58.19	72.10
Sep	2290	3.06	2.95	3.17	Sep	13	63.04	56.67	69.40
Oct	2323	1.26	1.18	1.33	Oct	15	67.81	31.28	104.35
Turbidity: Up-bay, SAV bed					DIN: Down-bay, SAV bed				
Apr	623	-0.49	-0.91	-0.08	Apr	3	3.89	-10.71	18.50
May	1924	0.89	0.41	1.37	May	3	8.46	-7.41	24.32
Jun	1530	4.87	4.75	5.00	Jun	3	34.76	12.40	57.12
Jul	676	2.75	2.53	2.97	Jul	3	52.05	7.58	96.52
Aug	1237	1.23	1.14	1.31	Aug	3	47.82	-17.95	113.60
Sep	1945	1.69	1.55	1.83	Sep	3	37.12	8.31	65.93
Oct	1299	5.02	4.65	5.40	Oct	3	37.99	0.49	75.48
pH: Up-bay, SAV bed					DIN: Up-bay, down-bay				
Apr	626	-0.08	-0.11	-0.06	Apr	10	10.09	-5.75	25.94
May	2189	-0.83	-0.85	-0.81	May	15	3.14	-8.96	15.23
Jun	1696	-1.43	-1.45	-1.42	Jun	13	15.38	-8.76	39.52
Jul	1732	-1.51	-1.53	-1.49	Jul	15	18.56	-24.28	61.41
Aug	2540	-1.41	-1.43	-1.39	Aug	13	17.32	-44.91	79.56
Sep	2679	-1.41	-1.43	-1.40	Sep	13	25.92	1.11	50.73
Oct	2582	-1.21	-1.23	-1.19	Oct	15	29.83	8.71	50.95
DO: Up-bay, SAV bed									
Apr	625	-0.37	-0.44	-0.29					
May	2189	-1.53	-1.61	-1.45					
Jun	1901	-2.91	-3.00	-2.81					
Jul	1948	-2.16	-2.25	-2.07					
Aug	2745	-1.54	-1.63	-1.46					
Sep	2878	-1.49	-1.55	-1.43					
Oct	2586	-2.30	-2.37	-2.23					

Figure captions

Figure 2.1 Location of the Susquehanna River and water quality sampling sites. Dark shaded area in the figure on the right indicates the SAV bed aerial extent in 2010.

Figure 2.2 Time series for (a) SAV relative abundance (1958-1983) and bed abundance (1984-2010), (b) bed area, and (c) perimeter depth. Solid vertical lines and grey shaded areas in the time series plots indicate estimated change-points ± 95% confidence intervals (conf. int.). Dashed lines indicate linear trends before and after each change-point.

Figure 2.3 1984-2010 SAV cover at Susquehanna Flats. Shades of gray indicate SAV density classes. Images were generated through digital analysis of aerial photography. Surveys were not flown in 1988.

Figure 2.4 1945-2010 time series for (a) spring daily mean total nitrogen loading and (b) growing season (June-October) mean Susquehanna River flow with 'wet years' (>75th percentile) and 'dry years' (<25th percentile) highlighted.

Figure 2.5 (a) Bi-plot illustrating relative loadings of water quality variables onto the first and second principal components (PC1 and PC2) and (b) correlation between river discharge and PC1.

Figure 2.6 Relationship between growing season mean Susquehanna River discharge and SAV bed abundance during (a) the transition time period (1999-2008) and (b) the stable time period (1984-1998; 2009-2010).

Figure 2.7 Mean percent change in bed abundance ± standard error (SE) during normal river flow years, dry years, and wet years. An asterisk indicates significant difference at the 0.05 level.

Figure 2.8 2007-2010 monthly means ± standard error (SE) for several water quality parameters at sampling stations located inside the SAV bed, up-bay, and, in the case of dissolved inorganic nitrogen, down-bay from the SAV bed. Except for DIN, all other SE values did not exceed the radius of the data points. NTU- nephelometric turbidity units.

Figures

Figure. 2.1

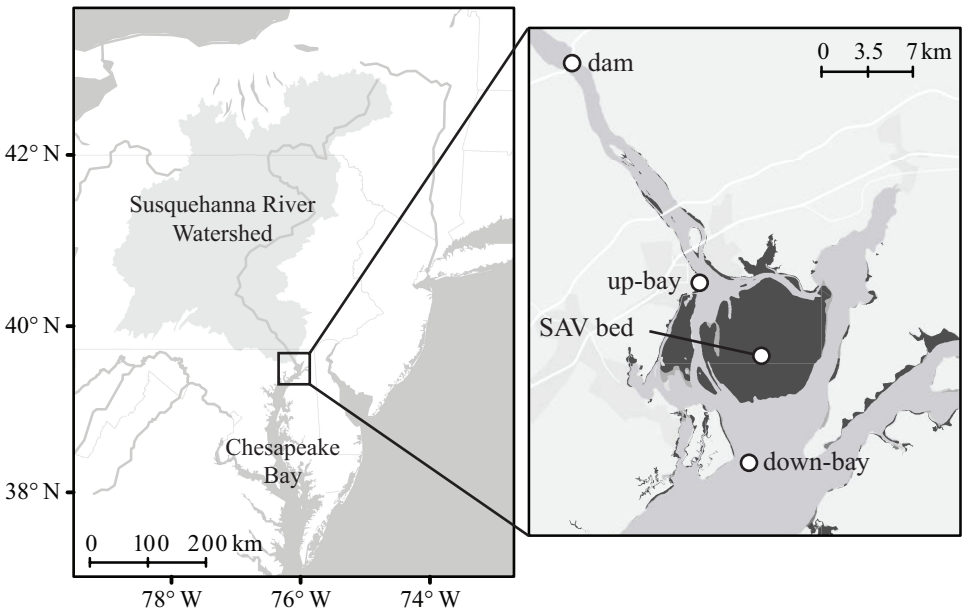

Figure 2.2

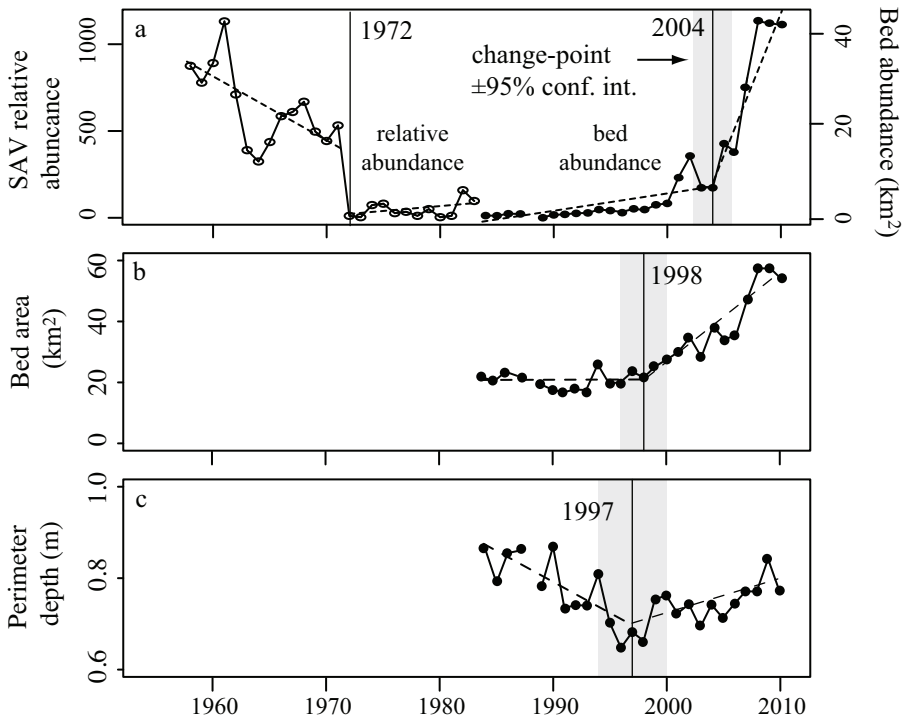
a
1972
2004
change-point
±95% conf. int.
relative
abundance
bed
abundance
SAV relative
abuncance
Bed abundance (km²)
b
1998
Bed area
(km²)
c
1997
Perimeter
depth (m)
1960
1970
1980
1990
2000
2010

Fig 2.3

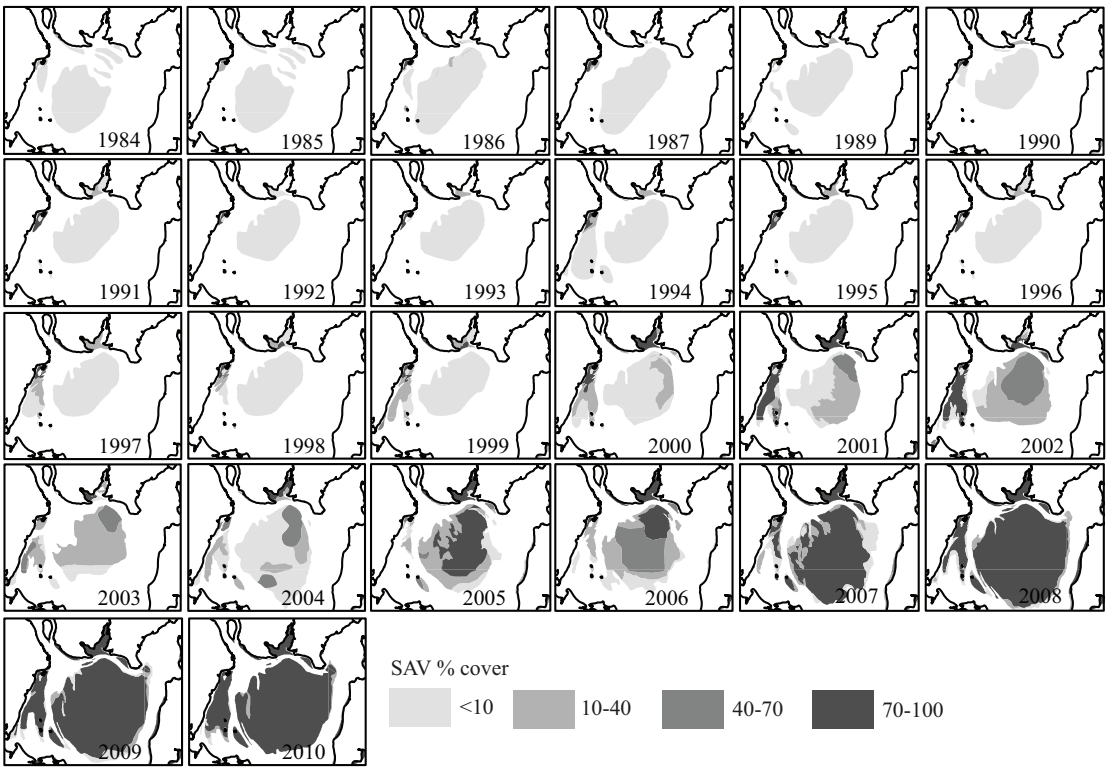
1984
1985
1986
1987
1989
1990
1991
1992
1993
1994
1995
1996
1997
1998
1999
2000
2001
2002
2003
2004
2005
2006
2007
2008
2009
2010
SAV % cover
<10
10-40
40-70
70-100

Fig. 2.4

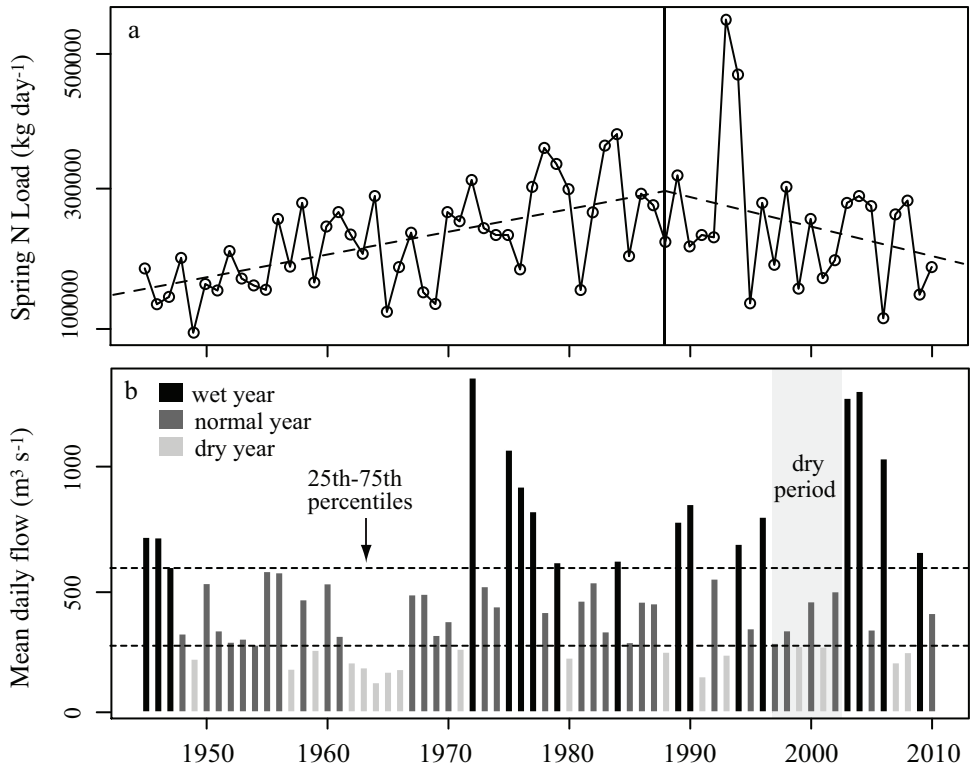
a
Spring N Load (kg day-1)
100000
300000
500000
b
wet year
normal year
dry year
25th-75th
percentiles
dry
period
Mean daily flow (m3 s-1)
0
500
1000
1950
1960
1970
1980
1990
2000
2010

Fig. 2.5

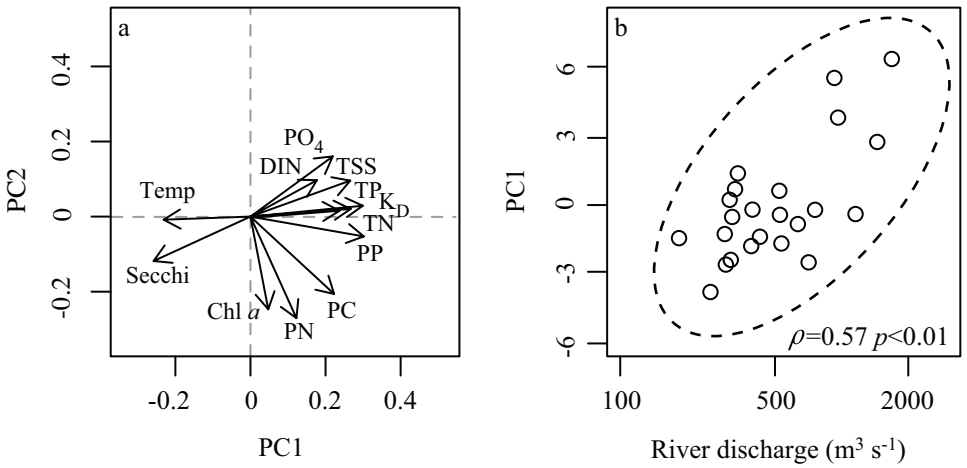
a
PO4
DIN
TSS
TP
KD
Temp
TN
PP
Secchi
Chl a
PC
PN
PC2
PC1
-0.2
0
0.2
0.4
b
PC1
River discharge (m3 s-1)
100
500
2000
ρ=0.57 p<0.01

Fig. 2.6

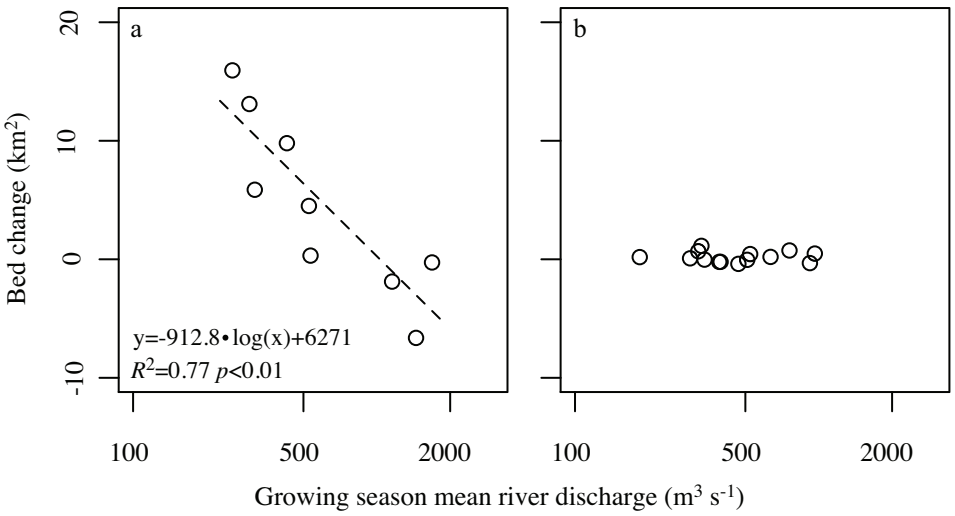
a
b
Bed change (km²)
20
10
0
-10
y=-912.8•log(x)+6271
R²=0.77 p<0.01
100
500
2000
100
500
2000
Growing season mean river discharge (m³ s⁻¹)

Fig. 2.7

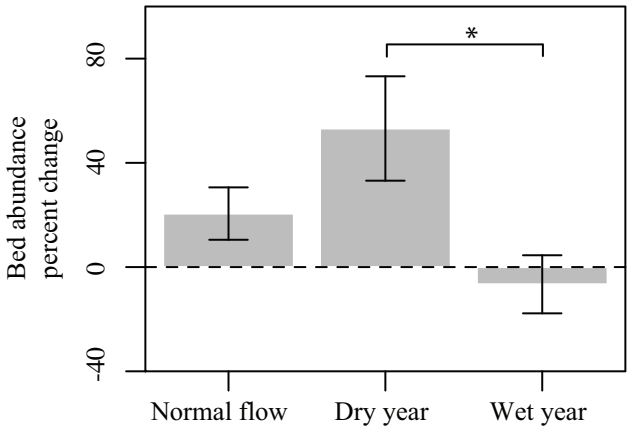
Bed abundance
percent change
-40
0
40
80
*
Normal flow
Dry year
Wet year

Fig. 2.8

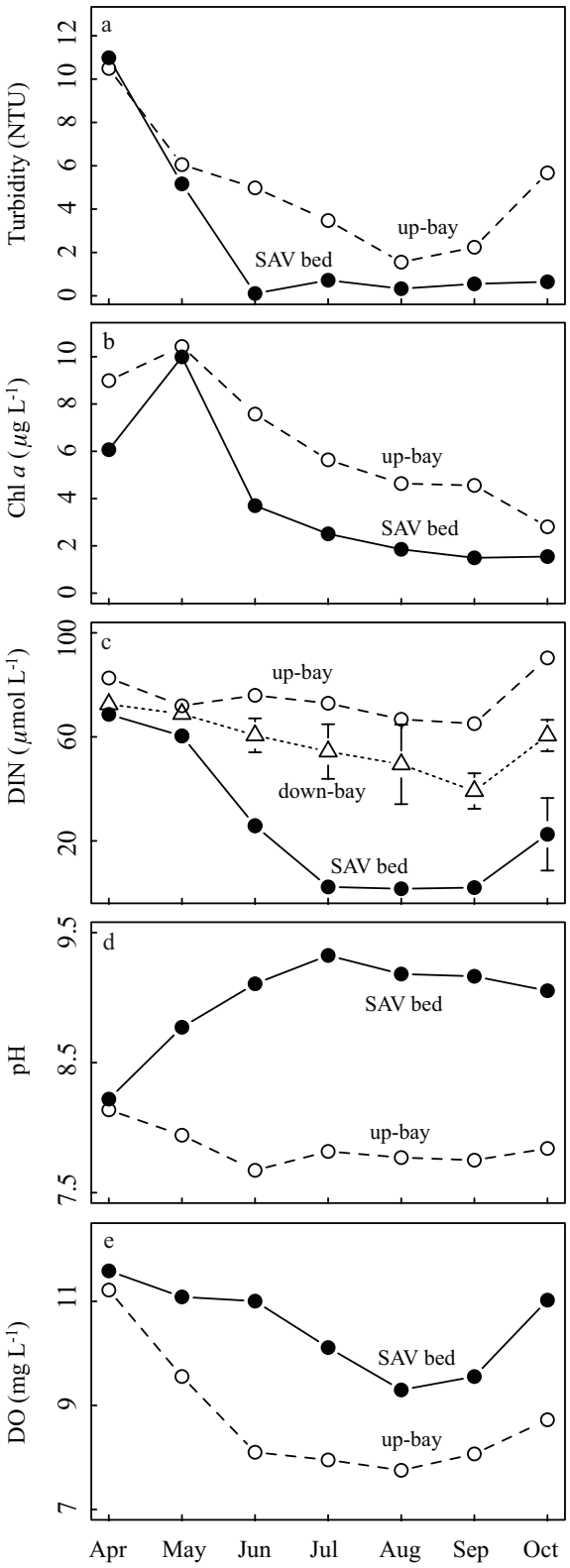
a
Turbidity (NTU)
0
2
4
6
8
10
12
up-bay
SAV bed
b
Chl a (μg L-1)
0
2
4
6
8
10
up-bay
SAV bed
c
DIN (μmol L-1)
20
60
100
up-bay
down-bay
SAV bed
d
pH
7.5
8.5
9.5
SAV bed
up-bay
e
DO (mg L-1)
7
9
11
SAV bed
up-bay
Apr
May
Jun
Jul
Aug
Sep
Oct

Chapter 3: Mechanisms of storm-related loss and resilience in a large submersed plant bed

Abstract

There is a growing emphasis on preserving ecological resilience, or a system's capacity to absorb or recover quickly from perturbations, particularly in vulnerable coastal regions. However, the factors that affect resilience to a given disturbance are not always clear and may be system-specific. We analyzed and synthesized time series datasets to explore how extreme events impacted a large system of submersed aquatic vegetation (SAV) in upper Chesapeake Bay and to identify and understand associated mechanisms of resilience. We found that physical removal of plants around the edge of the bed by high flows during a major flood event as well as subsequent wind-driven resuspension of newly deposited sediment and attendant light-limiting conditions were detrimental to the SAV bed. Conversely, it appears that the bed attenuated high flows sufficiently to prevent plant erosion at its inner core. The bed also attenuated wind-driven wave amplitude during seasonal peaks in plant biomass, thereby, decreasing sediment resuspension and increasing water clarity. In addition, clear water appeared to "spill over" into adjacent regions during ebb tide, improving the bed's capacity for renewal by creating more favorable growing conditions in areas where plant loss had occurred. These analyses demonstrate that positive feedback processes, whereby an SAV bed modifies its environment in ways that improve its own growth, likely serve as mechanisms of SAV resilience to flood

events. Although this work focuses on a specific system, the synthetic approach used here can be applied to any system for which routine monitoring data are available.

Introduction

Although intense storm events, such as hurricanes and floods, can restructure even the most robust ecosystems (Rappaport and Whitford 1999), estuaries and coasts have become particularly vulnerable over the past several decades due to degradation associated with chronic anthropogenic stressors, including eutrophication (Taylor et al. 1995; Carpenter et al. 1998; Cloern 2001), increasing hypoxia (Diaz and Rosenberg 2008), and climate change (Najjar et al. 2010). In addition, overfishing (Jackson et al. 2001) and habitat loss (Lotze et al. 2006) threaten the biodiversity that enriches estuaries (Duffy et al. 2015). Loss of seagrass and other submersed aquatic vegetation (SAV) beds is particularly troubling because of the valuable ecosystem services they provide (Costanza et al. 1997; Barbier et al. 2011), such as enhanced nutrient cycling (Caffrey and Kemp 1990), shoreline protection through attenuation of waves and currents (Koch 2001), and habitat and food provisioning for a host of important organisms (Orth et al. 2006; Ralph et al. 2013).

Coupled to threats from human-induced perturbations are projected increases in the frequency and intensity of extreme storm events (IPCC 2014), which leads to the question of whether these impaired ecosystems can withstand or rebound from such events (Cardoso et al. 2008; Grilo et al. 2011). To address this concern, we need to understand the underlying mechanisms that influence the resilience of a system, which we define here as its ability to resist or quickly recover from disturbances (Folke 2006).

Previous work has documented a suite of storm-related mechanisms of SAV loss and resilience. For example, extreme currents, waves, wind, and sediment loading during storm events can break, uproot, or bury plants (Preen et al. 1995; Cabaço et al. 2008) and pulses of suspended sediment or nutrients and subsequent algal blooms can degrade water clarity, thereby decreasing the amount of light available for plant photosynthesis (Moore et al. 1997; Longstaff and Dennison 1999). Meanwhile, plant diversity may buffer against total bed loss (Lande and Shannon 1996; Reusch et al. 2005), and a number physiological and morphological plant acclimation strategies allow for persistence despite decreased light availability (Longstaff and Dennison 1999; Maxwell et al. 2014). In addition, biophysical feedbacks, through which plant beds alter ambient physical conditions in ways that enhance their own growth, may also help plant beds absorb storm impacts (De Boer 2007). For example, healthy plant beds decrease shear stress exerted on the seabed, thereby reducing sediment resuspension and enhancing suspended particle deposition (Gambi et al. 1990; Granata et al. 2001; Peterson et al. 2004). SAV can also take up water column nutrients (McGlathery et al. 2007) and enhance nitrification and denitrification (Caffrey and Kemp 1990; Bartoli et al. 2008), thereby decreasing nutrient availability, and, in turn, algal biomass. In both cases, the plant bed, itself, acts to increase the amount of light reaching leaf surfaces (Gruber and Kemp 2010). If plant loss does occur, recovery potential depends on post-disturbance growing conditions and species-specific rates of clonal growth and seedling recruitment (Walker et al. 2006).

Despite this broad mechanistic understanding of plant responses to storm events, observed dynamics are often difficult to predict because drivers and responses are typically system-specific (Tomasko et al. 2005). For example, the environmental characteristics of a given location, including temperature and salinity, shape the composition of SAV species, which differ in their tolerance to any given stressor (Orth et al. 2010). In addition, local geographic features, such as bathymetry and proximity to tributaries can influence the relative magnitude of stressors that accompany storm events (Campbell and McKenzie 2004; Maxwell et al. 2014). Thus, detailed information about the biological and physical characteristics that are unique to a given system may help elucidate the mechanisms that drive its dynamics.

Here, we investigate the dynamics underlying the response of an SAV bed to storm events using an example from the tidal fresh upper Chesapeake Bay. In 2011, the U.S. mid-Atlantic region experienced two major back-to-back storms. The first, Hurricane Irene, traversed Maryland coastal waters on 27-28 August, producing sustained winds >15 m s^{-1} in the upper bay but relatively little rainfall. The second was a stalled tropical weather system (the remnants of Tropical Storm Lee) that generated near-record flooding for several days in early September throughout the watershed of the Susquehanna River, the largest tributary of Chesapeake Bay. Several years prior, SAV had rapidly recolonized a large shoal in an area of the upper bay, known as Susquehanna Flats, forming the largest SAV bed in the bay (Gurbisz and Kemp 2014). However, a substantial portion of the bed was lost by the fall of 2011 following the storms. In this paper, we analyze and synthesize publically available monitoring data, which we supplement with additional field samples and a simple

hydrodynamic model, to infer the mechanisms driving loss and resilience of this large, dense and continuous meadow to the 2011 storm events. Our goal is not only to interpret drivers of change in this system, but also to provide an example of how this type of synthetic analysis can be used to yield insights into ecosystem dynamics.

Methods

Study site

Susquehanna Flats, located in the tidal freshwater upper Chesapeake Bay, is a broad shoal (~1 m average depth) surrounded by deeper channels (ranging from ~2 to >6 m) and smaller shoals with narrow flanking beds along the west and north (Fig. 3.1). The shoals form a subaqueous delta of the Susquehanna River, which discharges, on average, 1100 m^3 s^{-1} at Conowingo Dam 16 km north of the river mouth. Historically, the Flats and the general region supported dense populations of native SAV, punctuated by a rapid increase and decrease of the non-native *Myriophyllum spicatum* in the late 1950s (Bayley et al. 1978). However, SAV populations experienced dramatic decline following record flooding that accompanied Tropical Storm Agnes in June 1972 (Bayley et al. 1978). Plant aerial cover and density on the Flats remained sparse until the early 2000's, when the trajectory of the large bed suddenly changed, with the bed attaining a size (~50 km^2) that may have mirrored its historic extent. This rapid recovery corresponded to enhanced water clarity during an extended dry period and modest long-term reductions in nutrient loading (Orth et al. 2010; Gurbisz and Kemp 2014). Co-dominant SAV species include wild celery (*Vallisneria americana*), water stargrass (*Heteranthera dubia*), Eurasian watermilfoil (*Myriophyllum spicatum*), and *Hydrilla verticillata*. In the

Chesapeake Bay region, these species attain peak biomass in the late summer, spreading asexually via rhizome elongation from established patches, or sexually from dispersing seeds. Many of these freshwater species are also capable of dispersing and establishing from fragments (Sculthorpe 1967).

Data sources and collection methods

We compiled a suite of publically available monitoring data that were collected between 2007-2013 at a range of sampling intervals by several agencies (Table 3.1). Our analyses focused on: (1) annual "peak" SAV area cover and density, (2) standard water quality variables measured by the Maryland Department of Natural Resources (MDNR) at sites located inside and outside of the SAV bed, including turbidity, chlorophyll *a* (Chl *a*), total suspended solids (TSS), and the vertical diffuse downwelling attenuation coefficient (K_d), and (3) external drivers of water quality, including river discharge (measured at Conowingo Dam) and wind speed (measured at the CBIBS buoy) (Fig. 3.1). Sample site locations were constrained by the fact that the monitoring data had already been collected independent of this project. We calculated SAV bed area weighted for plant density using a multiplier based on median values of crown density categories (<10%; 10-40%; 40-70%; 70-100%) to estimate an index of total plant biomass, which we call ''bed abundance'' (Moore et al. 2000; Rybicki and Landwehr 2007). All SAV data and analyses presented in the text are for the large central bed occupying the shoal; however, the maps and time series plot presented in Fig. 3.1 also include smaller flanking beds.

We supplemented these monitoring datasets with additional field samples following the two storms in 2012-2014. We collected replicate plant samples near the

water quality monitoring sensor inside the SAV bed at monthly intervals starting in July in 2012 and May in 2013 and ending in October each year. We also collected biomass samples in August 2014. Number of replicates varied (n=3-10) to account for patchy SAV cover early in the growing season (5-10 replicates) and relatively homogeneous plant cover during peak plant biomass (3 replicates). We sampled plant material to a sediment depth of ~20 cm with an acrylic corer (15.5 cm diameter, 35 cm long) and washed each sample to remove sediment. We separated samples into above- and below-ground living tissues and oven dried them at 60^{o}C to constant weight (~ 24-48 hours). To measure epiphytic material, we collected three replicates of ~10 cm apical sections for each of the dominant species present at each biomass sampling location by placing a plastic bag over individual shoots underwater to obtain a bag containing the plant segment, associated epiphytic material, and ambient water (Twilley et al. 1983). We washed any epiphytic material that had not already detached from plant leaves into the bag containing ambient water for each sample. We filtered the water onto pre-weighed 45 mm glass fiber filters, which we then dried and weighed. We also dried and weighed plant segments to obtain a measure of epiphyte mass per unit plant biomass.

We also measured key water quality variables at several additional stations when plant biomass was collected in 2012-2013 as well as along a transect in August 2014 four times during a tidal cycle starting in the middle of the plant bed and ending ~1.5 km south of the plant bed. For each sample, we passed a measured water volume through pre-weighed and ashed filters (45 mm GFF), which we then rinsed with deionized water to remove salts. We dried and weighed the filters to determine TSS

concentrations. We analyzed additional filters for Chl *a* concentrations. The filters were extracted in the dark with 90% acetone, sonicated, filtered, and read on a fluorometer (10-AU, Turner Designs). We measured dissolved inorganic nitrogen (DIN) and dissolved inorganic phosphorous (DIP) in the filtered water colorimetrically (Shimadzu UVmini-1240) (Parsons et al. 1984). In addition, we measured vertical profiles of photosynthetically active radiation (PAR) at select stations using a scalar (4pi) quantum sensor (Li-Cor) to compute K_d. We also measured turbidity, Chl *a*, dissolved O_2, pH, temperature, and salinity at each site using a YSI 6600 sensor package.

Statistical analyses

Our overall data analysis approach was to characterize how the system changed after the extreme weather events that occurred in 2011 and to determine relationships among physical, chemical, and biological variables to explore potential drivers of change in the system.

To describe change in properties of the plant bed, we tested for differences in monthly mean plant and epiphyte biomass between 2012, 2013, and 2014 using Student's *t*-test. We also tested whether plant loss based on annual aerial surveys flown in late summer (Orth et al. 2010) was related to location within the plant bed and April-September maximum river discharge. To conduct this analysis, we calculated distance from the edge of the large central plant bed as a measure of location within the bed. Using ArcGIS software, we created a grid of equally spaced (500 m) sampling points on top of each SAV bed polygon for years during which SAV loss occurred (2003, 2006, 2009, 2011) as well as each previous year. We

excluded 2012 because, although there was plant loss, maximum discharge was only 2860 m^3 s^{-1}. We suspect, as discussed below, that the effects of the 2011 flood event carried over into 2012 and caused additional plant loss despite relatively low flow conditions that year. We measured the distance from each point to the perimeter of the plant bed prior to loss and we recorded the points at which plant loss occurred between years. We then used logistic regression, which is commonly applied for binary (e.g., plant loss, no plant loss) response variables (Hosmer and Lemeshow 2000), to analyze the relationship between the probability of SAV loss, distance from the outer edge of the plant bed, and maximum river discharge. We used the Pearson χ^2 test to assess model fit, in which a significant *p*-value indicates evidence for lack of fit.

We investigated the magnitude of change in water quality across time and space by calculating monthly mean differences between paired (inside vs. outside the bed) continuous monitoring observations of turbidity and Chl *a*. We used bootstrap resampling (resamples=1000) with corrected accelerated percentiles (Efron 1987) to calculate 95% confidence intervals for the mean differences (confidence intervals that include 0 indicate no difference in means). We also used Student's t-test to test for differences in nutrient (DIN, DIP) concentrations inside and outside the plant bed before and after the 2011 flood event in both spring and summer.

We used ordinary least squares linear regression to model relationships among TSS, YSI Chl *a*, turbidity, and K_d with data from concurrent grab samples measured at or near established stations located inside and outside SAV bed. In addition, because K_d is only measured 2-4 times per month, we used these relationships to

estimate a more detailed K_d time series derived from continuous April-October Chl *a* and turbidity data spanning 2010 to 2013 at the SAV bed monitoring site. We then used this time series to calculate percent of surface light through the water (PLW) at 1 m depth using the Lambert-Beer relationship ($PLW=100*e^{-Kd*z}$, where z=water depth) to show how the light environment changed over time inside the SAV bed. To account for additional light attenuation by epiphytic material, we used monthly epiphyte data, where available, to estimate percent light at the leaf surface (PLL) according to the methods outlined in Kemp et al. (2004).

We also estimated net ecosystem production (NEP) at the same site using continuous oxygen, temperature, and wind speed data following previously published methods (Caffrey et al. 2014; Howarth et al. 2013). Because the plants appear to be the dominant organism at this site in terms of biomass, we assume that NEP is primarily a measure of SAV metabolic activity. We can, therefore, use NEP to illustrate shorter time-scale changes in bed productivity and investigate potential mechanisms of change in production, such as light limitation. We used linear mixed-effects models to test for differences in monthly mean NEP and the variables that affect NEP (viz., PLW, insolation, and temperature) between 2010, when the bed was at its pre-storm peak, and subsequent post-storm years (2011 to 2013). The model tested for differences in the intercept (i.e., mean) given year and month. Mixed models are preferential in this case over analysis of variance or time series methods because they can explicitly account for correlation structure that is inherent in time series data and also handle large spans of missing data (Pinheiro and Bates 2000), which occurred here during winter months when monitoring sensors were removed

from the water. We used bootstrap resampling to construct 95% confidence intervals for the differences in means (Efron 1987).

We also used a linear mixed-effects model to (1) explore the extent to which river discharge and wind speed were related to turbidity at inside and outside the SAV bed sites and (2) to test whether the effect of wind speed changed after the fall 2011 flood event. Log-transformed turbidity was the response variable. Fixed effects were river discharge and wind speed, and random effects included wind speed in relation to: (1) the 2011 flood event (before, after), (2) season (spring=April-June; summer=July-September), and (3) site (inside or outside the SAV bed). We initially also included wind direction; however its effect was not significant, so we excluded it from the model. We constructed a series of simplified models by excluding the random effects one at a time, and we compared these models to the full model to determine whether each variable improved model fit (Laird and Ware 1982). We then used bootstrap resampling to construct 95% confidence intervals for differences between relevant random coefficients (i.e., differences in the effect of wind speed on turbidity across sites and seasons before and after the flood event).

In all cases, we checked that raw data and model residuals met test assumptions (e.g., normality, independence, and heteroskedasticity), and we made relevant transformations (e.g., log transformation) as necessary.

Hydrodynamic model

We also developed a simple hydrodynamic model based on the same principles as the models of Fagherazzi et al. (2003) and Mariotti and Fagherazzi (2013) in an effort to strengthen our hypotheses and to provide surrogate data for

variables that we believed were important but missing. The model simulates flow and bottom stress in an idealized embayment system with geometry that is broadly based on the lower Susquehanna River and Susquehanna Flats region, assuming constant river flow interacting with a standing wave tide. It was developed for a constant width channel (6 m deep) adjacent to variable width subtidal flats (1.5 m deep) with and without SAV. The model solves first for the longitudinal flow changes required to conserve water volume as the tide rises and falls and as the subtidal flats widen and narrow. Flow is then partitioned between the channel and the flats to account for the differing influences of friction on flow over the channel and the shoal, assuming a slowly varying steady state shallow water balance between horizontal pressure gradient and vertical stress gradient. In the absence of SAV, the bottom drag coefficient is the same everywhere. In the presence of SAV over the flats, the drag is increased following the methods of Chen et al. (2007), with a user-specified ratio between the channel and flats drag coefficients simulating the effects of different plant densities. Finally, the lateral flows between channel and flats are adjusted to re-establish volume conservation. The fraction of the drag responsible for sediment transport (the "skin friction") is calculated following the methods of Chen et al. (2007) as well. More model details are available in Appendix I.

We used the open source software package R to carry out statistical analyses, run the model, and generate plots.

Results

Density-weighted plant cover ("bed abundance") of the large central bed decreased by 43% between 2010 and 2011, then by another 20% in 2012, followed by

slight (~1%) recovery in 2013 (Fig. 3.2). Logistic regression showed that the probability of plant loss decreased with distance into the plant bed and increased as river discharge increased (Table 3.2). There was also a significant positive interaction between distance into the plant bed and river discharge. In other words, most plant loss occurred around the outer edge of the plant bed, and higher flows led to greater overall plant loss (Fig. 3.3a); however, the proportion of loss at any given distance from the edge of the bed increased nonlinearly as river discharge increased (Fig 3b). In addition, plant biomass in August and September was significantly greater in 2013 than 2012 (Table 3.3, Fig. 3.4a) and possibly also in August 2014 compared to 2012 ($p=0.05$). There was no significant difference between biomass in August 2013 and 2014 nor were there any significant differences in below-ground biomass between years. August, September, and October epiphyte biomass levels were significantly less in 2013 than 2012 (Fig. 3.4b).

NEP was lower during the spring of 2011-2013 and greater in summer of 2012-2013 compared to NEP calculated before the storm events in 2010, as indicated by 95% confidence intervals for differences in monthly means (i.e., mixed model intercepts) that did not include 0 (Fig. 3.5a and 5e). Peak NEP occurred 1 month later in 2011 compared to 2010 and 2 months later in 2012 and 2013. PLW was generally lower after the storm events compared to 2010 (Fig. 3.5b and 5f) and, for years when epiphyte data were collected (2012 and 2013), epiphyte cover increased PLW by 15%. However, despite overall lower light levels compared to 2010, PLW during the summer of 2011-2013 and PLL in 2013 still exceeded 30% for a portion of the growing season. There were no differences in insolation after the flood event (Fig.

3.5d and 3.5h) and, although temperature was different from pre-storm means during some months, these differences did not appear to systematically coincide with differences in NEP (Fig. 3.5g-h).

In general, monthly mean turbidity before 2011 was lower inside the plant bed compared to a nearby monitoring station located outside the plant bed (Fig. 3.6a). For several months following the fall 2011 storm events and into spring of 2012, turbidity was greater inside the plant bed by ~10-30 turbidity units. The difference was much less (0 to 1 NTU) during late summer-early fall 2012. Turbidity was again greater inside the plant bed by ~10 to 15 NTU in spring 2013 but then it decreased by ~5 NTU inside the plant bed in summer 2013. Monthly mean water column Chl *a* was also consistently lower inside the plant bed by ~3-7 $\mu g\ l^{-1}$ before 2011 (Fig. 3.6b). Chl *a* was generally lower inside the plant bed in spring and summer of 2011 as well but by only ~1 $\mu g\ l^{-1}$. However, in spring and early summer of 2012 and May of 2013, Chl *a* was ~ 5-10 $\mu g\ l^{-1}$ greater inside the plant bed. Seasonal peaks in Chl *a* after the flood event appear to lag those of turbidity by ~1-2 months. Regression analysis showed that TSS (but not Chl *a*) was a statistically significant predictor of turbidity (Fig. 3.7). Together, turbidity and Chl *a* measured by monitoring sondes predicted K_d by the following formula: $K_d = 0.95 + 0.08 * \text{turbidity} + 0.03 * \text{Chl } a$ ($p < 0.001$, $R^2 = 0.74$). Mean summer DIN increased from 0.62 ± 0.29 to 13.63 ± 4.73 $\mu mol\ l^{-1}$ inside the plant bed; however this difference was not statistically different [t(5.12)=-1.87, p=0.12], nor were any other comparisons of DIN or DIP before and after the flood event.

Visual examination of turbidity, river discharge, and wind speed time series suggests that both river discharge and wind had an effect on turbidity but the wind effect increased inside the plant bed after the flood event (Fig. 3.8). For example, although Hurricane Irene generated high sustained winds, turbidity only increased marginally both inside and outside the plant bed. During the flood event, however, turbidity increased dramatically, exceeding 600 NTU at both sites. After the flood, turbidity was, at times, more than 250 NTU greater inside the plant bed compared to the monitoring site outside the bed, particularly during wind events. Results from the linear mixed model support these inferences. Susquehanna River discharge and wind speed each had a significant positive effect on turbidity (Table 3.4). Including timing in relation to the flood event, site, and season improved model fit, meaning that these variables modified the effect of wind speed on turbidity. Specifically, the effect of wind speed on turbidity increased inside the bed after the flood event (95% confidence interval, CI, for the difference in coefficients=0.0005, 0.0019), the effect was less in the summer compared to the spring (CI=-0.0023, -0.0006), and the effect in the spring was greater inside the bed compared to outside the bed (CI=0.0012, 0.0022).

Water quality transect data show that by August 2014, turbidity, and thus suspended particle concentrations, were generally lower inside the plant bed (Fig. 3.9a-c). At high tide, turbidity inside the bed slightly increased starting around 500 m from the edge of the bed (Fig 3.9b). However, at low tide, turbidity was consistently low to the edge of the bed and slightly lower for ~800 km beyond the outer edge of the bed compared to values measured at the same sites at high tide (Fig. 3.9c). Lower

turbidity around the southern outer edge of the bed is consistent with the apparent clear water plume emanating from the bed (Fig. 3.9a). PLW, calculated using depth at mean water and an estimate of K_d derived from turbidity and Chl *a* data collected at transect sites, was highest in the inner core of the plant bed, slightly lower around the inner and outer edge of the bed, and lower around the southern end of the transect, where the water was both deeper and more turbid (Fig. 3.9 d-e).

Model simulations for cases with and without the SAV bed on the flats with flow based on peak Susquehanna River flow in September 2011 (20,000 m^3 s^{-1}) at maximum ebb tide show that even in the absence of SAV, the flow and bottom stress over the flats were much lower than in the channel (Fig. 3.10). Minimum flows and bottom stresses generally occurred in the wide central region of the shoal, intermediate values occurred in the northern and southern narrow regions of the shoal, and the greatest values occurred in the northern river channel and the southern exit channel. When SAV were present, they greatly increased the total drag coefficient over the shoal, which greatly decreased flow over the shoal and enhanced flow in the channel (i.e., the flow pattern without SAV is greatly exaggerated with SAV). As a result, skin friction (the stress acting on the bottom sediments) was greatly reduced relative to the no SAV case. Without SAV, the minimum and maximum bottom stress values on the shoal were 1.4 and 3.2 Pa, respectively, but in the presence of SAV, skin friction on the shoal varied between 0.1-0.3 Pa. It is important to note that the total stress over the shoal with SAV remains similar to the no SAV case; the difference is that the drag of the plants dominates the total stress in

the SAV case, while the drag of bottom sediments dominates the total stress in the no SAV case.

Discussion

In contrast to the near-complete SAV loss that resulted from Tropical Storm Agnes in 1972, the persistence of large portions of the bed on Susquehanna Flats and its beginnings of recovery in 2013 following two severe storms in August and September 2011 demonstrates its resilience to a strong perturbation. Our analysis of a number of monitoring parameters, additional field studies, and modeling suggests that several critical biophysical interactions between the bed and its environment coupled to the physical characteristics of the region allowed the bed to survive and start to recover, particularly after the September 2011 flood event, which produced near-record flow and sediment loading rates.

Resistance to sediment loading

While poor water clarity associated with particle deposition and subsequent resuspension likely caused some plant loss and decreased plant production during and after the September 2011 flood event, it appears that reduced sediment resuspension during periods of peak biomass in 2012 and 2013 led to improved water clarity. We argue that this positive feedback between the plant bed and suspended particle concentrations served as a mechanism of bed resilience to high rates of sediment loading generated by the flood.

Before September 2011, turbidity and planktonic Chl *a* were lower inside the plant bed (Fig. 3.5a and 3.5b), a pattern consistent with previous studies (Moore

2004; Gruber and Kemp 2010; van der Heide et al. 2011). In contrast, higher turbidity inside the plant bed during the months immediately after the flood event in September 2011 and the subsequent two springs suggests that the flood had a lingering effect on suspended particle concentrations. Elevated Chl *a* inside the plant bed during late spring and early summer in 2012 and 2013 and greater epiphyte biomass in 2012 compared to 2013 (Fig. 3.4b, Table 3.3) imply effects on algal production as well. Because K_d, which is indicative of the amount of light available to plants, was related to both turbidity and planktonic Chl *a*, greater than normal values of these variables inside the plant bed after the flood event could have negatively affected the plant bed through light limitation.

Although the plants, on average, received enough light to survive through 2011-2013, as April-October median percent light through the water (PLW) and percent light at the leaf surface (PLL) at 1 m depth were > 13% and 9%, respectively (Dennison et al. 1993; Kemp et al. 2004), episodic extremes in turbidity that were not captured by data aggregated across the growing season could have caused plant mortality, particularly around the deeper outside and southern edges of the SAV bed (Moore et al. 1997; Longstaff and Dennison 1999). For example, PLW was <3%, a lethal light level for most freshwater macrophytes (Middleboe and Markager 1997), for ~ 1 week during the September 2011 flood event and for periods of 1 to several days throughout the following spring (Fig. 3.5b). In addition, light limitation could have altered plant phenology and limited plant production. For instance, PLW was <30%, the threshold light level below which production in these plants generally decreases (Blackburn et al. 1961; Harley and Findlay 1994), until July-August in

2012 and 2013. Light limitation early in the growing season could, thus, account for the apparent delay of annual peak production (Fig. 3.5a). Furthermore, because summer PLW and PLL were generally higher in 2013 compared to 2012, lower production rates associated with light limitation may also be responsible for lower biomass in 2012.

However, despite unusually poor springtime water clarity inside the plant bed after the flood event, light conditions improved by late summer in 2012 and 2013. Concurrent temporal patterns in plant biomass, turbidity, and Chl *a* suggest that the bed, itself, caused this improvement. For example, turbidity and Chl *a* decreased (Fig. 3.6) and PLW increased inside compared to outside the plant bed by August in 2012 and July in 2013 (Fig. 3.5c). These patterns coincided with increases in monthly plant biomass to 55 g m^{-2} and 41 g m^{-2} respectively (Fig. 3.4), suggesting that, after accumulating sufficient plant volume, the bed improved water quality and increased light availability, thereby allowing for increased plant production during the summer months.

Our analyses indicate that greater than usual wind-driven resuspension in the absence of plants and reduced resuspension when plants were present generated the observed patterns in turbidity. Because turbidity was related to both TSS (Fig. 3.7) and wind speed (Table 3.4), we can infer that higher wind speeds, in general, led to greater concentrations of suspended particles. The increased effect of wind on turbidity inside the plant bed during the spring after the flood (Fig. 3.8) further suggests that the September 2011 flood event created an environment on the shoal in which bottom sediments were highly resuspendible, probably due to substantial

deposition (Palinkas et al. 2013) of loose, unconsolidated sediment (Ward 1985; Sanford 1994; Sanford 2008) and creation of open scour channels by high flows (Luhar et al. 2008). Subsequent wind events then generated turbid conditions through resuspension by wind-forced waves, particularly during the spring when plants had yet to germinate or had just begun to emerge. However, the diminished effect of wind on turbidity during the summer when plant biomass was high (Fig. 3.4) implies a bed effect on turbidity. In general, the vertical transfer of turbulent stress to the seabed and, thus, sediment resuspension decreases when canopy drag surpasses a critical threshold due to increasing plant height and density (Ward et al. 1984; Luhar et al. 2008, Gruber et al. 2011). Therefore, it appears that once the bed reached a critical biomass, canopy drag dissipated wind-driven wave energy and stabilized the seabed, thereby allowing more light to reach the leaf surface to support photosynthesis (De Boer 2007; Chen et al. 2007).

Similar patterns in Chl *a* (Figs. 3.4b and 3.6b) and higher epiphyte biomass in the summer of 2012 compared to 2013 suggest that increased inputs of particle-bound nutrients and subsequent resuspension events may also be linked to greater than normal planktonic and epiphytic algae production in 2012 and early 2013. Although differences in DIN and DIP before and after the flood event were not statistically significant, the increase in summer DIN inside the plant bed, although not statistically significant, qualitatively suggests that nitrogen concentrations were greater than normal after 2011. Furthermore, differences in dissolved nutrients in response to increased inputs may not have been be detected because of rapid nutrient assimilation associated with algal and plant growth (Malone et al. 1996). We infer that dissolved

nutrient loading during the flood event did not likely cause elevated nutrient concentrations in the bed because water residence time in the upper Chesapeake Bay during high flow events is relatively short. As a result, dissolved nutrients generally pass through the region with little assimilation (Schubel and Pritchard 1986). However, decomposition of particulate organic nitrogen and desorption of particulate phosphorous can increase concentrations of porewater ammonium and phosphate (e.g., Kemp et al. 1984, Romero et al. 2006) and sloughing of organic epiphytic material during high flows can further add to the sediment nutrient pool (Fonseca et al. 1982). Resuspension events can enhance the rate of nutrient flux from the seabed to the water column through release of porewater solutes (Tengberg et al. 2003; Ståhlberg et al. 2006) and, thus, fuel algal growth. Conversely, the decrease in Chl *a* during the summer of 2012 and 2013 could be linked to decreased sediment resuspension and associated dissolved nutrient flux to the water column (Madsen et al. 2001). Furthermore, plant nutrient uptake (Cornelisen and Thomas 2006) and enhanced denitrification (Caffrey and Kemp 1990; Risgaard-Petersen et al. 2000) with increased water residence time inside the plant bed (Nixon et al. 1996; Lara et al. 2012) may also have decreased nutrient concentrations and, therefore, algal production.

Resistance to high flows

River discharge during the 2011 flood event exceeded 20,000 $m^3 s^{-1}$, a value surpassed only three times previously since monitoring of Susquehanna River flow began in the late 1800's. While mechanical plant breakage, dislodgement, or scour and associated uprooting due to high flows likely caused substantial plant loss (Preen

et al. 1995; Fonseca and Bell 1998), our analyses and model simulations suggest that the bed was also resilient to high flows by attenuating currents and shunting flow around the shoal and into surrounding channels.

The amount of force required to break or dislodge plants is highly variable depending on SAV species and sediment composition (Schutten et al. 2005), making the relative role of these processes difficult to assess. Our model simulations do suggest, however, that sediment scour, root exposure, and associated plant uprooting could have occurred, perhaps in conjunction with breakage or dislodging. Generally, bottom shear stresses that are greater than ~0.1 to 0.3 Pa result in sediment movement at a rate that depends on the difference between the applied stress and the threshold stress (Allen 1985). When modeled river flow was 20,000 m^3 s^{-1}, bottom stresses across a substantial area of the southern region of the flats exceeded this threshold (Fig. 3.10d), indicating incipient scour. In addition, although the modeled bottom stresses responsible for sediment transport were relatively small, the total drag forces were quite large, comparable to shear stresses simulated in our "no-SAV" scenario (Fig. 3.10b). These total stresses (about 3 Pa) were borne primarily by the plants, which might have been selectively broken or dislodged. Once thinning of the plant bed started for any reason, the system would tend towards unstable behavior. Any local loss of the protective SAV barrier would lead to greater local sediment scour, which, in turn, would lead to further plant loss, and so on. It is, therefore, possible that unstable plant loss and sediment scour associated with strong currents may have resulted in uprooting that caused large areas of plant loss during the flood. The increases in velocity and bottom stress were likely focused in the southern region of

the model domain both because of the constriction in width, and because maximum ebb tidal currents increase from north to south to conserve tidal volume transport. In addition, when the ebbing tide combined with southward river flow, velocity further accelerated in the southern region, thereby increasing bottom stress.

On the other hand, our results also suggest that the plant bed attenuated flow during the flood event, as shown by relationships between the spatial distribution of plant loss and river discharge during high flow years. For example, the decreasing probability of plant loss with increasing distance from the outer edge of the plant bed (Fig. 3.3a) implies that inner regions of the bed were protected during flood events. The analysis also showed that as river discharge increased, the probability of loss at any given distance into the bed increased, suggesting that at higher flow rates, this protective capacity decreases. For these reasons, larger plant beds are generally more resilient to storm events because their inner core is protected (Gruber et al. 2011; Orth et al. 2012).

Model simulations support the idea the inner bed was sheltered from high flows. Bottom stresses on the shoal for the case without SAV were well above the threshold required to erode and transport sandy sediments (Figs. 3.10a and 3.10b); however, bottom stresses were near or below this threshold when SAV were present, particularly in the widest part of the shoal (Figs. 3.10c and 3.10d). This occurs because, in addition to attenuating turbulence in the vertical dimension, canopy drag also dissipates the horizontal transfer of momentum from the leading edge toward the center of a plant bed (Luhar et al. 2008). Furthermore, the plant bed diverts flow from the shoal into the channel, resulting in decreased velocities on the shoal and

acceleration of currents in the channel (Gambi et al. 1990; Chen et al. 2007; Luhar and Nepf 2013).

Recovery following loss

In addition to serving as a mechanism of resistance to disturbance, we suggest that positive feedback processes are also important for this bed's recovery. The region of higher turbidity around the edge of the plant bed during high tide (Fig. 3.9b) suggests that particles are transported into the bed with the rising tide. However, the large area of low turbidity outside the bed during low (Fig. 3.9c) tide implies that clear water drains out of the bed with the ebbing tide, creating the clear water "plume" evident in the aerial photograph (Fig. 3.9a). Because PLW inside the plant bed and in the plume region is greater than the minimum light required for plant survival (13% of surface irradiance), recovery in this region is likely limited by the rate at which the plants can expand clonally or establish satellite colonies from fragments and seedlings. Light levels below this threshold at sites outside of the plume suggest that inadequate light could limit recovery in this region. However, if we use turbidity and Chl *a* data from the plume region to calculate PLW at the southern most transect sites (1.5 m deep), light at the bottom would be 17%, exceeding the minimum threshold. If the plume of clear water expands into deeper water as the bed expands southward, this process of local a feedback effect "spilling over" into adjacent regions could be a key mechanism for the bed's recovery to its pre-storm extent.

Inferences about recent and historical weather events

Although sediment scour and poor water clarity associated with the September 2011 flood event were likely the primary drivers of plant loss, it is worth noting that decreased plant production in spring 2011 compared to 2010 (Fig. 3.5a-b) may have weakened the plant bed's ability to withstand the flood. With precipitation in March 2011 greater than six times above average, elevated turbidity that spring (Fig. 3.6a) likely decreased PLW (Fig. 3.5d), and, thus, also plant production (Alcoverro et al. 1999; Longstaff and Dennison 1999). In addition, below average water temperatures in April 2011 could have delayed plant germination and further decreased plant production (McFarland and Shafer 2008), rendering the bed more susceptible to loss in the face of additional turbidity pulses (Cabello-Pasini et al. 2002; Yaakub et al. 2014; Fraser et al. 2014).

In addition, the inferences developed herein may help explain historical patterns of SAV abundance. In 1972, precipitation in the Susquehanna River watershed during Tropical Storm Agnes generated a 100- to 200-year flood that destroyed nearly the entire Susquehanna Flats SAV bed, with only sparse regrowth for several decades (Bayley et al. 1978; Kemp et al. 2005; Gurbisz and Kemp 2014). Based on the observed effects of the 2011 flood event, the magnitude of flooding likely exceeded the capacity of the bed to attenuate flow in 1972, leading to catastrophic plant loss. In fact, in a model run with comparable river flow (30,000 m^3 s^{-1}), bottom stresses on the vegetated shoal ranged from 0.3 to 0.7 Pa (not shown), values that lie within or surpass the threshold range for sediment motion. It is also possible that the 1972 bed was less dense than the 2011 bed, considering its trajectory

of decline prior to Tropical Storm Agnes (Bayley et al. 1978; Kemp et al. 2005), and, therefore, less capable of attenuating and diverting flows. The seasonal timing of the 1972 storm also likely exacerbated bed damage because storms that occur near peak plant biomass are generally more destructive to SAV than those that occur after (Wang and Linker 2005). With presumably more sediment deposition and plant loss compared to the 2011 flood, resuspension in the absence of vegetation likely generated turbid conditions for an extended period of time, leading to a self-reinforcing bare-sediment state (Scheffer et al. 1993).

Concluding comments

These analyses suggest that the ultimate effect of a flood event on submersed plant populations depends on the balance between mechanisms of plant loss and resilience, which involve complex biological, physical, and chemical interactions between a plant bed and its environment. In this case, although there was substantial SAV loss in response to a major flood event, the system was also remarkably resilient, apparently owing to strong biophysical feedback processes carried out by a large, dense, healthy SAV bed. Future work should aim to quantify threshold river flow rates beyond which plant beds cannot recover as well as the extent to which bed size and previous disturbances affect the tipping point. Whether genetic diversity interacts with these processes to enhance resilience is another important focus for additional research.

This paper also demonstrates how synthetic analysis of diverse datasets can be used to address ecological questions (Carpenter et al. 2009). We followed synthesis methods similar to those outlined in Kemp and Boynton (2011). For example, initial

plots of data across time and space allowed for visualization of relevant patterns and trends. This preliminary information was then used to guide statistical approaches for more in-depth analysis. In addition, a simulation model was helpful for analyzing mechanisms and providing surrogates for missing but important variables. While alone, individual datasets may not be particularly meaningful, together and in the context of theory and other studies, they can be used to construct compelling explanatory models for ecological phenomena.

Tables

Table 3.1 Summary of publically available data sources

Data description	Source	Duration	Frequency
Water quality	Maryland Department of Natural Resources http://mddnr.chesapeakebay.net/eyesonthebay/	2007-present	4-6 h^{-1}
SAV cover	Orth et al. http://web.vims.edu/bio/sav/index.html	1984-present	1 y^{-1}
River discharge	United States Geologic Survey http://waterdata.usgs.gov/usa/nwis/uv?01578310	1967-present	1 h^{-1}
Meteorological	Chesapeake Bay Interpretive Buoy System http://buoybay.noaa.gov/locations/susquehanna	2008-present	4-6 h^{-1}

Table 3.2 Logistic regression results showing distance from the outer edge of the plant bed and April-September mean river discharge as predictors of the probability of plant loss. The non-significnant *p* value for overall model fit shows that there is no evidence for lack of fit. Bold: $p<0.05$

Predictor	Coefficient	SE	*Z*	*p*
Constant	-3.40	0.96	-3.59	**<0.001**
Distance	$9.2\text{x}10^{-3}$	$3.3\text{x}10^{-3}$	-2.83	**<0.01**
Discharge	$2.0\text{x}10^{-3}$	$5.1\text{x}10^{-4}$	3.91	**<0.001**
Distance:discharge	$3.6\text{x}10^{-6}$	$1.6\text{x}10^{-6}$	2.28	**<0.05**
Overall model fit		χ^2	df	*p*
Hosmer-Lemeshow test		8.14	8	0.4200

Table 3.3 Differences in monthly mean plant and epiphyte biomass between years. Student's *t*-test was used to test for differences in June-October above and belowground plant biomass as well as epiphyte biomass between 2012-2013, 2012-2014 and 2013-2014. Only statistically significant results are shown. Bold: $p \leq 0.05$

Sample dates	*t*	df	*p*	2012 mean	2012 SD	2013 mean	2013 SD
Above ground plant biomass							
August	-2.54	7	**<0.05**	60.69	14.36	146.10	93.63
September	-2.42	12	**<0.05**	71.68	48.01	195.89	149.97
Epiphyte biomass							
August	2.21	14	**<0.05**	2.12	3.41	0.18	0.19
Septmeber	2.54	26	**<0.05**	0.91	0.75	0.42	0.37
October	4.11	20	**<0.01**	1.02	0.78	0.23	0.18

Table 3.4 Relationships between environmental variables and turbidity, as shown by linear mixed effects regression models. Fixed effect predictor variables include Susquehanna River discharge and wind speed. Random effects include timing in relation to the September 2011 flood (before or after), site (inside or outside the SAV bed), season (spring=April, May, June; summer=July, August, September). Random effects were sequentially removed to investigate whether each significantly affected model fit. Model improvement by including first order autoregressive (AR1) correlation structure is also demonstrated

Fixed effect parameter estimates

Predictor	Estimate	SE	*t*	*p*
Discharge	0.00020	0.00002	9.854	<0.0001
Wind speed	0.00056	0.00027	2.091	<0.05

Effect of random terms

Model	*df*	*AIC*	*BIC*	Log-likelihood	Likelihood ratio	*p* value
Maximal	13	189	253	-81		
Maximal - site	10	460	509	-220	277.2	<0.0001
Maximal - timing	10	584	633	-282	401.1	<0.0001
Maximal - season	10	566	616	-273	383.4	<0.0001
Maximal - slope (wind speed)	7	242	276	-114	65.0	<0.0001
Maximal + AR1	14	-605	-536	317	795.8	<0.0001

Figure captions

Fig. 3.1 The study site, Susquehanna Flats, is located in upper Chesapeake Bay near the mouth of the Susquehanna River. Water quality and plant samples were collected inside and outside the SAV bed. Wind data came from the Chesapeake Bay Interpretive Buoy System (CBIBS) buoy, and river flow data was measured at the Conowingo Dam. The SAV bed, as indicated by the dark gray shape, was drawn based on aerial photographs taken in 2010

Fig. 3.2 (a) Time series of SAV bed abundance (1958-2013). Data from 1958-1983 (open circles) represent relative SAV abundance data derived from field sampling by Bayley et al. 1978 and the Maryland Department of Natural Resources (*unpubl.*). Data for 1984-2013 (solid circles) represent SAV abundance data derived from aerial imagery. We concatenated the time series visually to the best of our ability; however it is important to note that they are based on different measurement scales. (b) Maps of Susquehanna Flats showing SAV spatial distribution and density cover (shades of grey) before (2010), immediately after the September 2011 flood event (2011), and two years following the event (2012-2013)

Fig. 3.3 Effect of the interaction between distance from the edge of the plant bed and April-September mean river discharge on probability of SAV loss. Trend lines were determined by logistic regression analysis

Fig. 3.4 2012-2014 monthly (a) plant and (b) epiphyte biomass. Asterisks indicate a significant difference at the 0.05 (*) and 0.01 (**) levels

Fig. 3.5 (a-d) Time series for daily net ecosystem production (NEP) and variables that may control NEP. (e-h) Differences between 2010 and 2011-2013 monthly means for the same variables with 95% confidence intervals, which were calculated by bootstrapping linear mixed effect model coefficients. Intervals that include 0 indicate no difference

Fig. 3.6 Mean monthly differences $\pm$ 95% confidence interval between measurements made inside and outside the plant bed (i.e., daily measurements at the outside the bed site were subtracted from those made inside the bed and those daily differences were averaged for each month) for (a) turbidity and (b) Chl *a*

Fig. 3.7 Relationship between total suspended solids (TSS) and turbidity

Fig. 3.8 Time series for (a) turbidity measured inside (gray) and outside (black) the plant bed, (b) 2-day moving average of Susquehanna River discharge measured ~16 km upriver at Conowingo Dam, and (c) wind velocity measured at the mouth of the Susquehanna River and smoothed using a 13-hour moving average

Fig. 3.9 (a) Aerial photo of the SAV bed in 2013 (shaded light gray), the "plume" of clear water emanating from its southern edge, and water quality transect sampling

sites (black dots). (b-c) Turbidity data for high and low tide, respectively. Dashed circles indicate areas of increased turbidity in the inner edge region at high tide and lower turbidity immediately outside the plant bed at low tide. (d) Mean water depth at transect sites. (e) Percent light through the water (PLW) calculated using turbidity and Chl *a* (to estimate K_D) and depth data. 13%, indicated by the dashed line, is the minimum light requirement for upper Bay SAV

Fig. 3.10 Hydrodynamic model output showing water velocity (left) and bottom stress (right) in the central channel (6 m deep) and later shoals (1.5 m) at peak ebb tide with river flow comparable to the September 2011 flood (20,000 m^3 s^{-1}). The top panels represent the case without SAV on the shoal and the bottom panels are for the case with SAV

Figures

Fig. 3.1

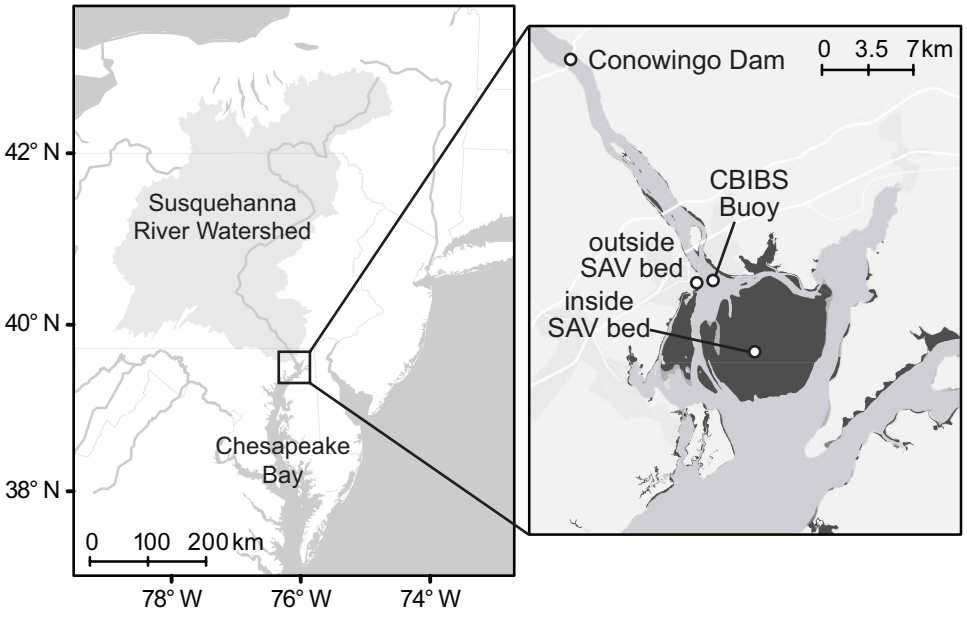

Fig. 3.2

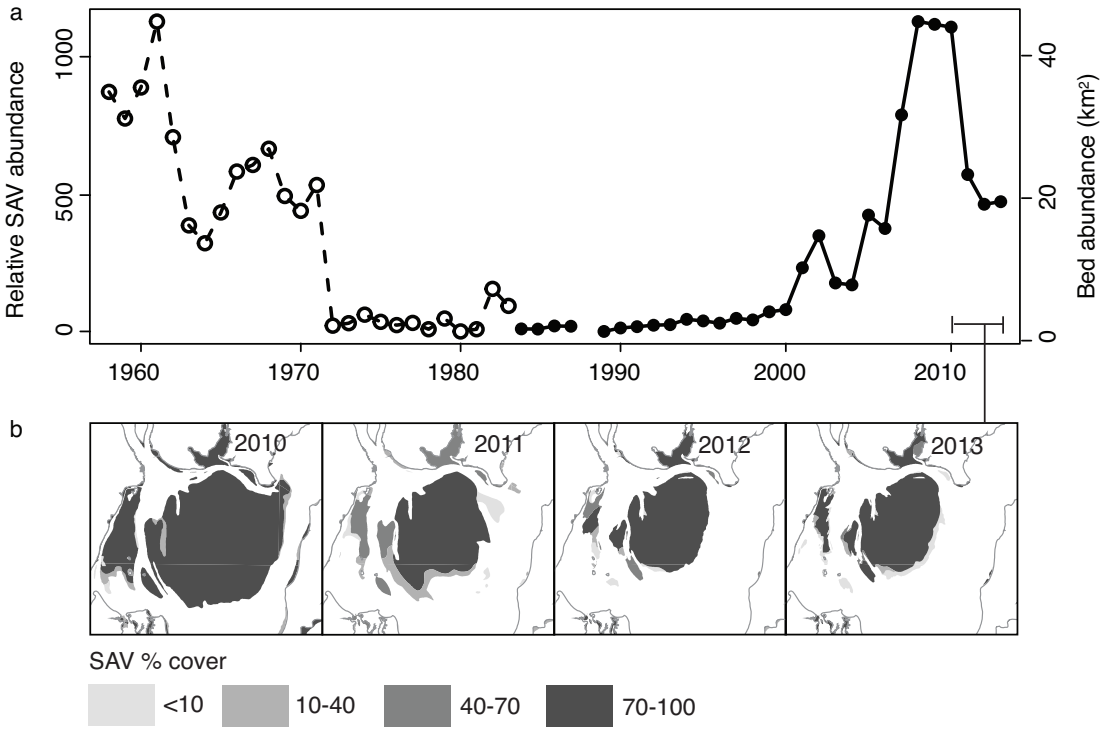
a
Relative SAV abundance
0
500
1000
Bed abundance (km²)
0
20
40
1960
1970
1980
1990
2000
2010
b
2010
2011
2012
2013
SAV % cover
<10
10-40
40-70
70-100

Fig. 3.3

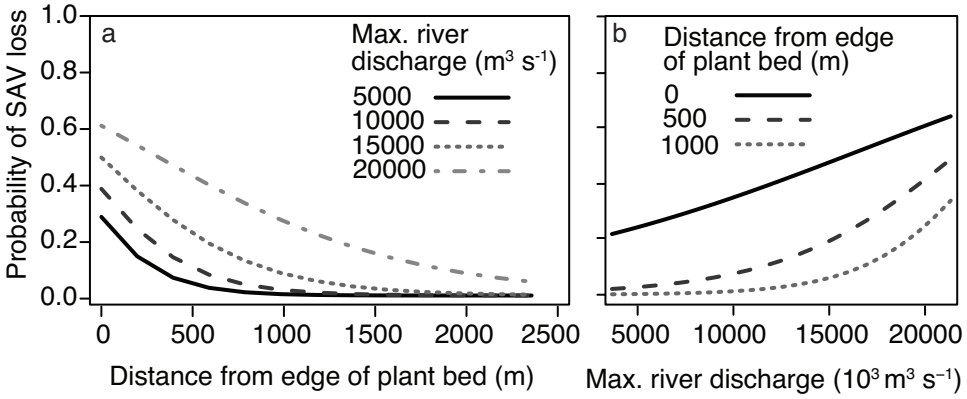
Probability of SAV loss
1.0
0.8
0.6
0.4
0.2
0.0
a
Max. river discharge (m³ s⁻¹)
5000
10000
15000
20000
0
500
1000
1500
2000
2500
Distance from edge of plant bed (m)
b
Distance from edge of plant bed (m)
0
500
1000
5000
10000
15000
20000
Max. river discharge (10³ m³ s⁻¹)

Fig. 3.4

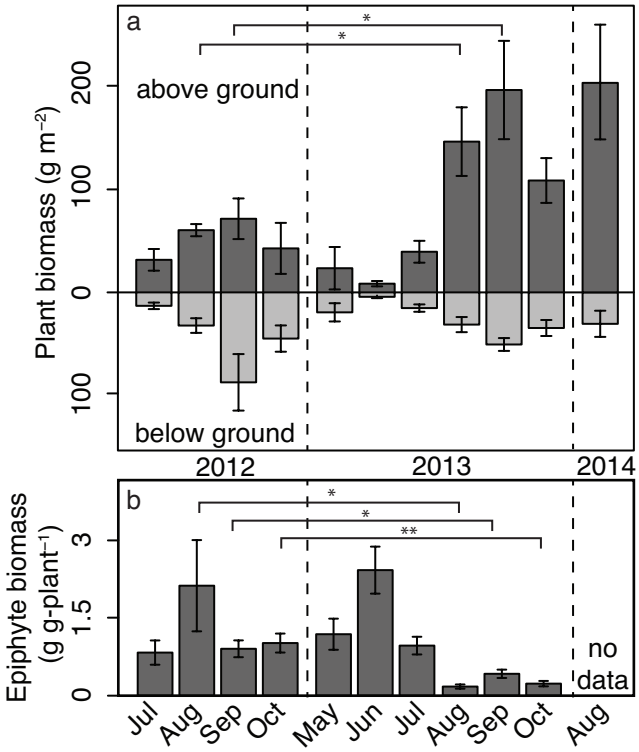
a
above ground
below ground
Plant biomass (g m⁻²)
200
100
0
100
2012
2013
2014
b
Epiphyte biomass (g g-plant⁻¹)
3
1.5
0
no data
Jul
Aug
Sep
Oct
May
Jun
Jul
Aug
Sep
Oct
Aug

Fig. 3.5

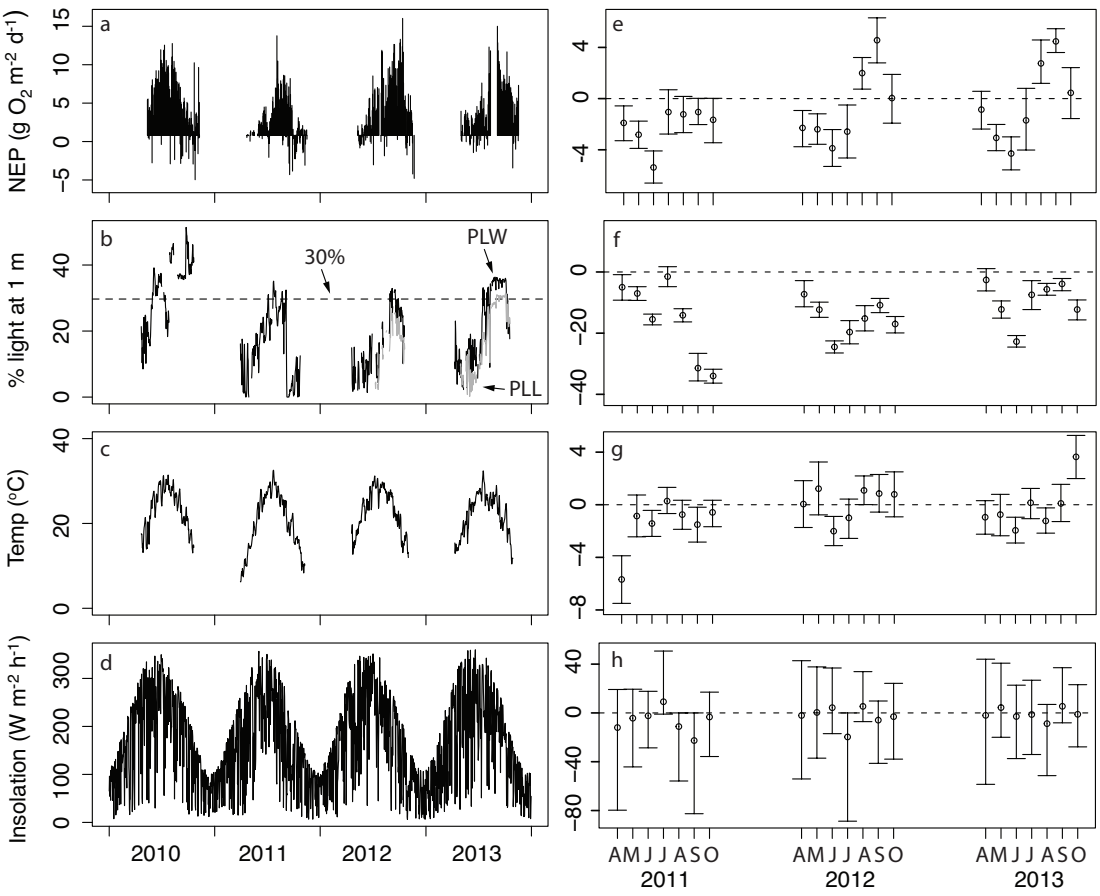
a
b
c
d
e
f
g
h
NEP (g O_2 m^{-2} d^{-1})
% light at 1 m
Temp (°C)
Insolation (W m^{-2} h^{-1})
30%
PLW
PLL
2010
2011
2012
2013
A M J J A S O

Fig. 3.6

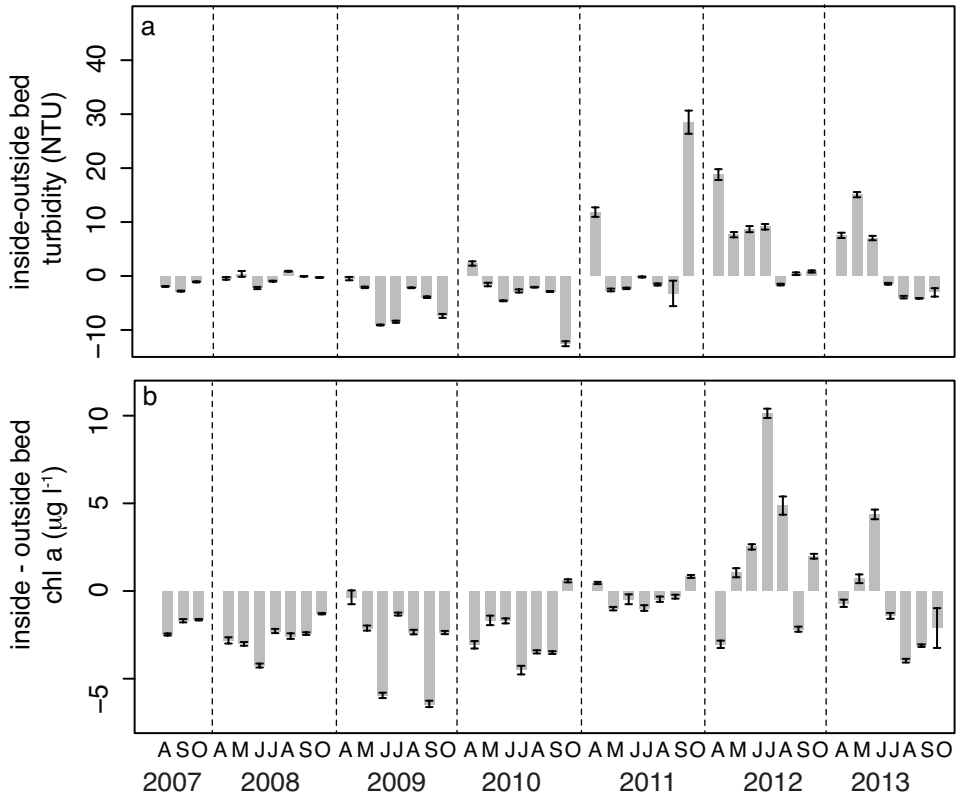
a
inside-outside bed
turbidity (NTU)
40
30
20
10
0
−10
b
inside - outside bed
chl a (μg l-1)
10
5
0
−5
A SO A M J J A SO A M J J A SO A M J J A SO A M J J A SO A M J J A SO A M J J A SO
2007
2008
2009
2010
2011
2012
2013

Fig. 3.7

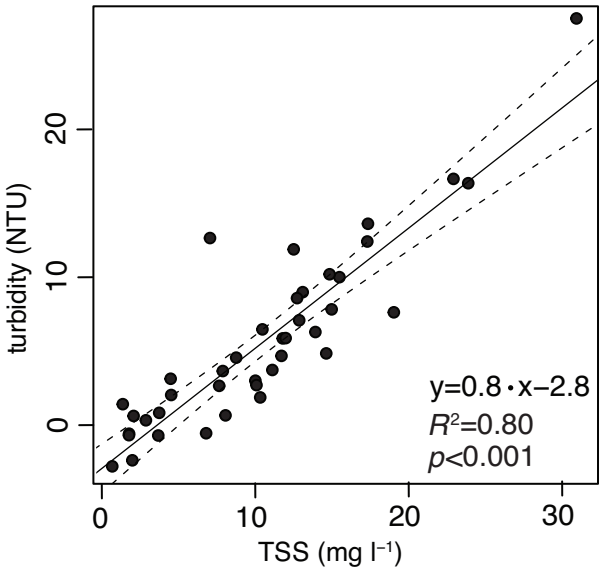

Fig. 3.8

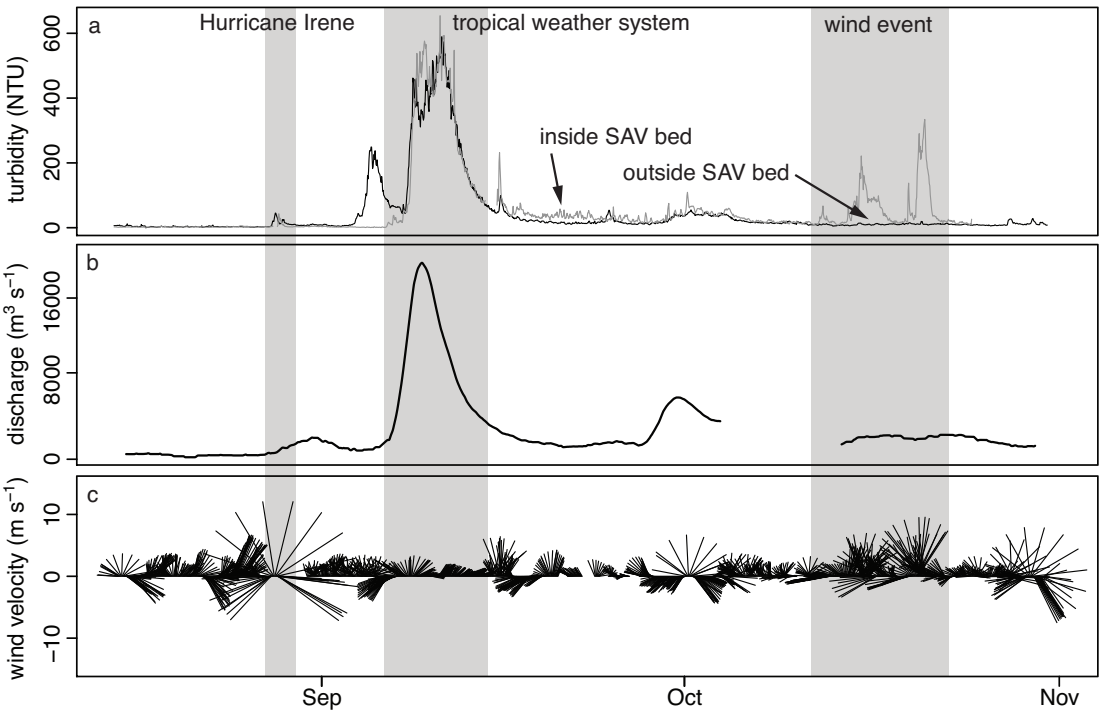
a
Hurricane Irene
tropical weather system
wind event
inside SAV bed
outside SAV bed
turbidity (NTU)
0
200
400
600
b
discharge (m^3 s^{-1})
0
8000
16000
c
wind velocity (m s^{-1})
−10
0
10
Sep
Oct
Nov

Fig. 3.9

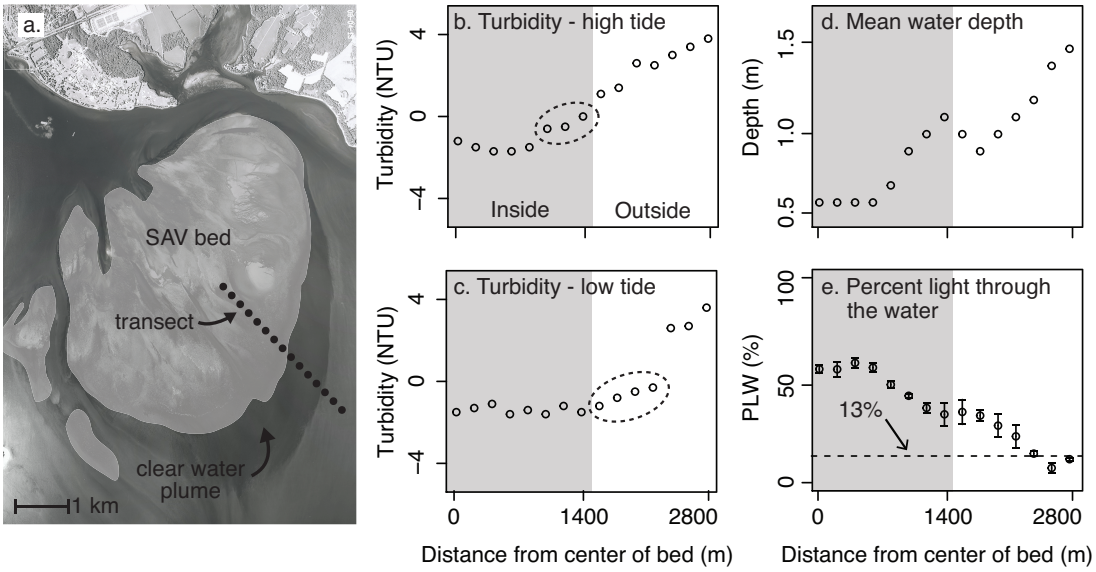
a.
SAV bed
transect
clear water
plume
1 km
b. Turbidity - high tide
Turbidity (NTU)
Inside
Outside
c. Turbidity - low tide
Distance from center of bed (m)
d. Mean water depth
Depth (m)
e. Percent light through
the water
PLW (%)
13%
Distance from center of bed (m)

Fig. 3.10

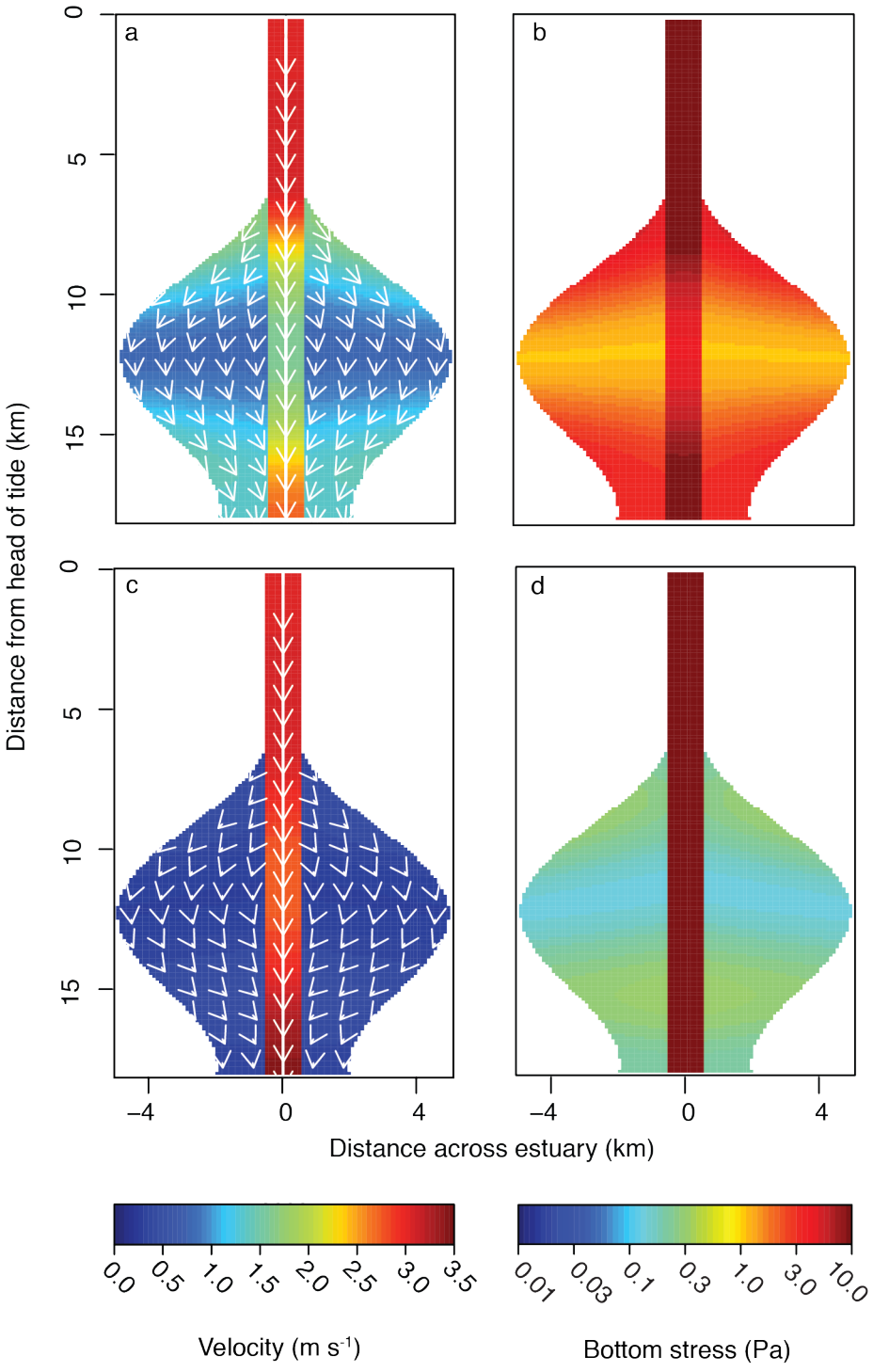
a
b
c
d
0
5
10
15
Distance from head of tide (km)
−4
0
4
Distance across estuary (km)
0.0
0.5
1.0
1.5
2.0
2.5
3.0
3.5
Velocity (m s-1)
0.01
0.03
0.1
0.3
1.0
3.0
10.0
Bottom stress (Pa)

Chapter 4: Interactive effects of physical and biogeochemical feedback processes in a large submersed plant bed

Abstract

Submersed plants are sensitive to high rates of nutrient loading because excess algal growth creates light-limiting conditions. However, submersed plant beds can also locally modify nutrient cycling through feedback loops whereby algal growth is limited and plant growth is enhanced. Most studies on the effect of SAV beds on nutrient cycling concentrate on either biogeochemical or physical controlling mechanisms. However, we hypothesize that a holistic ecosystem-scale approach could yield insights into how these processes interact. We measured a suite of physical and biological processes in a large SAV bed in upper Chesapeake Bay and developed a simple, 1-D reactive transport model to investigate potential mechanisms driving SAV bed effects on nutrient cycling. We observed substantially lower concentrations of dissolved inorganic nitrogen and phosphorous (DIN and DIP) inside the SAV bed relative to outside the bed during the summer. Denitrification in the sediment (mean N_2-N flux in August = 50 μmol m^{-2} h^{-1}) and plant nutrient assimilation (August rates=385 μmol N and 25 μmol P m^{-2} h^{-1}) were mechanisms of nutrient removal. We also found that advective transport and tidal dispersion decreased inside the SAV bed and water residence time, therefore, increased as the plant bed developed. As a result, there was more time for biological processes to

reduce DIN and DIP concentrations. Together, these processes create conditions that allow SAV to outcompete phytoplankton and epiphytic algae, as water column nutrient concentrations were low enough to limit microalgae growth, while sediment porewater concentrations were generally sufficient to satisfy SAV nutritional demand. The results from this study suggest that interactions between physical and biological feedbacks in SAV beds can play a key role in structuring shallow aquatic ecosystems.

Introduction

Seagrass and associated submersed aquatic vegetation (SAV) are rooted vascular plants that often serve as the foundation of shallow aquatic ecosystems. Although humans highly value SAV for the ecosystem services they provide, such as habitat structure for diverse and economically important fauna (Costanza et al. 1997), these plants are also sensitive to anthropogenic stresses (Orth & Moore 1983, Dennison et al. 1993, Kemp et al. 2005). Of particular concern is excess nutrient loading and associated algal blooms, which have been linked to widespread SAV loss because high algal concentrations decrease light penetration through the water column (Waycott et al. 2009). However, SAV beds can also affect local nutrient concentrations, which, in turn, can limit algal growth and improve growing conditions (Valiela et al. 1997, Havens et al. 2001, McGlathery et al. 2007).

For example, SAV roots leak oxygen and dissolved organic matter into the surrounding sediment, which can enhance rates of denitrification in eutrophic systems where nitrate is abundantly available to both autotrophs and denitrifying bacteria (Caffrey & Kemp 1990, An & Joye 2001, Risgaard-Petersen 2004). Because denitrification converts nitrate to dinitrogen gas, labile nitrogen is removed from the

system and substrate availability for algal blooms is limited. In addition, SAV retain nutrients in their tissue, thereby temporarily sequestering nutrients that would otherwise fuel algal growth during the growing season (Risgaard-Petersen & Ottosen 2000).

SAV beds can also modify the physical environment. Generally, the effects of SAV beds on physical processes are described in terms of their ability to improve water clarity. For example, drag exerted by plants on moving water diminishes momentum transfer into SAV beds and decreases shear stress exerted on the bottom (Luhar et al. 2008). As a result, suspended particles tend to sink, resuspension decreases, and light penetration through the water, therefore, increases (Gacia et al. 1999, Koch 2001). However, effects on water movement can also interact with biogeochemical processes. For instance, when organic particles deposited inside an SAV bed are mineralized, porewater nutrient concentrations increase (Kemp et al. 1984, Hemminga et al. 1991, Gruber & Kemp 2010), which can support plant growth. Furthermore, reduced shear stress on the seabed can potentially limit nutrient flux from the sediment to the overlying water, thereby retaining porewater nutrients for plant root access and limiting availability for benthic algae and phytoplankton uptake in the water column (Koch 1999). SAV beds can also decrease tidal exchange with adjacent waters (Rybicki et al. 1997), which increases water residence time inside the plant bed (Nepf et al. 2007). When a parcel of water is in contact with the sediment and plants for a longer period of time, the extent to which assimilation and denitrification can remove nutrients increases and water column concentrations decrease (Nixon et al. 1996, Dettmann 2001, Seitzinger et al. 2006).

Most studies on the effect of SAV beds on nutrient cycling focus on either physical or biogeochemical controlling mechanisms. However, a holistic ecosystem-scale perspective could yield insights into how these processes interact that discrete studies, alone, cannot address. Here, we measure and integrate a suite of physical and biogeochemical parameters and rate processes in an SAV bed using a large stand of submersed plants in upper Chesapeake Bay as an example system. Our goals are 1) to investigate the mechanisms driving SAV bed effects on environmental conditions, 2) determine the extent to which interactions among physical and biogeochemical processes influence these effects, and 3) make inferences about implications for ecosystem structure and resilience.

Methods

Study site

Susquehanna Flats is a large (~50 km^2) shoal (~1 m deep) flanked by deeper (up to ~8-9 m) channels located in the tidal fresh upper Chesapeake Bay that formed as a subaqueous delta of the Susquehanna River (Fig. 4.1). Historically, the region was renowned to anglers and waterfowl hunters for supporting abundant fish, duck, and geese populations, which thrived among the large, diverse SAV beds that covered the shoal. In the 1960's, SAV at the flats began to decline as water quality became increasingly degraded (Bayley et al. 1978, Kemp et al. 2005). Then, in June 1972, catastrophic flooding during Tropical Storm Agnes destroyed most of the SAV in the region. There was little regrowth until the early 2000s, when a large, dense SAV bed suddenly repopulated nearly the entire shoal (50 km^2) in conjunction with improved water clarity during several consecutive dry years and modest long-term reductions in

nutrient loading to the estuary (Orth et al. 2010, Gurbisz & Kemp 2014). Another major flood occurred in September 2011. However, this time, only half the bed was lost, demonstrating some degree of resilience to extreme weather events (Gurbisz et al. 2016). Currently, a mixed assemblage of freshwater SAV species, including *Vallisneria americana*, *Heteranthera dubia*, *Myriophyllem spicatum*, and *Hydrilla verticillata* occupy ~25 km^2 of the shoal. Although this is only half of its maximum extent, the bed is nonetheless the largest continuous stand of SAV in Chesapeake Bay.

Monitoring data description and sources

We accessed publically available water quality monitoring data measured at the Up-bay, Bed 2, and Down-bay sites (Fig. 4.1c) from the Chesapeake Bay Program Data Hub (http://www.chesapeakebay.net/data) and the Maryland Department of Natural Resources (MDDNR) Eyes on the Bay website (Bed 2 and Up-bay sites; http://www.eyesonthebay.net). We also downloaded wind and current velocity data measured at the Susquehanna buoy from the National Oceanic and Atmospheric Administration (NOAA) Chesapeake Bay Interpretive Buoy System (CBIBS; http://buoybay.noaa.gov/locations/susquehanna) and river discharge data measured at the Conowingo gauging station (~16 km up-river) from the United States Geologic Service (USGS) National Water Information System (http://waterdata.usgs.gov/usa/nwis/uv?01578310).

Field measurements

We measured a suite of physical and biogeochemical properties and processes during two sets of field deployments. In 2013, we installed 2 PVC platforms, each housing an automated water sampler (ISCO 2700) at the Bed 1 site (MLLW=0.2 m) and the Edge site (MLLW=0.7 m) (Fig. 4.1c). We also deployed a bottom-mounted Nortek acoustic Doppler profiler (ADP) adjacent to each platform. We installed an additional automated water sampler adjacent to a data sonde maintained by MDDNR attached to a bulkhead outside of but near the SAV bed at the Up-bay site (Fig. 4.1c). These instruments were deployed for 6 days when plant biomass was low (July 8-13) and again when biomass was high (September 15-20). When we installed the platforms and instruments in both July and September, we inserted triplicate dialysis pore water samplers ("peepers") into the sediment at the Edge, Bed 1, and Bed 2 sites (Hesslein 1976).

We programmed water samplers to collect ~900 ml of ambient water every 2 h from ~20 cm above the bottom in the case of the platform samplers and ~1 m below the surface in the case of the bulkhead sampler. We filled the inside of the samplers with ice so that water samples would remain chilled until we retrieved them. Each day, we replaced the ice, retrieved the sample bottles, and replaced them with empty bottles. We vacuum filtered the water samples through glass fiber filters and froze the filters and filtrate to store for later chemical analysis. ADPs measured velocity and water depth every 10 min throughout the water column with a 5-cm blanking distance and 10-cm bins at the Bed 1 site and a 30-cm blanking distance and 30-cm bins at the Edge site, which was deeper. The peepers contained five holes covered by a 0.2 μm

polycarbonate membrane centered at 5, 8, 11, 15, and 20 cm below the sediment surface. We filled the peepers with N_2-sparged deionized water prior to installation and retrieved them after 10 days. Upon retrieval, we filtered the pore water into vials and stored the samples on ice until returning to the lab, where they were frozen. Samples for Fe analysis were immediately fixed with hydrochloric acid.

In August 2014 and May-June 2015, we measured water velocity in the deep channel adjacent to the SAV bed (MLLW=8 m) and in a relatively shallow channel, which we call the "cut", in the middle of the SAV bed (MLLW=1.5 m). We deployed a ring with an acoustic Doppler current profiler (ADCP) that measured velocity in 0.5 m bins starting at 1.2 m above the bottom in the deep channel and a small tripod with an ADV that measured velocity at 0.9 m above the bottom in the "cut" (Fig. 4.1d). Both instruments were programmed to collect data every 10 min for 13 d in early in the growing season (May 29-June 10 2015) and 5 d during peak SAV biomass (August 11-15 2014).

We also measured the flux of dissolved gasses (N_2 and O_2) and nutrients (NH_4^+, NO_x, DIP), across the sediment-water interface at 5 sites across the bed when instruments were deployed in August 2014 and May 2015, and, additionally, in August 2015. The sites included two northern and two southern locations and one location near the middle of the bed. The northern and southern sites were selected such that each pair contained one site inside the SAV bed and one outside the bed (Fig 4.1d). At each site, we collected three replicate 6.35 cm diameter sediment cores and ~40 l of ambient water. Upon returning to HPL, we placed the cores in environmental chambers set to ambient temperature (27^{o}C August 2014, 25^{o}C May

2015, 27°C August 2015) and aerated them with aquarium bubblers overnight. The next day, we incubated the sediment cores plus one "blank" core containing only water from each site under dark and illuminated conditions (150 μE for all cores in May and sites 1 and 5 in August; 38 μE for sites 2-4 in August to simulate shading by the plant canopy) and collected a time course of water samples according to the methods outlined in Gao et al. (2012). For each core, sediment-water flux rates were calculated as the rate of change for each dissolved gas or nutrient in the light and dark, corrected for water column rates measured in the blank cores. We also measured sediment surface Chl *a* and grain size. We used a cut-off syringe to subsample sediment from the top 1 cm of each core, then placed samples in 15 ml centrifuge tubes and froze them for later Chl *a* analysis. Samples for sediment grain size analysis were collected in duplicate push cores at each site.

In August 2014, we conducted an additional experiment two days after collecting the cores to determine the effect of nitrate concentration on flux rates. We divided water from Site 4, which had an ambient nitrate concentration of 9.9 μmol l^{-1}, into three 20-l containers and added additional nitrate to amend the water in each container to a concentration of either 14.5, 58.3, or 100.7 μmol l^{-1}. We replaced the overlying water in each of the three sediment cores from each site with water from one of each of the three nitrate-amended containers. We also included one "blank" core containing no sediment for each nitrate concentration and then ran incubations as described above.

In addition, we measured water quality along a north-south transect across the bed four times during the tidal cycle while instruments were deployed in 2014 (Aug

14-15) and 2015 (June 5-6). This transect was located adjacent to but not directly aligned with the transect described above to take advantage of easier navigation through a slightly deeper but nonetheless vegetated trough in the bed. We collected ~1 l of water every 400 m in the northern portion of the transect and every 600 m in the southern portion and immediately placed samples on ice. After completing each transect, we filtered the water samples in the field through glass fiber filters using a 60 ml syringe. Filters and filtered water samples were transported on ice and frozen within 4 h for storage until later analysis.

We also measured SAV biomass at the SAV bed sites (Edge, Bed 1, and Bed 2) during each of the 2013 deployments and the three SAV bed sites (Sites 2, 3, and 4) during the 2014 and 2015 deployments. We additionally collected monthly biomass samples at the Bed 1 and Bed 2 sites in June-October 2012 and May, June, August, and October 2013 to capture change in biomass across the full growing season. We sampled plant material to a sediment depth of ~20 cm with an acrylic corer (15.5 cm diameter, 35 cm long) and rinsed each sample with ambient water to remove sediment. Number of replicates varied (n=3-10) to account for patchy SAV cover early in the growing season (5-10 replicates) and relatively homogeneous plant cover during peak plant biomass (3 replicates). Samples were stored chilled for < 2 d.

Laboratory analyses

Filters and sediment Chl *a* samples were extracted in the dark with 90% acetone and read on a fluorometer (10-AU, Turner Designs). We measured nitrate+nitrite ($NO_x = NO_3^- + NO_2^-$), ammonium (NH_4^+), and dissolved inorganic phosphorous (DIP) in ambient and sediment-water flux samples water

colorimetrically (Shimadzu UVmini-1240) following the methods outlined in Parsons et al. (1984). Dissolved gasses (N_2 and O_2) from the sediment flux experiments were measured as ratios to Ar using high-precision membrane-inlet mass spectrometry at HPL (Kana et al. 1994). Sediment grain size was measured by wet and dry sieving the top 2 cm of each push core. We measured plant length and biomass by separating plant samples into above- and below-ground living tissues, measuring shoot lengths, and oven drying the samples at 60^{o}C to constant weight (~24-48 hours). We ground a subset of dried plant and root samples collected across the growing season (n=17 from the Bed 2 site and n=18 from 6 other sites distributed around the SAV Bed) to measure the carbon, nitrogen, and phosphorus content of plant tissue. Particulate C and N samples were processed using a CE-440 elemental analyzer (Exeter Analytical) and particulate P samples were digested in 1 mol l^{-1} HCl (Aspila et al. 1976) and analyzed colorimetrically for DIP.

Data analyses

We used analysis of variance (ANOVA) and *t*-tests to quantify spatial and temporal differences in N_2-N flux rates and pore water nutrient concentrations. We used linear regression to test for relationships between N_2-N flux, sediment Chl *a*, and NO_x concentration, and analysis of covariace (ANCOVA) to test whether there were spatial differences in flux rates after controlling for NO_x concentration. Raw data and model residuals were tested to ensure normality, heteroscedasticity, and independence assumptions were met and data were transformed as necessary to meet the assumptions. In addition, we used a linear mixed effect approach to test for monthly across-site differences in routinely monitored water column nutrient concentrations.

This method is appropriate because it has relaxed assumptions about independence and can explicitly account for autocorrelation structure in time series (Pinheiro and Bates 2000). Site and month were treated as random effects on the intercept, which means that mean values for each water quality parameter were calculated for each site and month. We used bootstrap resampling (n=1000) to calculate the mean difference with 95% confidence intervals between sites within each month (Lyubchich et al. 2015). Confidence intervals that encompass zero are not considered statistically "significant."

We also estimated monthly (April-October) rates of net community dissolved inorganic nitrogen (DIN) and dissolved inorganic phosphorous (DIP) assimilation using dissolved O_2 data measured continuously by MDDNR from 2007-2015 at the Bed 2 site (Fig 4.1c). We first used the open-water method developed originally by Odum (1956) and more recently refined by Howarth et al. (2013) and Caffrey et al. (2014) to calculate monthly mean net daily ecosystem production rates, as reflected by O_2 production and consumption. We accounted for atmospheric O_2 exchange according to theoretical saturation values that change as a function of temperature and salinity and a reaeration coefficient based on an empirical relationship with wind speed (Marino & Howarth 1993). We assume that production was carried out by a combination of SAV, benthic macroalgae (*Lyngbya woleii*), and epiphytic algae. We then used a photosynthetic quotient of 1, (Burris 1981, Kemp et al. 1986), to convert O_2 production to CO_2 assimilation. Next, we used C:N and C:P molar ratios of 13:1 and 294:1, respectively, to convert C assimilation to N assimilation. These are the

average C:N and C:P ratios for SAV and *Lyngbya* tissue samples collected at the Bed 2 site.

Results

Trends in plant biomass and water quality

Seasonal patterns: There were pronounced seasonal differences in several water quality parameters measured inside and outside the SAV bed (Fig 4.2a-c) that coincided with increases in SAV biomass (Fig. 4.2d). Mixed effect model results illustrate the magnitude of the differences (Fig. 42e-j). For example, NO_x + NH_4^+, or dissolved inorganic nitrogen (DIN), decreased substantially inside the SAV bed, with concentrations up to ~70 μmol l^{-1} less than those measured outside the SAV bed (Fig. 4.2e and h). DIN was composed primarily of NO_x (96%, on average across sites and sample dates). In addition, there were seasonal increases in DIP at the Up-bay and Down-bay sites but not inside the SAV bed (Fig. 4.2b), which led to lower DIP concentrations inside the bed particularly during the summer and fall (Fig. 4.2f and i). While Up- and Down-bay Chl *a* concentrations were generally highest during the late spring to early summer, there were two peaks inside the SAV bed, one in May and one in September, and a decrease during mid summer (Fig. 4.2c). As a result, July Chl *a* was lower inside the SAV bed compared to Up-bay and Down-bay (Fig. 4.2g and j).

Patterns at high temporal frequency: Automated water sampler deployments and concurrent plant biomass measurements show spatial and seasonal differences in water quality during low (July 2013) and high (September 2013) biomass at high

temporal resolution. Log-transformed biomass at the Bed 1 site increased between July and September [$t(18)=-4.1$, $p=0.0006$] (Fig. 4.3). There was no significant increase at the Edge site because plant cover was patchy, leading to high variance. DIN at the bed site decreased between July (mean=41.9, SD=5.8 μmol l^{-1}) and September (mean=13.3, SD=15.4 μmol l^{-1}) (Fig. 4.4). Although there were no significant differences in DIP, concentrations were generally lower inside the plant bed in both July and September (mean difference between Bed 1 and Up-bay=0.18, SD= 0.11 μmol l^{-1}; mean difference between Bed 1 and Edge=0.13, SD=0.2 μmol l^{-1}) and decreased at all three sites between July and September (mean decrease at all 3 sites=0.49 μmol l^{-1}). There were semi-diurnal patterns in the DIN and Chl *a* time series, but only during September, when SAV biomass was higher.

Patterns at high spatial frequency: Transect measurements show differences in water quality during low (May) and high (August) biomass at high spatial resolution. SAV biomass measurements from August 2014 were abnormally high (>1000 g m^2), we believe due to sampling error (we may have collected plants outside of the sampling area because they were tangled with plants inside the sampling area). We present August 2015 data collected at the same site as a proxy because we believe they represent more realistic summer biomass values. Log-transformed biomass was greater in August 2015 compared to May 2015 at Site 2 [$t(2)=-3.9$, $p=0.05$], Site 3 [$t(6)=-4.3$, $p=0.006$], and Site 4 [$t(5)=-3.1$, $p=0.03$] (Fig. 4.3). Water quality transect data show that there was a strong gradient of decreasing DIN from outside to inside the bed, but only in August, when SAV biomass was high (Fig. 4.5a-b). DIP followed a different seasonal pattern, whereby concentrations decreased from high to low

across the bed when SAV biomass was low but remained consistently low across space during high SAV biomass (Fig. 4.5c-d).

Rate measurements

Denitrification: N_2-N fluxes across the sediment-water interface (Fig. 4.6a) are used as a proxy for denitrification rates. Mean ± SD N_2-N fluxes across sites during the two August experiments were 43.6±31.1 μmol m^2 h^{-1} in the dark and 57.1±23.6 μmol m^2 h^{-1} in the light (May results are not reported because time series were too noisy to calculate flux rates). For August 2014 and 2015 N_2-N fluxes in the light, there were no significant effects of site [$F(4, 18)=1.8$, $p=1.8$], sediment Chl *a* ($R^2=0.005$, $p=0.74$), or NO_x concentration ($R^2=0.04$, $p=0.21$) on denitrification. There was a marginally significant site effect on dark denitrification rates [$F(4, 19)=2.889$, $p=0.05$]. According to a Tukey post-hoc test, the flux rate at Site 4 was significantly less than that at Site 1 ($p < 0.05$). However, after controlling for NO_x concentration, there was no significant site effect [$F(1, 36)=0.32$, $p=0.58$]. There was a significant relationship between dark N_2 flux and NO_x concentration (Fig. 4.6b). Sediment Chl *a* concentration was not related to dark or light flux rates ($R^2=0$, $p=0.96$). Sediment grain size and Chl *a* concentrations, and sediment-water flux rates for additional parameters are presented in Appendix II (Table AII.1 and Fig. AII.1).

Because we only have denitrification data for August, we used the average light rate and the predicted dark rate according to our empirically derived relationship with NO_x (we used monthly mean NOx concentrations, Figs. 4.2 and 4.7) multiplied by the number of day and night hours each day to calculate daily mean rates for April-October (Fig. 4.7a). The assumption that August rates are representative of

those for the entire growing season is flawed, as denitrification rates can vary seasonally (Kemp et al. 1990). However, our intention was to compare these rates to autotroph assimilation rates. Because plant assimilation varies seasonally across a much broader range than denitrification (Caffrey & Kemp 1992), we consider this extrapolation of denitrification rates to be reasonable. Derived rates ranged from 1.1 to 1.5 mmol m^{-2} d^{-1}.

Autotroph assimilation: Plant C production was 83.6 mmol m^{-2} d^{-1}, on average, with a maximum rate of 230.3 mmol m^{-2} d^{-1}. N and P uptake rates ranged from 1.8 to 10.6 and 0.1 to 0.7 mmol m^{-2} d^{-1}, respectively. Both followed a seasonal cycle similar to that of SAV biomass, with a peak in mid summer and minima in the spring and fall (Fig 4.7). N assimilation rates were similar to denitrification rates in the spring and fall but >8 times greater in the summer.

Physical processes

Physical data collected during the 2013 and 2014-2015 deployments illustrate flow patterns across space and time. In general, current velocities followed a semi-diurnal pattern that coincided with the tidal cycle (Figs. 4.8 and 4.9). At most sites, there was net-southward flow due to the influence of Susquehanna River outflow, which follows a step-like pattern because river discharge is controlled by timed releases from a hydroelectric dam.

During the 2013 deployments, river flow was 60% greater in July (996 m^3 s^{-1}) compared to September (402 m^3 s^{-1}). Mean current speed, calculated using east and north velocity components to reflect the magnitude of measured velocities, was 56% greater at the CBIBS buoy (0.09 vs. 0.04 m s^{-1}), 36% greater at the Edge site (0.11 vs.

0.07 m s^{-1}), and the same at the Bed 1 site (0.05 m s^{-1}) in July compared to September. Mean current speed was 22% greater at the Edge site compared to the CBIBS buoy in July and 75% greater in September. In addition, the dominant flow direction, or the angle of the principal axis of the velocity time series, shifted from 337^{o} in July at the Bed 1 site (oriented northwest-southeast, Fig. 4.10a), to 16^{o} in September (oriented northeast-southwest Fig. 4.10b). Physical data from additional sites in 2013 are available in Appendix II (Figs AII.2 and AII.3).

During the 2014 and 2015 deployments, river flow was 9% greater in August (608 m^3 s^{-1}) than in May-June (560 m^3 s^{-1}) (Fig. 4.9). Current speed measured by the ADCP in the channel was also 9% greater in August (0.25 m s^{-1}) compared to May-June (0.23 m s^{-1}); however velocity was 33% less (0.06 vs. 0.04 m s^{-1}) at the CBIBS buoy and 57% less (0.07 vs. 0.03 m s-^{1}) at the ADV site in August compared to May-June. Current speed was 69% less at the ADV site compared to the ADCP site in May-June and 88% less in August. Velocity at the ADV site was in-phase with velocity measured at all other sites in May-June, whereby flow was generally northward during flood tide and southward during ebb tide. However, velocity at the ADV site was out of phase with the other sites in August, in which case currents flowed up-bay during ebb tide and down-bay during flood tide.August ADV data are cut short due to equipment malfunction. Additional physical data from 2014-2015 are available in Appendix II (Figs AII.4–AII.6).

Pore water and plant tissue nutrient concentrations

There were several between-site and between-month differences in pore water dissolved nutrient concentrations (Fig 4.11, Tables 4.1 and 4.2). Specifically,

NH_4^+ was greater at the Bed 2 site compared to Bed 1 and Edge in July (Fig. 4.11a) and Bed 1 in September (Fig. 4.11b), DIP was lower at the Bed 2 site compared to Bed 1 and Edge in September (Fig. 4.11d), and Fe was lower at the Edge site compared to both other sites in July (Fig. 4.11e) and the Bed 1 site in September (Fig. 4.11f). In addition, NH_4^+ at Edge and Bed 1 sites increased, and DIP and Fe at the Bed 2 site decreased between July and September (Table 4.2). Most pore water DIN and DIP samples were greater than nominal pore water half-saturation concentrations for tidal fresh SAV communities in Chesapeake Bay, with the exception of DIP measured at the Bed 2 site (Fig. 4.11d). Pore water nitrogen was composed primarily of NH_4^+(95% on average across all sites and sampling dates). Generally, there was a negative relationship between mean Fe and DIP concentrations measured at each site (Fig. 4.12). Pore water nutrient profile plots are available in Appendix II (Fig. AII.7).

Plant tissue nitrogen and phosphorus content ranged from 1.7-4.1 and 0.2-0.6%, respectively (Fig. 4.13a-b). Tissue C:N molar ratios ranged from 10.2-25.6. C:P molar ratios ranged from 163.0-435.4. Tissue C:N ratios appear to follow a seasonal pattern, with increasing ratios from June to September and decreasing ratios into October (Fig. 4.13b), although the only significant difference was between July and September [$F(4,21)=3.5$, $p=0.02$]. There were no significant between-site differences for C:N [$F(5,12)=1.4$, $p=0.28$] or C:P ratios [$F(3,8)=0.18$, $p=0.90$].

Discussion

Perhaps the most striking trends we observed were the large seasonal differences in DIN and DIP inside the SAV bed relative to up-bay and down-bay sites. The concurrent increase in plant biomass suggests that the SAV bed has the

capacity to dramatically alter local DIN and DIP concentrations. In the sections that follow, we develop an explanatory model for the biological and physical mechanisms driving these changes in dissolved inorganic nutrient concentrations inside the plant bed and discuss potential ecological implications.

Mechanisms of decreased DIN inside the plant bed

Our results show that denitrification is one mechanism of DIN removal from the system. The literature on denitrification in SAV beds reports a wide range of results, from enhanced denitrification relative to outside the SAV bed (Caffrey & Kemp 1992, Flindt 1994, Cornwell et al. 1999) to no difference or decreased rates inside the SAV bed (Rysgaard et al. 1996, Welsh et al. 2000, Bartoli et al. 2008). Our sediment flux measurements show no difference between sites once the nitrate concentration in overlying water is accounted for, probably because the primary factor controlling denitrification is nitrate availability (McGlathery et al. 2007). It is possible, however, that our sediment water flux experiments may not have captured the mechanisms that are thought to enhance denitrification because our cores did not contain plants. For example, leaking oxygen from plant roots can increase nitrification (the oxidation of NH_4^+ to nitrate) because the process is carried out by obligate aerobes (Cornwell et al. 1999). In addition, exudation of dissolved organic matter from roots increases the supply of substrate upon which respiratory processes depend (Karjalainen et al. 2001).

Autotroph assimilation appears to be a more important mechanism of DIN loss in the plant bed, particularly in the summer when estimated community assimilation rates were >8 times greater than denitrification rates. This is not

surprising, considering the large amount of SAV biomass that accumulates through the growing season. Our estimated net primary production rates are comparable to those measured for submersed vascular plants in other systems, which generally fall between 80 and 250 mmol C m^{-2} d^{-1} but can range from <80 to >400 mmol C m^{-2} d^{-1} (Duarte and Cebrian 1996). It is important to note, however, that our rates are for the whole autotrophic community, which includes mats of *Lyngbya woleii*. Furthermore, *Lyngbya* is a diazotroph and is known to fix N, albeit at low rates, in this system (~0.007 nmol N g^{-1} h^{-1}, J. O'Neil, *unpubl.).* Determining the relative contribution of different autotrophs to DIN assimilation and, possibly, production would require additional uptake and N-fixation rate studies.

Although the rate of biological N removal increases as the SAV growing season progresses, the magnitude of the increase does not seem to explain the observed seasonal decrease in DIN unless interactions with physical processes are also considered. For instance, automated water sampler data imply that DIN interacts with tidal flow, especially during peak SAV biomass. At first glance, it appears that DIN is advected into the SAV bed by tidal currents, as indicated by increasing DIN (Fig. 4.4) and concurrently increasing depth as the tide rises (Fig. 4.8). Nitrogen is assimilated and processed through denitrification, and low-N water then flows out of the bed with ebbing tidal currents (e.g., Bulthuis et al. 1984). Low DIN concentrations south of the bed support the idea that low-N water flows out of the bed with the ebbing tide (Fig. 4.5).

However, the magnitude of the observed decrease in DIN is not possible at the timescale of a tidal cycle. If we use assimilation plus dentrification rates from August

(431 μmol m^{-2} h^{-1}) and assume an average depth of 1 m, DIN in a 1 m^3 parcel of water containing a starting concentration of, say, 60.0 μmol l^{-1} traversing the bed over 6 hours would only decrease to 57.4 μmol l^{-1}). A decrease in DIN to, say, 5 μmol l^{-1} would take more than 5 days. This suggests that water residence time inside the plant bed would have to increase to ~5 days in order to achieve such low DIN concentrations. Meanwhile, with a slightly lower rate of biologically mediated N loss in May (273 μmol m^{-2} h^{-1}), the concentration of DIN would decrease to 27 μmol l^{-1} if water residence time was 5 days. Because May DIN was generally ≥40-60 μmol l^{-1} (Figs. 4.2 and 4.5) and also more spatially uniform across the bed (Fig. 4.5), exchange with water outside the bed must be greater and water residence time, therefore, must be shorter early in the growing season. This suggests that as the SAV bed develops, it has an increasingly important effect on flow, whereby exchange between the bed and surrounding channels decreases and water residence time increases.

Our current velocity measurements collected at several points during the SAV growing season support the idea that the bed affected flow. For example, flow attenuation is apparent in the ADCP and ADV data, which show that despite little change in river discharge or current speed in the main channel, current speed was, on average, 57% less at the ADV site in August 2014 compared to May-June 2015 (Fig. 4.9). This is consistent with other studies, which show that submersed aquatic plants exert drag on moving water, which decreases flow rates (Fonseca et al. 1982, Gambi et al. 1990, Luhar & Nepf 2013).

The bed also diverts flow around the shoal and into the main channel. This has been demonstrated in a previous modeling study of this system (Gurbisz et al. 2016)

as well as field and laboratory studies in other systems (Rybicki et al. 1997, Rominger & Nepf 2011). During our 2013 deployment, flow at the CBIBS buoy decreased approximately in proportion (by ~60%) with the decrease in river flow between July and September; however, flow at the Edge site, which is located near the main channel, only decreased by 36%. Furthermore, within each of these deployments, flow was greater at the Edge site than the CBIBS buoy, but the difference was much greater in September. This implies that water is shunted around the bed into the channel, and, accordingly, current velocities decrease inside the bed and increase in the channel (Fagherazzi et al. 2003).

Observed changes in flow direction are consistent with this explanation. When a dense plant bed occupies a shoal, the rate at which water level changes over the shoal often lags that in the channel, resulting in a relative water level difference and an associated cross-stream pressure gradient (Rybicki et al. 1997). If the gradient is sufficiently large, water tends to flow along the gradient in a direction that can potentially be perpendicular to flow in the channel. The change in flow orientation at the Bed 1 site between July and September 2013 follows this pattern (Fig. 4.10). Flow direction at the ADV site in 2014 did not change because currents likely followed the topography of the trough in which the instrument was deployed (Fagherazzi et al. 2003). However, the fact that velocity measured at this site was out of phase with velocity at the other sites but only when SAV biomass was high (Fig. 4.9) further implies that flow during peak biomass is dominated by a cross-stream pressure gradient generated by the presence of a dense plant bed, whereas flow early in the

growing season is dominated by a north-south pressure gradient generated by river discharge and northward propagating tidal waves.

We developed a simple 1-dimensional tidally-averaged reactive transport model to test our inferences regarding the interaction between flow and biological nitrogen removal processes (García et al. 2008, Hofmann et al. 2008). The model calculates the steady-state concentration of DIN along a northwest-southeast oriented transect (Fig. 4.1e) spanning the approximate length of the SAV bed (3600 m) divided into 9 segments (400 m each) by calculating advective and dispersive fluxes across the interface of each segment and biologically mediated DIN loss within each segment according to the equation

$$\frac{\partial \mathrm{DIN}}{\partial t} = \frac{\partial}{\partial x}\left(K\frac{\partial \mathrm{DIN}}{\partial x}\right) - \mathrm{u}\frac{\partial \mathrm{DIN}}{\partial x} - (\mathrm{assimilation} + \mathrm{denitrification}).$$

The dispersion coefficient, K, represents tidal dispersion, which we initially estimated assuming that K is proportional to the tidal excursion multiplied by tidal flow velocity ($K \propto U_{tide}L_{tide}$, Zimmerman 1976). Assuming L_{tide}≈1375 m and U_{tide}≈0.05 m s^{-1} (the mean current speed measured at the Bed 1 site during low biomass), K≈70 m^2 s^{-1} ($2.5x10^5$ m^2 h^{-1}). Tidal excursion (L_{tide}) was estimated according to the equation

$$L_{tide} = \frac{u_{max}T}{\pi}$$

where u_{max} is the maximum tidal velocity measured at the Bed 1 site (0.1 m s^{-1}) and T is the tidal period (12 h). For the case with high SAV biomass, we used an empirically-derived dispersion coefficient (K≈10 m^2 h^{-1}) from measurements made inside a stand of aquatic macrophytes (Lightbody & Nepf 2006). Advective velocity, u, represents net down-bay transport resulting from river outflow and was initially based on the means of north-south components of flow velocity measured inside the

SAV bed (-0.01 m s^{-1} during low SAV biomass and -0.005 m s^{-1} during high SAV biomass). We supplied DIN concentrations at the up-bay and down-bay boundaries and biological loss rates (i.e., the sum of plant assimilation and denitrification rates) based on the data presented in Figs. 4.5 and 4.7. We then used "inverse modeling" to estimate K and u for June and August, whereby we adjusted these parameters to produce model output that matched the tidally averaged DIN concentrations that we measured in our June and August water quality transects. We used the R package, *ReacTran*, to implement the model. All relevant equations and example code are described in Soetart & Meysman (2012).

Parameter values used to simulate June and August DIN concentrations (Fig. 4.14) are listed in Table 4.3. To simulate low DIN concentrations in the center of the bed in August, we decreased u and we decreased K linearly from the edge of the bed until it reached a constant value. This is consistent with lab and flume studies, which demonstrate that K eventually achieves a constant value as water traverses a stand of macrophytes (Nepf et al. 1997, Lightbody & Nepf 2006, Murphy et al. 2007). We also assigned greater K values in the southern half of the transect compared to the northern half in August, which is reasonable given that tidal flow increases as distance from the mouth of the river increases and the cross-sectional width of the basin constricts.

We conducted sensitivity analysis to illustrate the relative effect of u, K, and biological loss rates on SAV bed DIN concentrations in June and August by running the model with each parameter increased and decreased by 25%. The response of modeled DIN concentrations to changes in model parameters is small for the case

with low SAV biomass. This is because both advective and dispersive fluxes are large, thus overwhelming small parameter modifications. Change in DIN concentration across space inside the SAV bed is minimal during this time because a constant supply is delivered from outside the bed. On the other hand, DIN is more sensitive to changes in model parameters in August. Although river discharge was not substantially different when we conducted our June and August deployments and transect measurements, the flow regime across the plant bed changed dramatically due to increased SAV biomass, resulting in decreased advective and dispersive fluxes of N across the bed. Because fluxes are relatively small during this time, changes in model parameters have a greater effect on DIN concentrations.

The water residence time (T) for each box of the model can be calculated using the volume of water in each box (V, 400 m^3) and modeled flow rates into the boxes (Q, 36 m^3 h^{-1} during low SAV biomass and 13 m^3 h^{-1} during high biomass) according to the equation T=V/Q = 11 h during low biomass and 31 h during high biomass. The water residence time at any location along the transect can then be estimated by summing the cumulative residence times of all boxes north of a given location, assuming that a parcel of water enters the bed from the north and traverses the bed towards its southern edge. Residence times in the center of the bed would, therefore, be 2 d during low biomass and 6.5 d during high biomass. These times are consistent with our estimates of the amount of time required to draw down DIN concentrations based on measured denitrification and assimilation rates.

Mechanisms of decreased DIP inside the plant bed

The processes controlling seasonal changes in DIP concentrations differ from those driving changes in DIN. While river outflow is the main source of DIN, primarily in the form of NO_3^-, increasingly greater down-bay DIP concentrations throughout the year suggest internal phosphorous cycling as an important DIP source. DIP concentrations in estuarine waters are often associated with salinity because the reduction of sulfate, which is abundant in seawater, to sulfide alters sediment biogeochemistry in ways that enhance the release of PO_4^{3-} bound to Fe (Froelich 1988, Jordan et al. 2008). For example, although PO_4^{3-} is released from iron oxyhydroxides under anoxic conditions in freshwater sediments, the resulting dissolved Fe remains available to precipitate PO_4^{3-} once reoxidized in the overlying oxic layer and PO_4^{3-} flux into the water column is, thus, minimal. In seawater, however, reduced sulfate (sulfide) tends to precipitate dissolved Fe, thereby removing sorption sites that would otherwise be available to PO_4^{3-}, leading to increased fluxes of PO_4^{3-} from the sediment. Salinity at the Down-bay site generally increases by ~4 PSU between June and October, when river discharge is typically lowest and seawater, can therefore, mix further up the bay. Release of particle-bound P associated with decreased river flow, and associated increasing salinity, and sulfide could, therefore be a source of seasonal increases in DIP. Concentrations likely remain low inside the SAV bed due to rapid autotroph assimilation and reduced exchange with waters outside the bed. The negative relationship between pore water DIP and dissolved Fe measured inside the bed (Fig. 4.12) is consistent with the idea that interactions with Fe are important in controlling DIP concentrations.

Our data also suggest sub-seasonal differences between DIN and DIP dynamics. For example, our DIN field measurements are generally consistent with routine water quality monitoring data (Figs. 4.2a, 4.4, 4.5a-b). However, our measured concentrations from automated water sampler deployments in July 2013 and transect sampling in June 2014-2015 at the Up-bay site were generally greater than 2007-2015 monthly means of monitoring samples collected up-bay from the SAV bed (Figs. 4.2b, 4.4, and 4.5c). This implies that DIP dynamics at shorter time scales may be more variable than DIN dynamics.

On the other hand, the factors controlling the spatial distribution of DIP across the plant bed appear to be consistent with those controlling DIN concentrations. We used autotroph phosphorous assimilation rates (Fig. 4.7b), DIP concentrations measured outside the SAV bed (Fig. 4.5c-d), and the advective velocity and dispersion coefficients derived through our DIN modeling exercise (Table 4.3) to simulate DIP concentrations across the SAV bed during low and high biomass. Modeled concentrations were generally consistent with those measured in June 2015 and August 2014 (Fig. 4.14). Note that we made the DIP assimilation rate a function of concentration to maintain positive values for the high biomass simulation because boundary concentrations were so low. In addition, although modeled DIN was more sensitive to model parameter adjustments for the case with high biomass, modeled DIP concentrations were not sensitive to parameter variability due to very low DIP concentrations. Generally, however, the fact that the model accurately predicts DIN and DIP concentrations using the same set of parameters suggests that physical

transport processes coupled with biological and biogeochemical processes are important in controlling both DIN and DIP concentrations across the SAV bed.

Ecological implications

Seasonally low water column DIN and consistently low DIP inside the SAV bed could have implications for the structure and function of the system. The generally accepted conceptual model of how shallow aquatic ecosystems respond to changes in nutrient concentrations describes a shift from benthic vascular plant dominance to microalgae dominance as nutrient loading increases, with increasing prevalence of benthic macroalgae as an intermediate step (Valiela et al. 1997, Havens et al. 2001, McGlathery et al. 2007). Phytoplankton and macroalgae thrive at higher nutrient concentrations because they have high nutrient uptake rates and, when abundant, they limit the amount of light available to submersed vascular plants. On the other hand, SAV thrive at low concentrations because they can satisfy their nutrient demand through root uptake from the porewater. Our data suggest that primary producer dynamics on the flats adhere to this model.

First, algal production inside the SAV bed is likely nutrient-limited during the summer. For example, the July Chl *a* minimum inside the SAV bed corresponds with the lowest monthly mean DIN concentration measured at this site (1.9 μmol l^{-1}). This concentration is also less than nitrogen half-saturation coefficients (K_N) for most phytoplankton species found in tidal fresh and oligohaline regions of Chesapeake Bay, which range from 1.8-2.1 μmol l^{-1} (Cerco 2000). DIP is also typically lowest in July (0.07 μmol l^{-1}), although this concentration is less than the DIP half-saturation concentrations (K_P) for only some phytoplankton species (typical K_P values range

from 0.03-0.1 μmol l^{-1}). July and August are also the only months when the DIN:DIP ratio (2:1 and 7:1 in July and August, respectively) is below the Redfield ratio (16:1), indicating that DIN limitation may be more important than DIP limitation of phytoplankton growth inside the plant bed during the summer. Although *Lyngbya* is persistently present inside the SAV bed, it has the capacity to fix N to satisfy its nutrient requirements. More work is needed to investigate the role of *Lyngbya* in primary producer dynamics in this system. Meanwhile, DIN concentrations Up-bay and Down-bay from the SAV bed are high (>40 μmol l^{-1}) year-round and DIP concentrations, although not exceedingly high (monthly means=0.13-0.94 μmol l^{-1}), are nonetheless greater than typical K_P values for Chesapeake Bay phytoplankton (Cerco 2000). This suggests that phytoplankton production outside the SAV bed is not nutrient limited.

In addition, even with low summer water column nutrient concentrations, SAV growth does not generally appear to be nutrient limited. Although the K_N and K_P values for SAV leaf uptake (13.6 and 0.9 μmol l-1, respectively) (Cerco & Moore 2001) exceed summer water column concentrations at some SAV bed sites, half-saturation coefficients for root uptake (K_N=67.9 and K_P=4.5 μmol l^{-1}) are generally less than or equal to average summer pore water DIN and DIP concentrations (Fig. 4.11). One exception is September pore water DIP at the Bed 2 site (Fig. 4.11d). However, plant tissue C:P molar ratios (Fig. 4.12) are consistently greater than the ratio that is thought to indicate P limitation in aquatic vascular plants (474:1), suggesting that production is not P-limited (Duarte 2012). Plant tissue C:N ratios appear to follow a seasonally increasing trend, approaching values that indicate N

limitation (20:1) in September (Duarte 2012). However, only a few plant tissue samples contained a C:N ratio>20, supporting the hypothesis that nutrient availability does not generally limit SAV growth because sediment pore water nutrients can support plant nutritional requirements. The effect of the bed on internal nutrient cycling could, therefore, allow the system to maintain benthic vascular plant dominance despite relatively high external nutrient loading rates.

Concluding comments

This study demonstrates that the interactive effect of submersed plant beds on physical and biological processes is an important mechanism driving feedbacks between SAV and nutrient cycling. We found that the physical structure of the SAV bed at Susquehanna Flats interacts with flow such that water residence time inside the bed increases as plant biomass increases. As a result, there is more time for biological and biogeochemical processes, including plant assimilation and denitrification, to reduce water column nutrient concentrations. These feedbacks likely control the transition between primary producer communities in this shallow aquatic ecosystem. More information is needed, however, to be able to quantitatively predict how this and similar systems will respond to changes in nutrient loading or climatic conditions. For example, a unique aspect of this system is its large size. Other studies have shown that SAV bed size plays a role in the extent to which physical processes are modified (e.g., Gruber et al. 2011), but how do these processes interact with nutrient cycling as a function of bed diameter? Explicitly addressing this and similar spatial problems could be an important line of future inquiry.

Tables

Table 4.1 Between-site differences in log-transformed sediment pore water ammonium (NH_4^+) and dissolved inorganic phosphorous (DIP), as indicated by analysis of variance (ANOVA). Bold *p*-values indicate the presence of significant differences at the 0.05 level.

	df	sum sq	mean sq	F	p
Jul NH_4					
site	1	8.86	8.86	31.84	**<0.0001**
residuals	42	11.69	0.28		
Sep NH_4					
site	2	4.25	2.13	7.419	**0.002**
residuals	40	11.46	0.29		
Jul PO4					
site	2	26.30	13.13	0.441	0.646
residuals	41	1219.60	29.75		
Sep PO4					
site	2	10.35	5.17	9.729	**<0.0001**
residuals	41	21.80	0.53		
Jul Fe					
site	2	8.15	4.08	7.911	**0.001**
residuals	42	21.63	0.52		
Sep Fe					
site	2	4.96	2.48	3.36	**0.044**
residuals	42	30.98	0.74		

Table 4.2 Within-site differences between July and September log-transformed sediment pore water ammonium (NH_4^+) and dissolved inorganic phosphorous (DIP) as indicated by *t*-tests. Bold *p*-values indicate the presence of significant differences at the 0.05 level

	t	df	*p*
NH_4^+ Edge	-2.42	27.35	**0.022**
NH_4^+ Bed 1	-2.28	19.86	**0.034**
NH_4^+ Bed 2	-1.35	15.83	0.196
DIP Edge	-0.30	11.88	0.770
DIP Bed 1	-1.28	17.47	0.218
DIP Bed 2	2.21	21.53	**0.038**
Fe Edge	1.39	25.99	0.178
Fe Bed 1	2.02	10.07	0.060
Fe Bed 2	2.91	16.59	**0.010**

Table 4.3 Parameters used in the reactive transport model. Boundary DIN concentrations are from measurements made immediately up-bay and down-bay from the SAV bed. A single value for K represents constant tidal dispersion all model segment interfaces; a vector of coefficients represents different values for K across each segment interface

	Boundary DIN concentration ($\mu mol\ l^{-1}$)	Advective velocity (v) ($m\ h^{-1}$)	Dispersion coefficient (K) ($m^2\ h^{-1}$)	Internal losses ($\mu mol\ m^{-3}\ h^{-1}$)
June	70, 50	36	2.5×10^5	273
August	80, 20	13	100, 50, 10, 10, 10, 10, 10000, 15000, 20000, 25000	431

Figure captions

Fig 4.1 Study site (a) location and (b) bathymetry (0.5 m contours) and sampling sites for (c) the 2013 deployments, (d) the 2014-2015 deployments, and (e) the water quality transect. Rectangles along the transect represents the reactive model transect grid structure

Fig. 4.2 Monthly mean (a) dissolved inorganic nitrogen (DIN), (b) dissolved inorganic phosphorous (DIP), and (c) chlorophyll *a* (chl *a*), (averaged across 2007-2014) at the up-bay (dark gray), down-bay (light gray), and bed 2 (black) monitoring sites and (d) SAV biomass (averaged across 2012-2013) at the bed 2 site. Error bars represent standard error. Most DIN, DIP, and chl *a* data are from MDDNR. We collected all biomass samples and a subset of nutrient and chl *a* samples. (e-j) are bootstrapped mean differences between concentrations measured at the Bed 2 and Up bay sites (e-g) and Bed 2 and Down bay (h-j). Error bars represent 95% confidence intervals; solid circles represent differences in which the confidence interval does not include zero, and are thus considered "significant"

Fig. 4.3 Mean (a) biomass and (b) ratio of plant length to mean water depth at sites where instruments were deployed. Error bars represent standard error; horizontal bars indicate between-month differences at the $p<0.05$ (*), $p<0.01$ (**), and $p<0.001$ (***) significance levels

Fig. 4.4 Time series for dissolved inorganic nitrogen (DIN), dissolved inorganic phosphate (DIP), and chlorophyll a (chl a) measured during low SAV biomass (July) and high SAV biomass (September) 2013 at the Bed 1 (black circles), Edge (dark gray triangles), and Up-bay (light gray squares) sites

Fig. 4.5 (a-b) Dissolved inorganic nitrogen (DIN) and (c-d) dissolved inorganic phosphorus (DIP) measured along a transect during low SAV biomass (left panels) and high SAV biomass (right panels). Gray shaded area represents the location of the SAV bed

Fig. 4.6 (a) August (2014-2015) mean N_2-N fluxes measured by incubating sediment cores in environmental chambers and collecting a time series of dissolved gas samples from the overlying water in each core. (b) Relationship between nitrate + nitrite (NO_x) concentration in the overlying water and N2-N flux rates. Open and filled circles represent fluxes measured under ambient conditions and with amended NO_x concentrations, respectively

Fig. 4.7 Monthly mean (a) autotroph dissolved inorganic nitrogen (DIN) assimilation rates (black line, calculated through conversion of net O_2 production to CO_2 assimilation according to literature values for SAV photosynthetic quotients, and then to DIN assimilation stoichiometrically according to measured C:N molar ratios), denitrification rates (gray dashed line), measured through sediment-water N_2-N flux

experiments, and autotrophic dissolved inorganic phosphorous (DIP) assimilation, calculated using the same method as used for DIN

Fig. 4.8 Time series for river discharge, tidal height adjusted to mean lower low water (MLLW), and water velocity measured during low SAV biomass (July, left) and high SAV biomass (September, right) 2013

Fig. 4.9 Time series for river discharge, tidal height adjusted to mean lower low water (MLLW), and water velocity during low SAV biomass (June 2015, left) and high SAV biomass (August 2014, right)

Fig 4.10 East-west velocity components plotted against north-south velocity components at the Bed 1 site in July (a) and September (b) 2013 illustrate the dominant flow direction

Fig 4.11 Summary of pore water nutrient concentrations in July (a-b) and September (c-d) 2013 measured at the Bed 1 (white), Edge (light gray), and Bed 2 (dark gray) sites. Horizontal bars indicate between-site differences at the $p<0.05$ (*), $p<0.01$ (**), and $p<0.001$ (***) significance levels. Dashed lines indicate the half-saturation concentration for root uptake by tidal fresh SAV species in Chesapeake Bay (Cerco & Moore 2001)

Fig 4.12 Relationship between mean pore water Fe and DIP concentrations measured at the Edge, Bed 1 and Bed 3 sites during low and high SAV biomass. Error bars represent standard errors

Fig. 4.13 Plant tissue (a) percent nitrogen and (b) phosphorous plotted against carbon to nitrogen and carbon to phosphorous ratios for samples collected at all sites and on all sample dates (x- and y-axes reflect the range of values reported in the literature for comparison) and carbon to (c) nitrogen and (d) phosphorous ratios measured at the Bed 2 site across months. The horizontal bar indicates a significant difference at the (*) $p<0.05$ level. Dashed lines indicate C:N and C:P ratios that are generally considered to be growth-limiting for submersed macrophytes (Duarte 1990)

Fig. 4.14 Reactive transport model output (lines) and tidally averaged dissolved inorganic nitrogen (DIN) and dissolved inorganic phosphorus (DIP) concentrations (open circles) measured during low SAV biomsass (June 2015) and high SAV biomass (August 2014) and modeled responses when parameters were increased and decreased by 25% (gray shaded areas)

Figures

Fig. 4.1

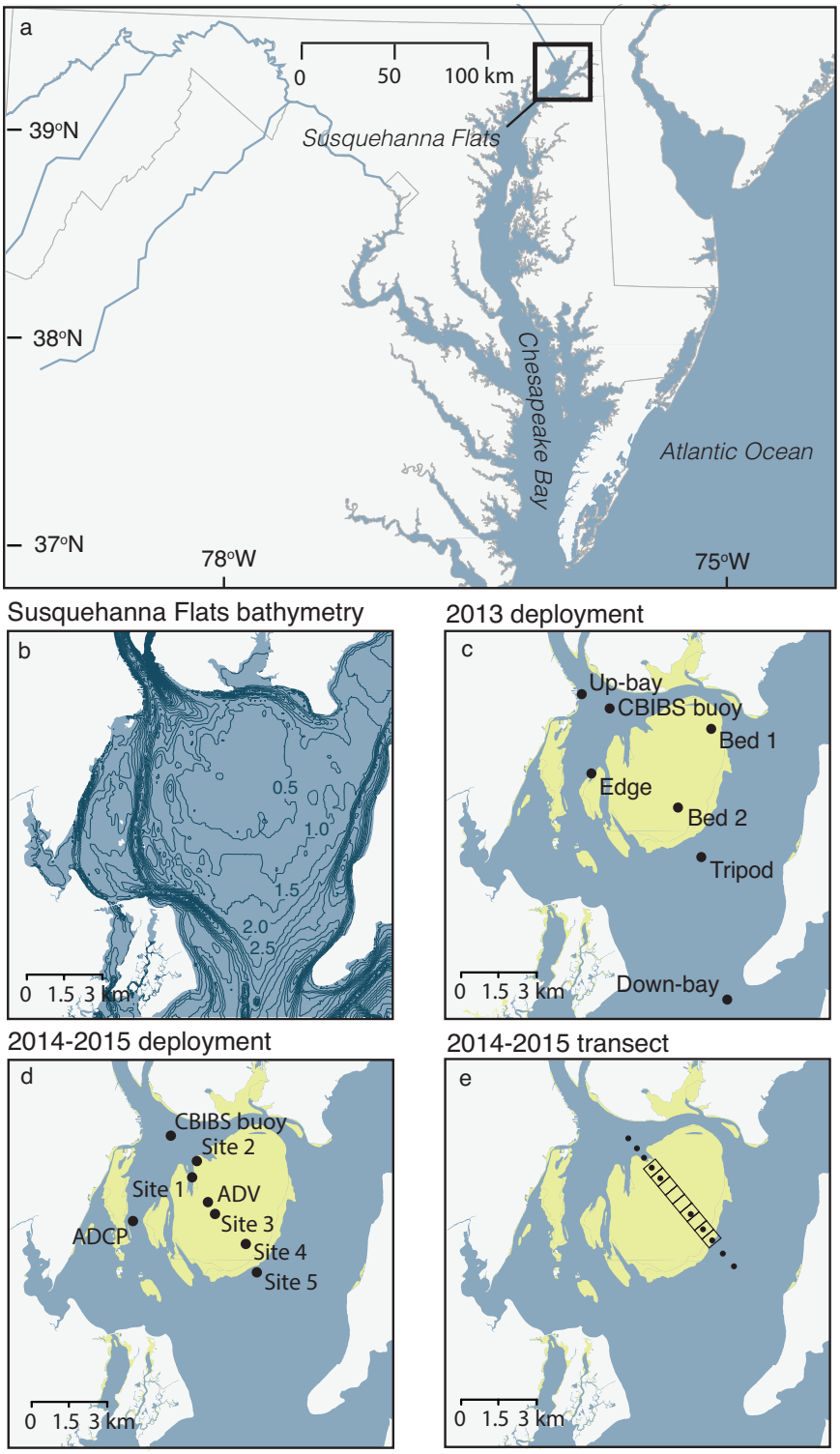

Fig. 4.2

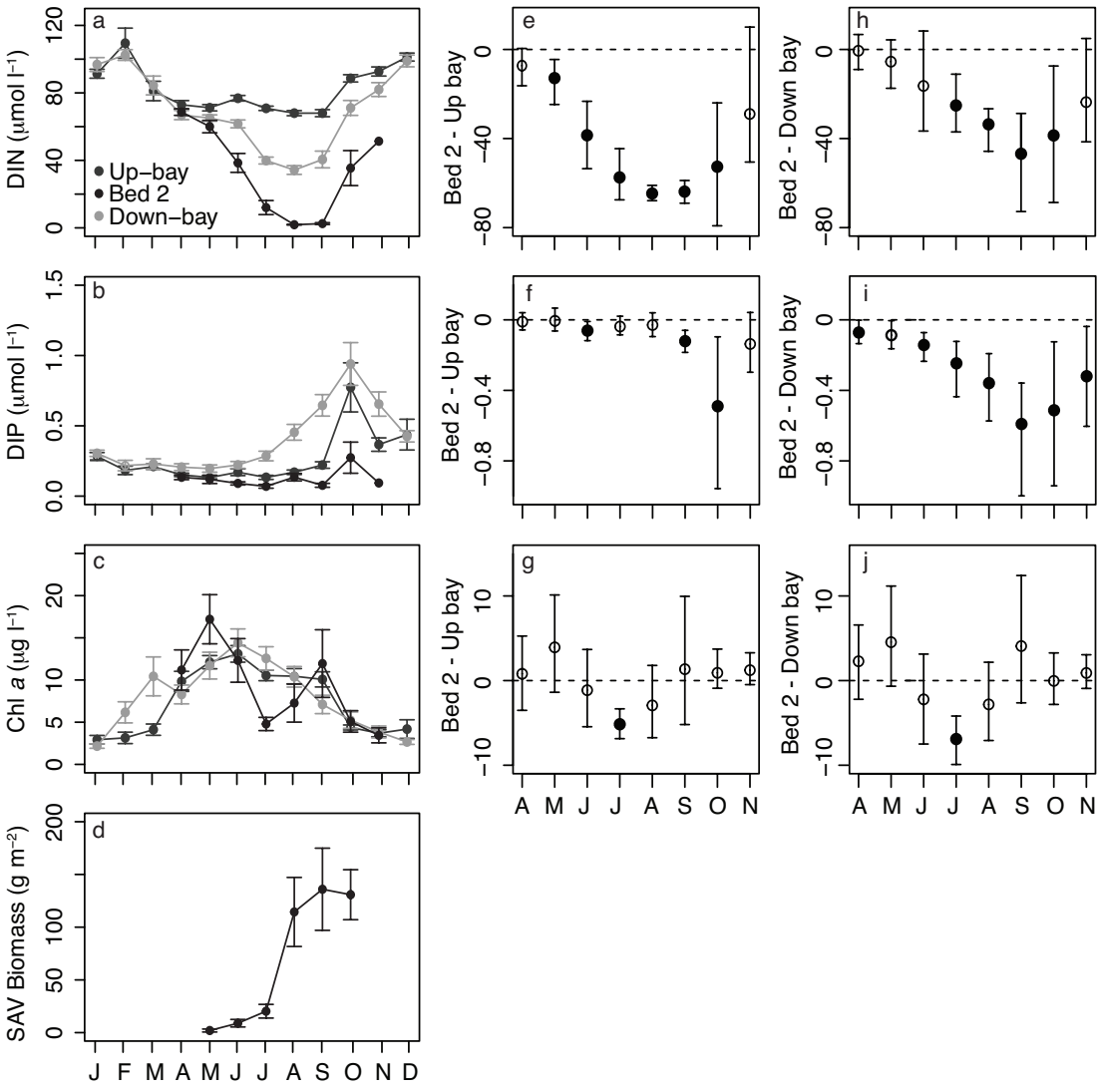
a
DIN (µmol l⁻¹)
Up–bay
Bed 2
Down–bay
b
DIP (µmol l⁻¹)
c
Chl a (µg l⁻¹)
d
SAV Biomass (g m⁻²)
J F M A M J J A S O N D
e
Bed 2 - Up bay
f
Bed 2 - Up bay
g
Bed 2 - Up bay
h
Bed 2 - Down bay
i
Bed 2 - Down bay
j
Bed 2 - Down bay
A M J J A S O N

Fig. 4.3

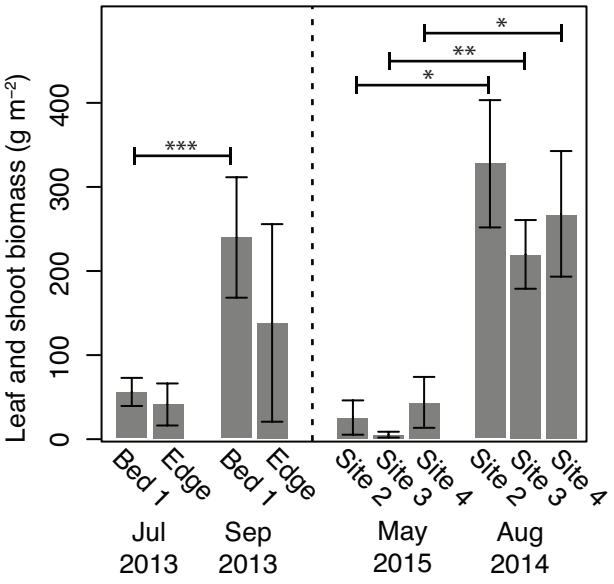
Leaf and shoot biomass (g m^{-2})
0
100
200
300
400
***
*
**
*
Bed 1
Edge
Bed 1
Edge
Site 2
Site 3
Site 4
Site 2
Site 3
Site 4
Jul 2013
Sep 2013
May 2015
Aug 2014

Fig. 4.4

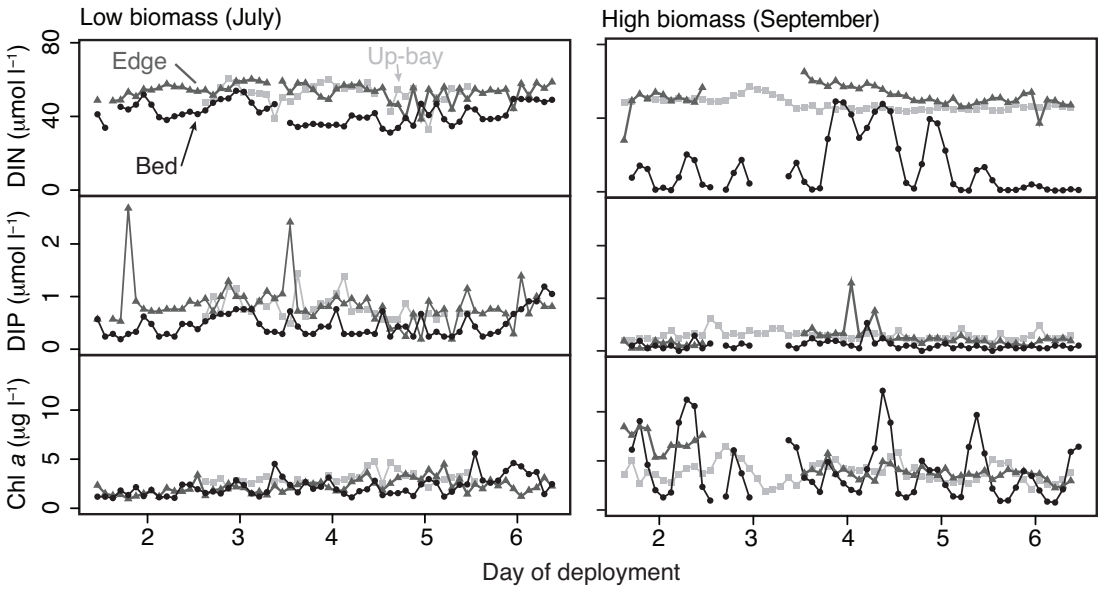
Low biomass (July)
High biomass (September)
Edge
Up-bay
Bed
DIN (μmol l⁻¹)
DIP (μmol l⁻¹)
Chl a (μg l⁻¹)
0
40
80
0
1
2
0
5
10
2
3
4
5
6
Day of deployment

Fig. 4.5

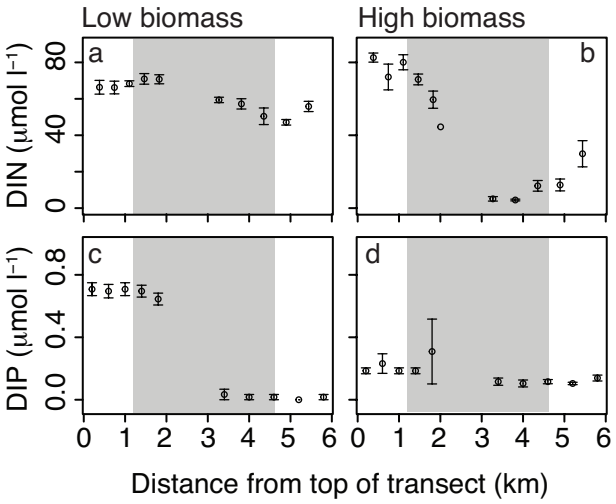
Low biomass
High biomass
a
b
c
d
DIN (µmol l⁻¹)
DIP (µmol l⁻¹)
0
40
80
0.0
0.4
0.8
0 1 2 3 4 5 6
Distance from top of transect (km)

Fig. 4.6

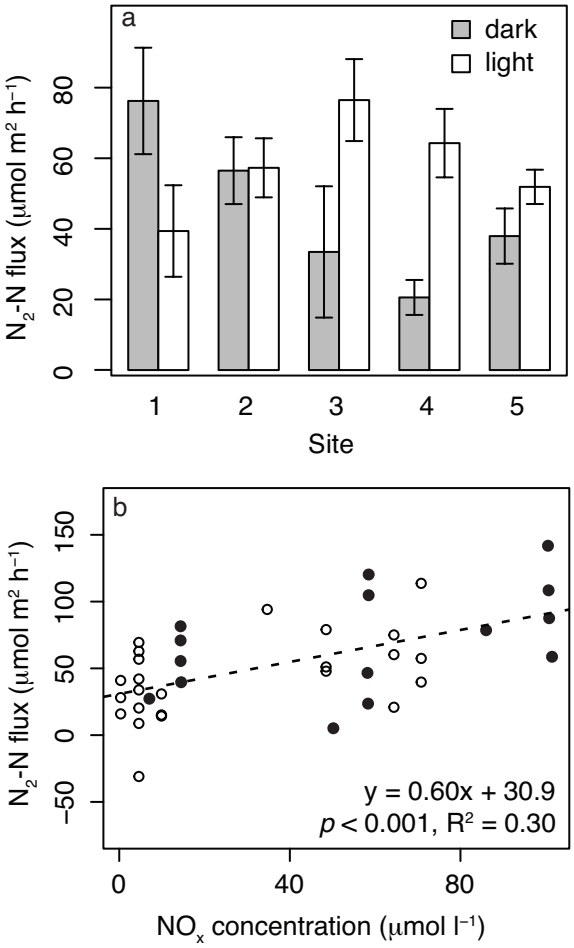
a
dark
light
N_2-N flux (μmol m^2 h^{-1})
0
20
40
60
80
1
2
3
4
5
Site
b
N_2-N flux (μmol m^2 h^{-1})
−50
0
50
100
150
y = 0.60x + 30.9
$p < 0.001$, $R^2 = 0.30$
0
40
80
NO_x concentration (μmol l^{-1})

Fig. 4.7

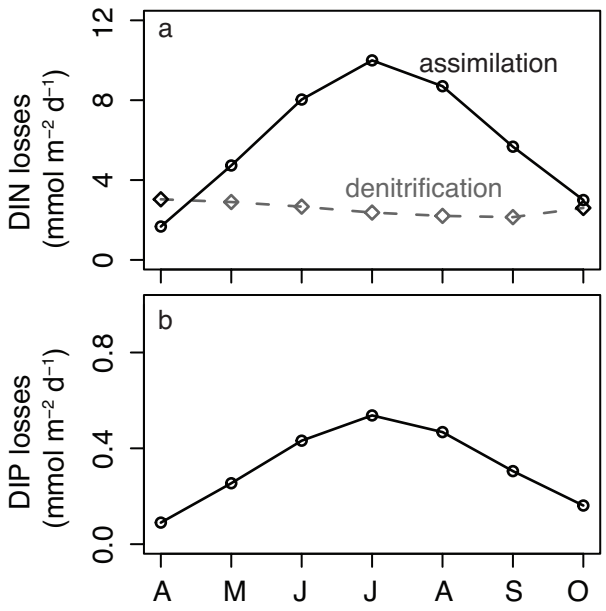
a
assimilation
denitrification
DIN losses
(mmol m^{-2} d^{-1})
0
4
8
12
b
DIP losses
(mmol m^{-2} d^{-1})
0.0
0.4
0.8
A
M
J
J
A
S
O

Fig. 4.8

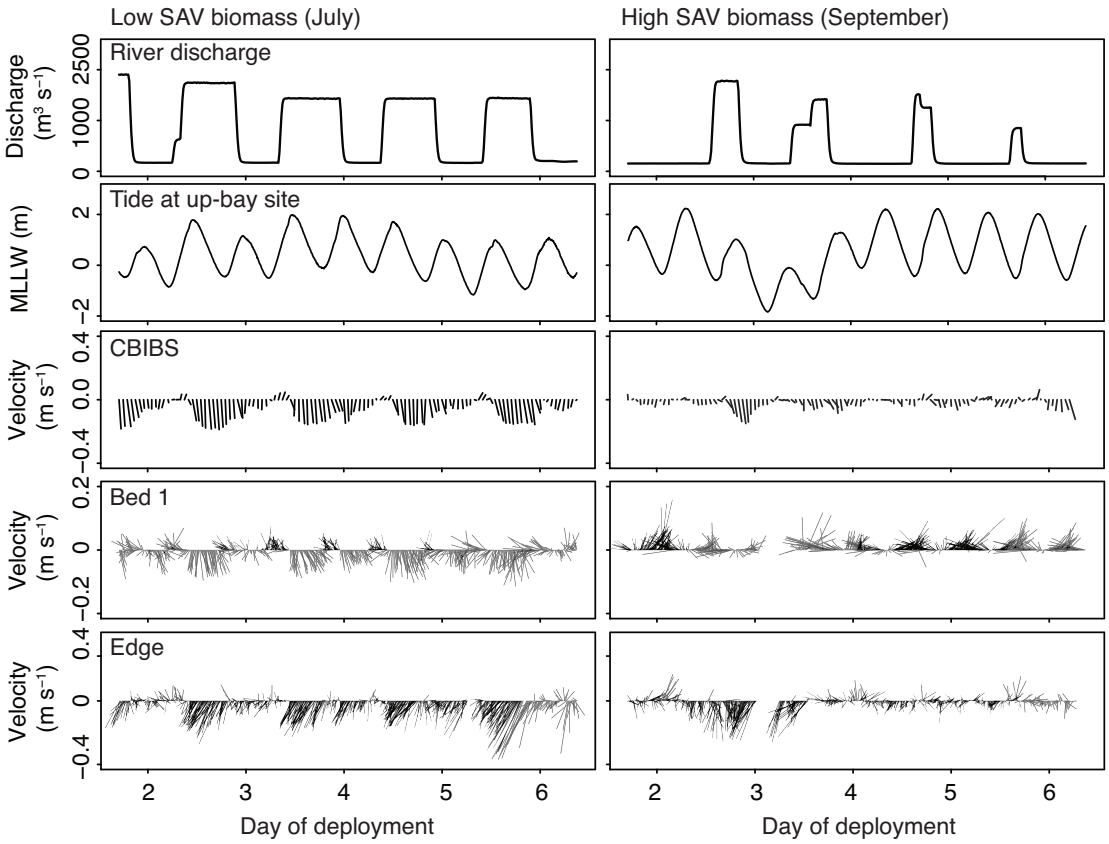
Low SAV biomass (July)
High SAV biomass (September)
River discharge
Discharge (m³ s⁻¹)
0
1000
2500
Tide at up-bay site
MLLW (m)
−2
0
2
CBIBS
Velocity (m s⁻¹)
−0.4
0.0
0.4
Bed 1
Velocity (m s⁻¹)
−0.2
0
0.2
Edge
Velocity (m s⁻¹)
−0.4
0
0.4
2
3
4
5
6
Day of deployment
Day of deployment

Fig. 4.9

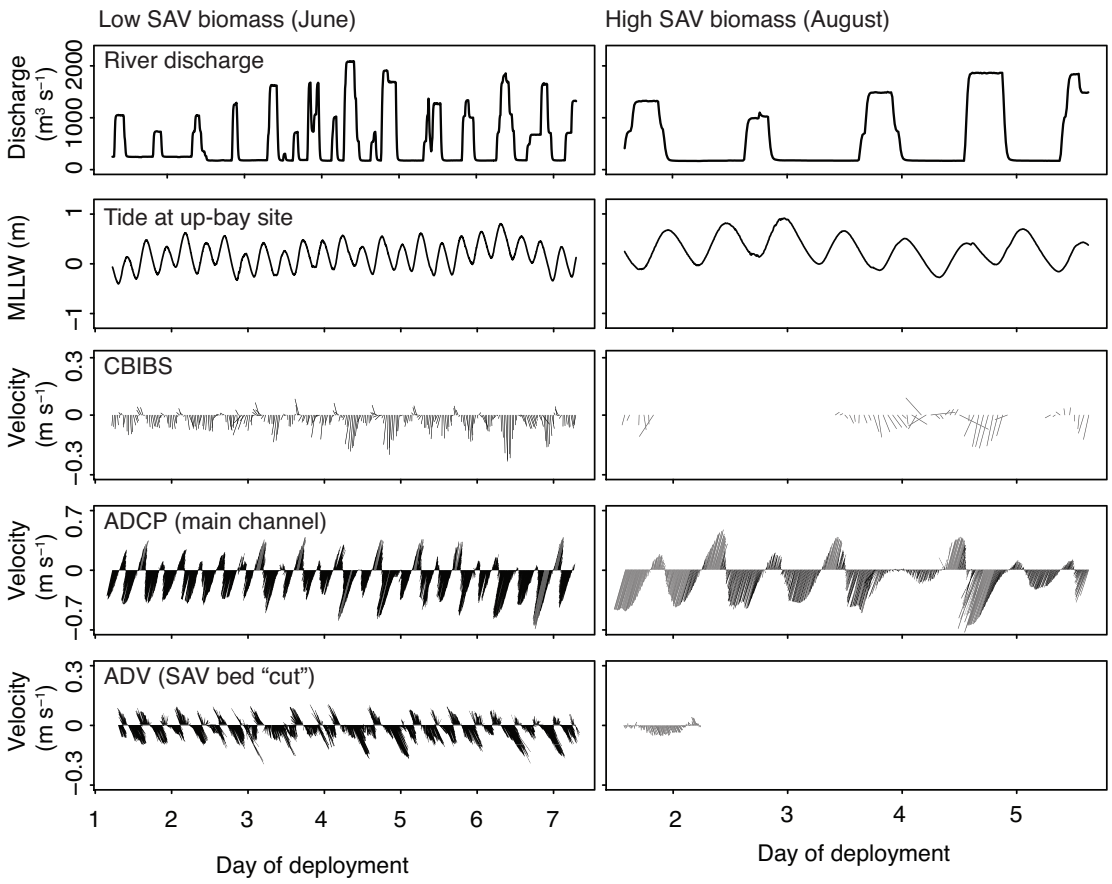
Low SAV biomass (June)
High SAV biomass (August)
River discharge
Discharge (m³ s⁻¹)
0 1000 2000
Tide at up-bay site
MLLW (m)
1 0 −1
CBIBS
ADCP (main channel)
ADV (SAV bed "cut")
Velocity (m s⁻¹)
0.3 0 −0.3
0.7 0 −0.7
1 2 3 4 5 6 7
2 3 4 5
Day of deployment
Day of deployment

Fig. 4.10

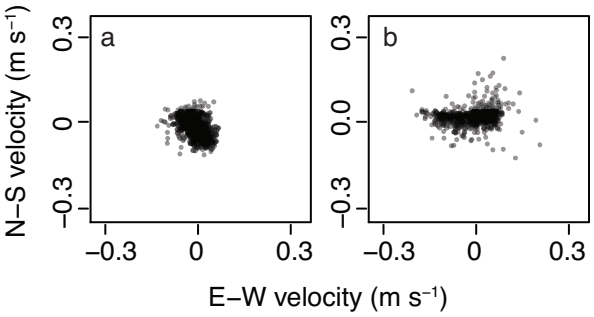

Fig. 4.11

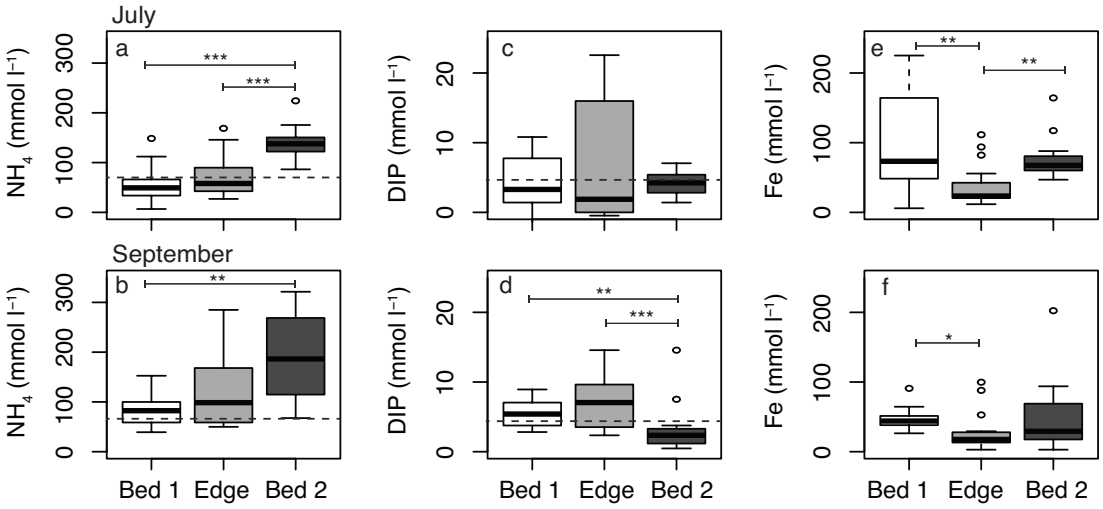
July
September
a
b
c
d
e
f
NH_4 (mmol l^{-1})
DIP (mmol l^{-1})
Fe (mmol l^{-1})
0 100 200 300
0 10 20
0 100 200
***
**
*
Bed 1
Edge
Bed 2

Fig. 4.12

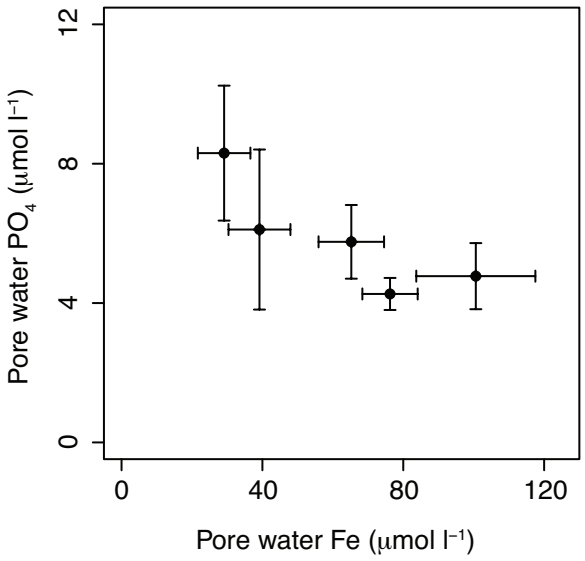

Fig. 4.13

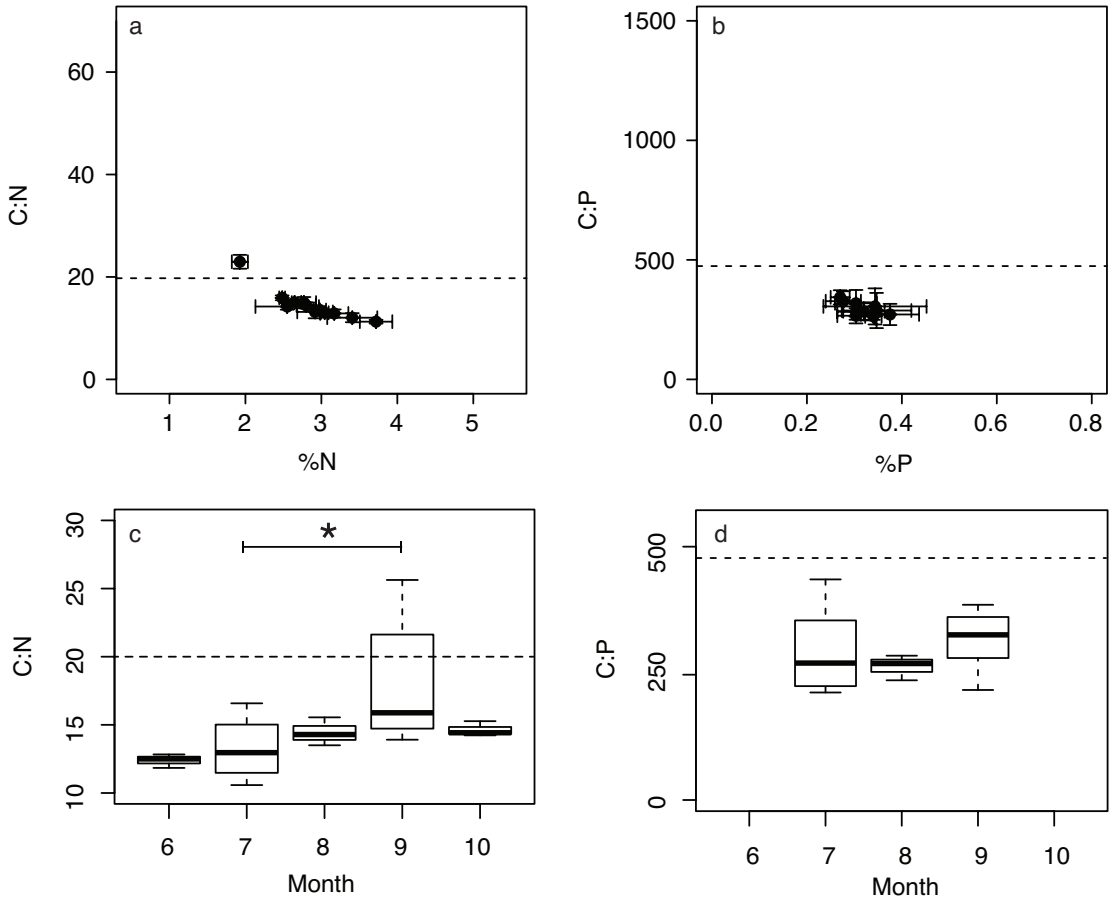

Fig. 4.14

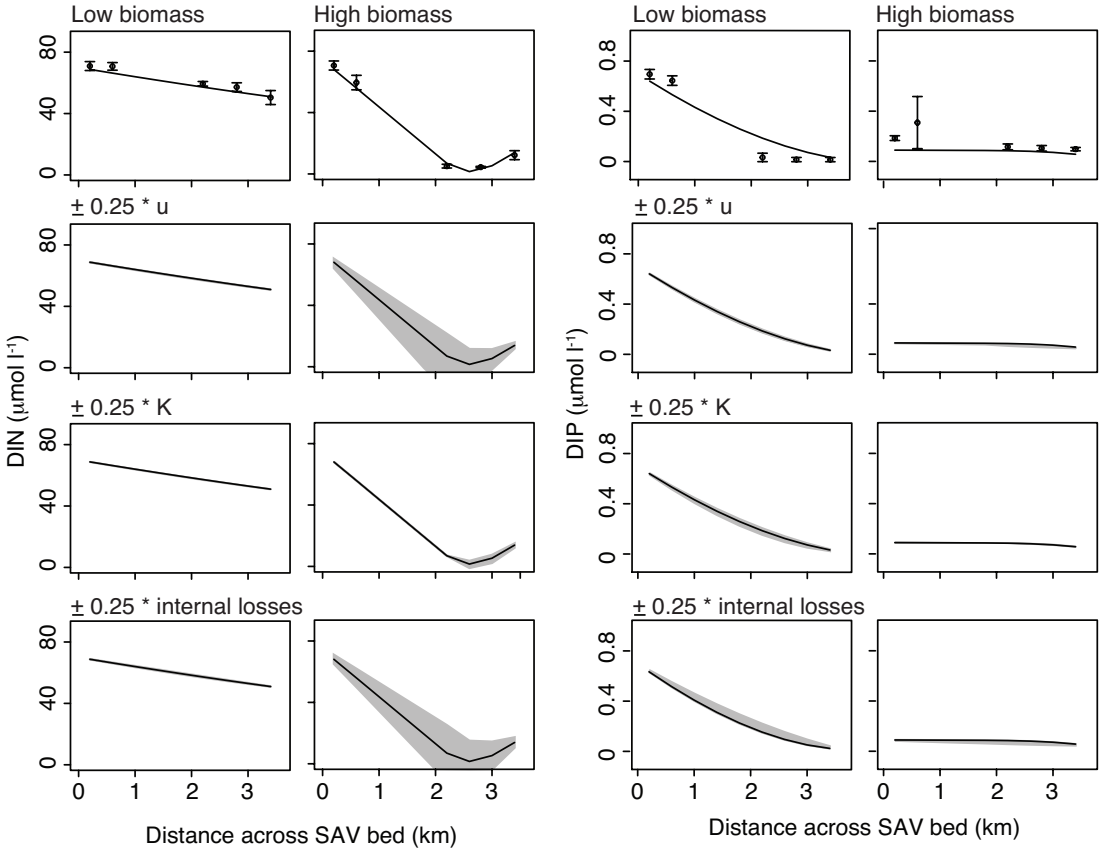
Low biomass
High biomass
Low biomass
High biomass
± 0.25 * u
± 0.25 * u
± 0.25 * K
± 0.25 * K
± 0.25 * internal losses
± 0.25 * internal losses
DIN (µmol l-1)
DIP (µmol l-1)
0
40
80
0.4
0.8
0
1
2
3
Distance across SAV bed (km)
Distance across SAV bed (km)

Chapter 5: Summary and synthesis

In the three preceding chapters, I used a combination of existing time series datasets, field data collection and experiments, and simple simulation models to quantify a suite of variables and processes in and around a large SAV bed in upper Chesapeake Bay. Together and in the context of theoretical and empirical literature, these synthetic analyses allowed me to draw inferences about the internal and external drivers of ecological dynamics in this system.

Chapter 2 showed that modest but statistically significant reductions in nutrient loading, coupled with a series of six consecutive dry years without a major flood event likely facilitated the SAV resurgence. Furthermore, seasonal differences in several water quality variables measured inside and outside the SAV bed implied the presence of strong positive feedback processes. These feedbacks may have played a role in the sudden nature of the recovery because they could have reinforced the state of the bed before and after the abrupt shift.

Chapter 3 showed that while scour and poor water clarity associated with sediment deposition during the 2011 flood event were mechanisms of plant loss, interactions between the bed, water flow, and waves served as mechanisms of resilience. Specifically, water was shunted around the bed and into the adjacent channel, resulting in lower flow velocities in the bed and higher velocities in the channel. Plants located towards the center of the bed were, therefore protected from

scour during the flood. In addition, the bed attenuated wind driven waves, leading to decreased resuspension of recently deposited sediments inside the bed and, thus, improved water clarity during periods of high SAV biomass following the flood. Furthermore, clear water from the inner core of the bed "spilled over" into adjacent regions in which plants were lost, thereby increasing the amount of light reaching the bottom and, thus, creating conditions favorable for regrowth. These positive feedback processes were mechanisms of resilience because they helped prevent plant loss and will potentially facilitate recovery.

Chapter 4 showed that interactions between physical and biogeochemical processes led to low nutrient concentrations inside the bed relative to outside the bed. For instance, as the bed developed and plant biomass accumulated throughout the growing season, it increasingly attenuated flow, thereby increasing water residence time inside the bed. As a result, there was more time for biological and biogeochemical processes, such as plant assimilation and denitrification, to draw down water column nutrient concentrations during the summer. Phytoplankton and epiphyte growth rates were likely nutrient limited, whereas sediment pore water concentrations were sufficient to satisfy SAV nutritional demand through root uptake. Interactions among these feedback processes, therefore, created conditions that precluded algal growth and reinforced vascular plant dominance in the system.

One recurring theme across all three chapters is the importance of feedback processes in controlling the structure and function of this ecosystem. A great deal of research has been undertaken over the past half-century to develop our understanding of the mechanisms driving ecological feedbacks and how they affect resilience and

ecosystem structure. For example, Holling (1973) and May (1977) drew from concepts in physics and engineering to develop the mathematical basis for how feedbacks influence resilience and breakpoints in natural systems. Scheffer (1990) applied the concepts of thresholds and feedbacks to aquatic ecosystems (i.e., shallow lakes) and Carpenter et al. (2001) demonstrated that the effect of internal processes on aquatic ecosystem structure can be shown through whole-ecosystem manipulative experiments. Many studies have subsequently built on these efforts to investigate, in detail, the mechanisms controlling biophysical (e.g., Peterson et al. 2004; Bouma et al. 2007; Carr et al. 2010; Luhar and Nepf 2013) and biogeochemical (e.g., Caffrey and Kemp 1992; Rysgaard et al. 1996; McGlathery et al. 1998; Eyre et al. 2010) feedback processes and how they affect shallow aquatic ecosystems.

My findings are relevant within this broader context because they demonstrate that a comprehensive, interdisciplinary approach involving diverse methods can be used to gain an in-depth understanding of the underlying mechanisms driving feedbacks in an SAV bed and how these processes influence the structure and dynamics of a particular system. In addition, although I show that feedbacks allow for SAV bed resilience to storm events and eutrophication, these processes are unable to act as a buffer beyond threshold rates of water flow, sediment loading, and/or nutrient loading. Furthermore, projected climatological increases in the frequency and intensity of extreme weather events call into question the future capacity of these systems to absorb and recover from disturbances. Management actions should aim to proactively cultivate resilient SAV ecosystems by mitigating stressors that can readily be controlled (i.e., anthropogenic nutrient and sediment sources).

Appendix I: Hydrodynamic model formulation and R code

The following R code, developed by L. Sanford and based on Fagherazzi et al. (2003), models flow in an idealized embayment system with geometry based on the lower Susquehanna River and the Susquehanna Flats region, assuming constant river flow interacting with a standing wave tide. The model is developed for a constant width deep channel adjacent to a variable width subtidal flat with and without grass. The initial solution considers the inviscid case, so all velocities are equal across any given cross-section. A second iteration considers the differing influences of bottom friction on flow over the channel and the shoals, assuming a slowly varying steady state shallow water balance between pressure gradient and vertical stress gradient. The script uses the R package pracma, which should be installed in advance of running the script.

Key parameters are river flow (Qr) and the square root of the ratio of the channel drag coefficient to the shoal drag coefficient (b), which represents increased drag on the shoal due to the presence of an SAV bed. $b = 1$ represents no SAV on the shoal. We use $b = 0.2$ to represent a dense SAV bed. The simulated velocities for $b = 0.2$ are consistent with a limited set of velocity measurements we made on the shoal and in the channel (Table A1.1).

River_flow	Observed	Modeled	Location
996	0.05	0.05	Shoal
402	0.04	0.05	Shoal
610	0.13	0.17	Channel

Table A1.1 Modeled vs. observed flow velocities

These parameters can be changed to simulate different river flows or SAV bed densities. The depth of the channel ($h1$) and shoal ($h2$) can also be modified.

```
rm(list=ls())
Qr = 1100
b = 1
h1 = 6
h2 = 1.5
```

The first step is to define model geometry. $w1$ represents the initial width of the river channel; $w2$ and $w3$ create the curved shape of the shoal. The total width (w) includes the curved shoal and straight channel. At its widest point, total width is 5 km on each side, for a total of 10 km. The length (x) begins at the head of tide and ends at Turkey Point. A represents the cumulative surface area for a given distance along x (x = 18 km).

```
library(pracma)
x = seq(0, 18000, 100)
w1 = 1000 * rep(1, length(x))
w2 = 0.25 * (x - 6000)
w2[w2 < 0] = 0
w3 = 3750 * (1 - cos(2 * pi/12000 * (x - 6000)))
w3[1:60] = 0
w = w1 + w2 + w3
w2 = w - w1
A = cumtrapz(x, w)
```

Next, we define tidal time-varying parameters in the channel ($h1$) and the shoal ($h2$). t (h) is a time vector that covers 1 M2 tidal cycle. omt is the tidal radian frequency (h^{-1}) and at is the tidal amplitude (m),

```
t=seq(0,12.42,0.1)
omt=2*pi/12.42
at=0.35
h1=h1+at*sin(omt*t)
h2=h2+at*sin(omt*t)
```

Total flow (Q) is calculated as a combination of river flow (Qr) and tidal flow.

```
Q=matrix(0,length(t),length(x))
dhdt=rep(0,length(t))
for (i in 1:length(t)){
    dhdt[i]=at*omt*cos(omt*t[i])/3600
    for (j in 1:length(x)){
        Q[i,j]=(Qr-A[j]*dhdt[i])
        }
    }
```

Next, we calculate potential flow velocities, where frictional effects are not considered.

```
Across=matrix(1,length(t),length(x))
U=matrix(0,length(t),length(x))
for (i in 1:length(t)){
    Across[i,]=w1*h1[i]+w2*h2[i]
  U[i,]=Q[i,]/Across[i,]
}
```

Now, we consider changes induced by the shallow water momentum balance and we partition flow and velocity between the channel and shoal.

```
U1=matrix(0,nrow(U),ncol(U))
U2=matrix(0,nrow(U),ncol(U))
Q1=matrix(0,nrow(Q),ncol(Q))
Q2=matrix(0,nrow(Q),ncol(Q))

for (i in 1:length(t)){
U1[i,]=Q[i,]/(h1[i]*w1+b*sqrt(h2[i]/h1[i])*h2[i]*w2)
U2[i,]=b*sqrt(h2[i]/h1[i])*U1[i,]
Q1[i,]=U1[i,]*w1*h1[i]
Q2[i,]=U2[i,]*w2*h2[i]
}

dU1dx=matrix(0,length(t),length(x))
dV1dy=matrix(0,length(t),length(x))
V2edge=matrix(0,length(t),length(x))
for (i in 1:length(t)){
    dU1dx[i,]=gradient(U1[i,],100)
    dV1dy[i,]= -1*dhdt[i]/h1[i]-dU1dx[i,]
    }
kk=which(w2>=0.1)
for (i in 1:length(t)){
    V2edge[i,kk]=dV1dy[i,kk]*w1[kk]/2*h1[i]/h2[i]
}
```

Calculate curvature of Flats shoal far boundary.

```
dwdx=gradient(w/2,100)
V2w=matrix(0,length(t),length(x))
for (i in 1:length(t)){
V2w[i,]=dwdx*U2[i,]
}

wgrid=100*c(0:round((max(w)/200),digits=0))
XY=meshgrid(x,wgrid)
U=array(0,dim=c(size(XY$X)[1],size(XY$X)[2],length(t)))
V=array(0,dim=c(size(XY$X)[1],size(XY$X)[2],length(t)))
for (i in 1:length(t)){
   for (j in 1:ncol(XY$X)){
       k1=which(XY$Y[,j]<=w1[j]/2) #channel
       k2=which((XY$Y[,j]>w1[j]/2)&(XY$Y[,j]<=w[j]/2)) #shoal
       U[k1,j,i]=U1[i,j]
       V[k1,j,i]=XY$Y[k1,j]*dV1dy[i,j]
       if (length(k2)>0){
           U[k2,j,i]=U2[i,j]
           V[k2,j,i]= -interp1(c(w1[j]/2,w[j]/2),c(V2edge[i,j],V2w[i
,j]),XY$Y[k2,j],method="linear")
       }
   }
}
```

Use velocity to calculate bottom stress (τ_b) according to the equation $\tau_b = 1000 *$

$0.0015 * u^2 + v^2$

```
wgrid=100*c(0:round((max(w)/200),digits=0))
XY=meshgrid(x,wgrid)
taub=array(0.001,dim=c(size(XY$X)[1],size(XY$X)[2],length(t)))
for (i in 1:length(t)){
    taub[,,i]=1000*0.0015*(U[,,i]^2+V[,,i]^2)
    }
```

Flip the grid to create the top half of the system for u, v and τ_b.

```
Uneg=array(0,dim=c((size(XY$X)[1]),size(XY$X)[2],length(t)))
Vneg=array(0,dim=c((size(XY$X)[1]),size(XY$X)[2],length(t)))
taubneg=array(0.001,dim=c((size(XY$X)[1]),size(XY$X)[2],length(t)))
for(i in 1:length(t)){
  Uneg[,,i]=flipud(U[,,i])
  Vneg[,,i]= -(flipud(V[,,i]))
  taubneg[,,i]=flipud(taub[,,i])
}

Uneg=Uneg[-51,,]
Vneg=Vneg[-51,,]
taubneg=taubneg[-51,,]
```

```
Unew=array(0,dim=c((2*size(XY$X)[1]-1),size(XY$X)[2],length(t)))
Vnew=array(0,dim=c((2*size(XY$X)[1]-1),size(XY$X)[2],length(t)))
taubnew=array(0.001,dim=c((2*size(XY$X)[1]-1),size(XY$X)[2],length(t
)))
for(i in 1:length(t)){
  Unew[,,i]=rbind(Uneg[,,i],U[,,i])
  Vnew[,,i]=rbind(Vneg[,,i],V[,,i])
  taubnew[,,i]=rbind(taubneg[,,i],taub[,,i])
}
```

Calculate mean u, v, and τ_b over all time steps.

```
Umean=apply(Unew,1:2,mean)
Vmean=apply(Vnew,1:2,mean)
taubmean=apply(taubnew,1:2,mean)
```

Appendix II: Supplementary tables and figures

Tables

Table AII.1. Sediment sand and mud fractions and sediment chl *a* (mean, standard deviation, mg m^{-2}) from sediment-water flux experiments.

Site	Date	% Sand	% Mud	Sediment chl *a*
1	8/4/14	96	4	9.2, 7.8
2	8/4/14	92	8	34.6, 37.3
3	8/5/14	65	35	12.9, 8.4
4	8/4/14	95	5	18.6, 14.8
5	8/5/14	95	5	12.9, 9.5
1	5/29/15	97	3	6.4, 0.8
2	5/29/15	94	6	9.1, 3.9
3	5/29/15	90	10	28.7, 13.5
4	5/29/15	93	7	13.8, 7.7
5	5/29/15	93	7	2.6, 1.5
1	8/26/15	96	4	5.1, 1.4
2	8/26/15	73	27	9.9, 3.0
3	8/26/15	54	46	17.2, 7.4
4	8/26/15	93	7	12.3, 1.8
5	8/26/15	92	8	7.7, 2.9

Figure Captions

Fig. AII.1 Sediment water flux rates for N2-n, nitrate+nitrite (NOx), ammonium (NH4), and oxygen (O2) in the dark (shaded bars) and under illumination (white bars).

Fig. AII.2 Time series plots from the 2013 deployments, including the same data as that presented in Fig. 8 but additionally including wind velocity and flow data collected at the Tripod and Bed 2 sites.

Fig. AII.3 East-west vs. north-south velocity components from July (left) and September 2013 (right) for all sites in which flow was measured.

Fig. AII.4 Time series plots from the 2014-2015 deployments, including the same data as that presented in Fig. 9 but additionally including wind velocity and flow data collected at Sites 2 and 4.

Fig. AII.5 Along-channel current velocities in the channel (gray line) and the "cut" inside the SAV bed (black line) in June (left) and August (right).

Fig. AII.6 East-west vs. north-south velocity components from May 2015 (left) and Aug 2014 (right)

Fig AII.7 Depth profiles of porewater nutrient concentrations in July (a-d) and September (e-h) 2013 measured at the SAV bed 1 (light green squares), bed 2 (dark green triangles) and edge (blue circles) sites.

Figures

Fig. AII.1

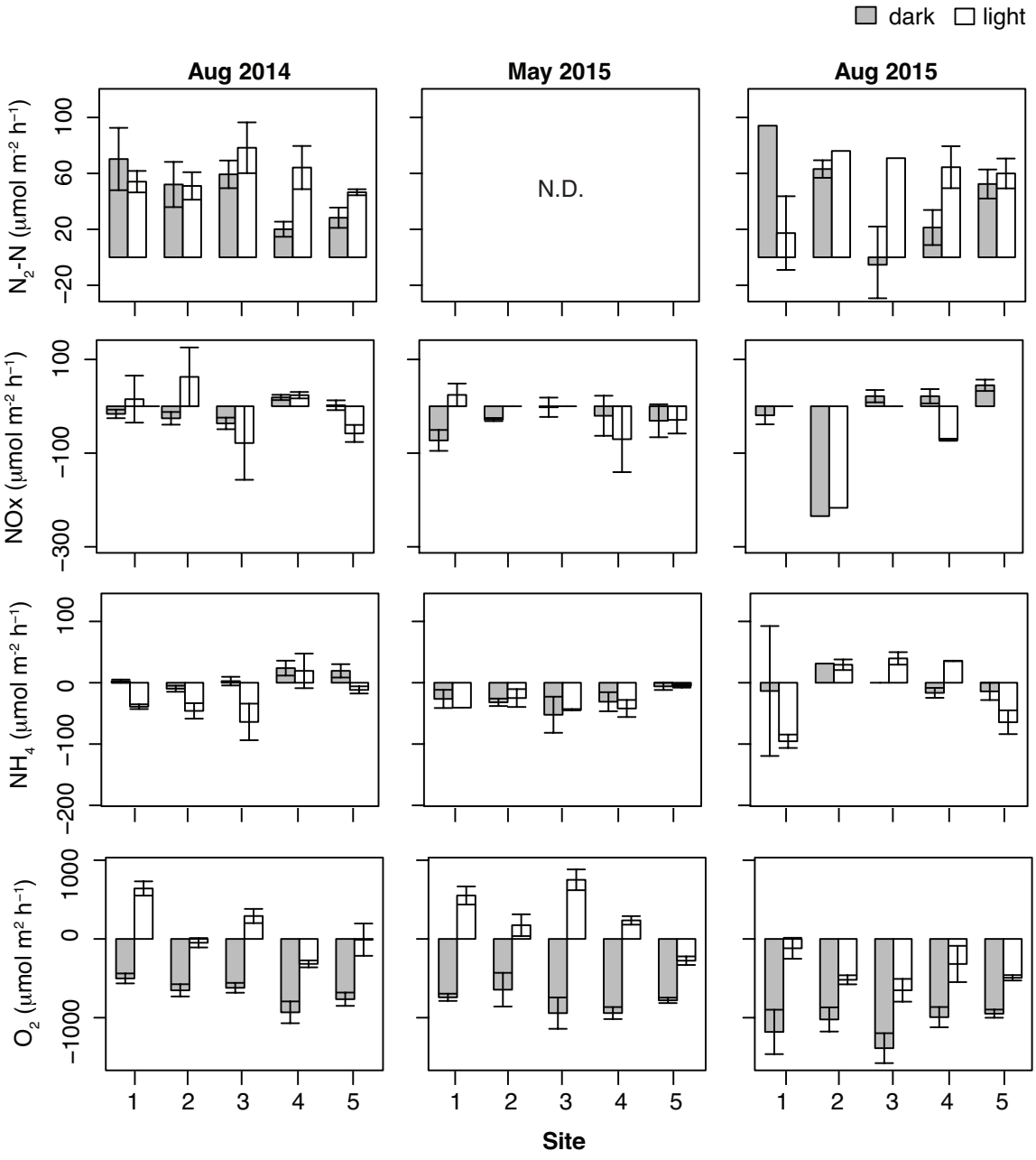

Fig. AII.2

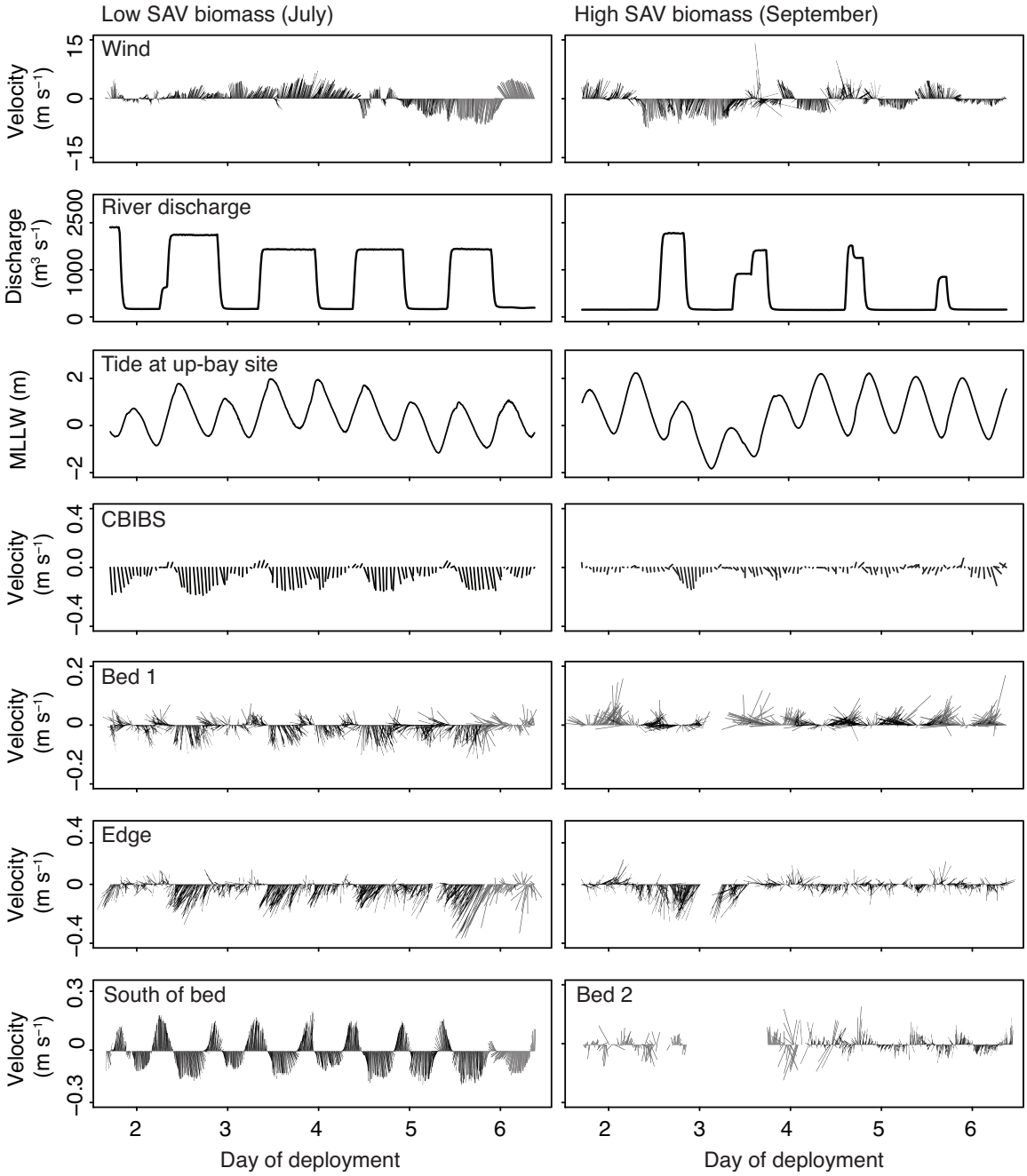
Low SAV biomass (July)
High SAV biomass (September)
Wind
Velocity (m s⁻¹)
15
0
−15
River discharge
Discharge (m³ s⁻¹)
0
1000
2500
Tide at up-bay site
MLLW (m)
2
0
−2
CBIBS
Velocity (m s⁻¹)
0.4
0.0
−0.4
Bed 1
Velocity (m s⁻¹)
0.2
0
−0.2
Edge
Velocity (m s⁻¹)
0.4
0
−0.4
South of bed
Bed 2
Velocity (m s⁻¹)
0.3
0
−0.3
2
3
4
5
6
Day of deployment
Day of deployment

Fig. AII.3

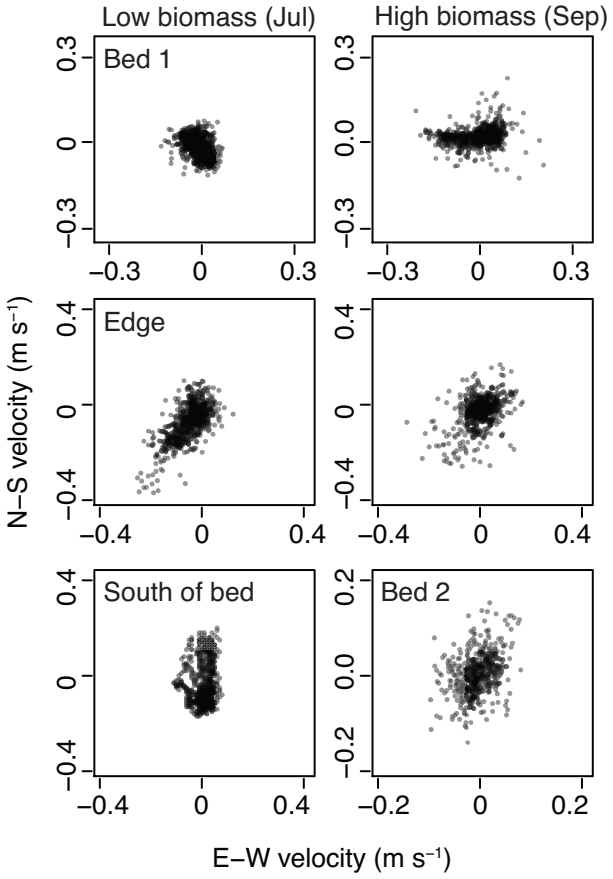
Low biomass (Jul)
High biomass (Sep)
Bed 1
Edge
South of bed
Bed 2
N–S velocity (m s⁻¹)
E–W velocity (m s⁻¹)

Fig AII.4

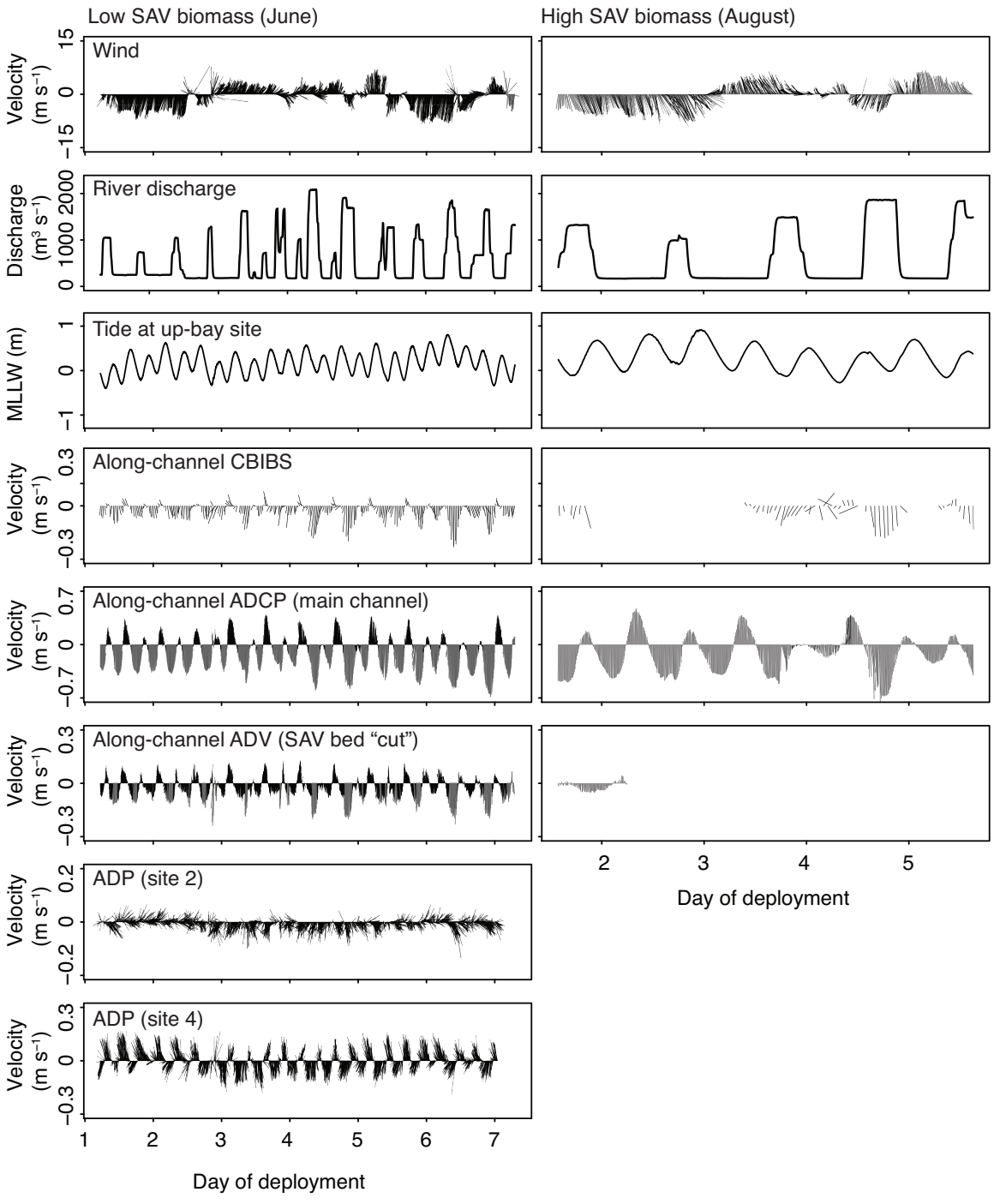
Low SAV biomass (June)
High SAV biomass (August)
Wind
Velocity (m s⁻¹)
15
0
−15
River discharge
Discharge (m³ s⁻¹)
0
1000
2000
Tide at up-bay site
MLLW (m)
1
0
−1
Along-channel CBIBS
Velocity (m s⁻¹)
0.3
0
−0.3
Along-channel ADCP (main channel)
Velocity (m s⁻¹)
0.7
0
−0.7
Along-channel ADV (SAV bed “cut”)
Velocity (m s⁻¹)
0.3
0
−0.3
ADP (site 2)
Velocity (m s⁻¹)
0.2
0
−0.2
ADP (site 4)
Velocity (m s⁻¹)
0.3
0
−0.3
1
2
3
4
5
6
7
Day of deployment
2
3
4
5
Day of deployment

Fig. A2.5

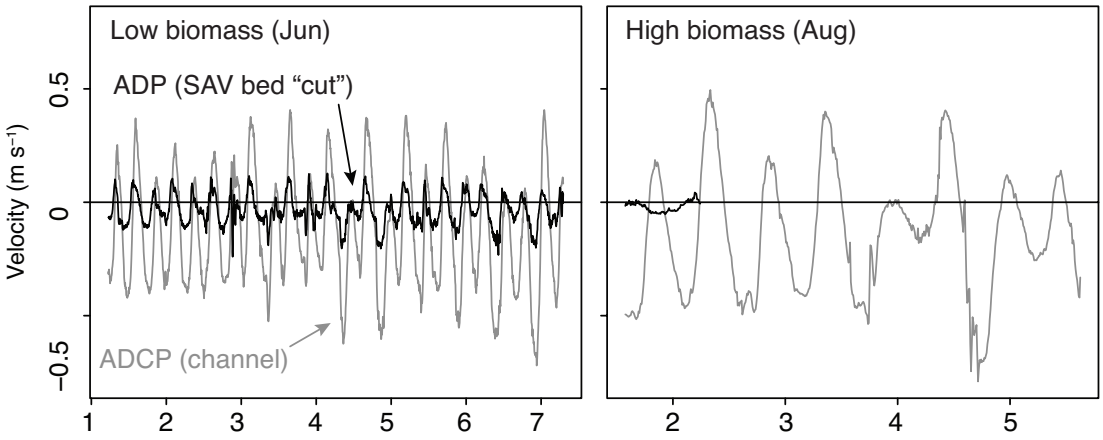
Low biomass (Jun)
High biomass (Aug)
ADP (SAV bed "cut")
ADCP (channel)
Velocity (m s⁻¹)
0.5
0
−0.5
1
2
3
4
5
6
7

Fig. AII.6

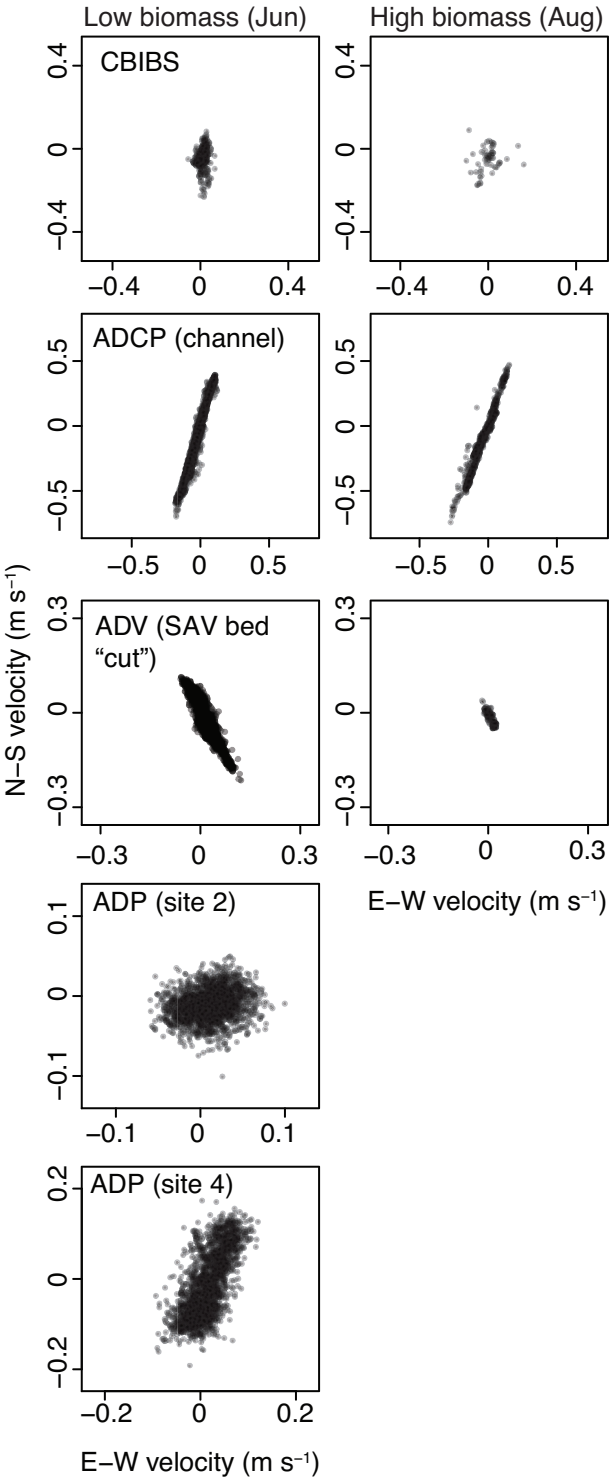
Low biomass (Jun)
High biomass (Aug)
CBIBS
ADCP (channel)
ADV (SAV bed "cut")
ADP (site 2)
ADP (site 4)
N–S velocity (m s⁻¹)
E–W velocity (m s⁻¹)
E–W velocity (m s⁻¹)

Fig. AII.8

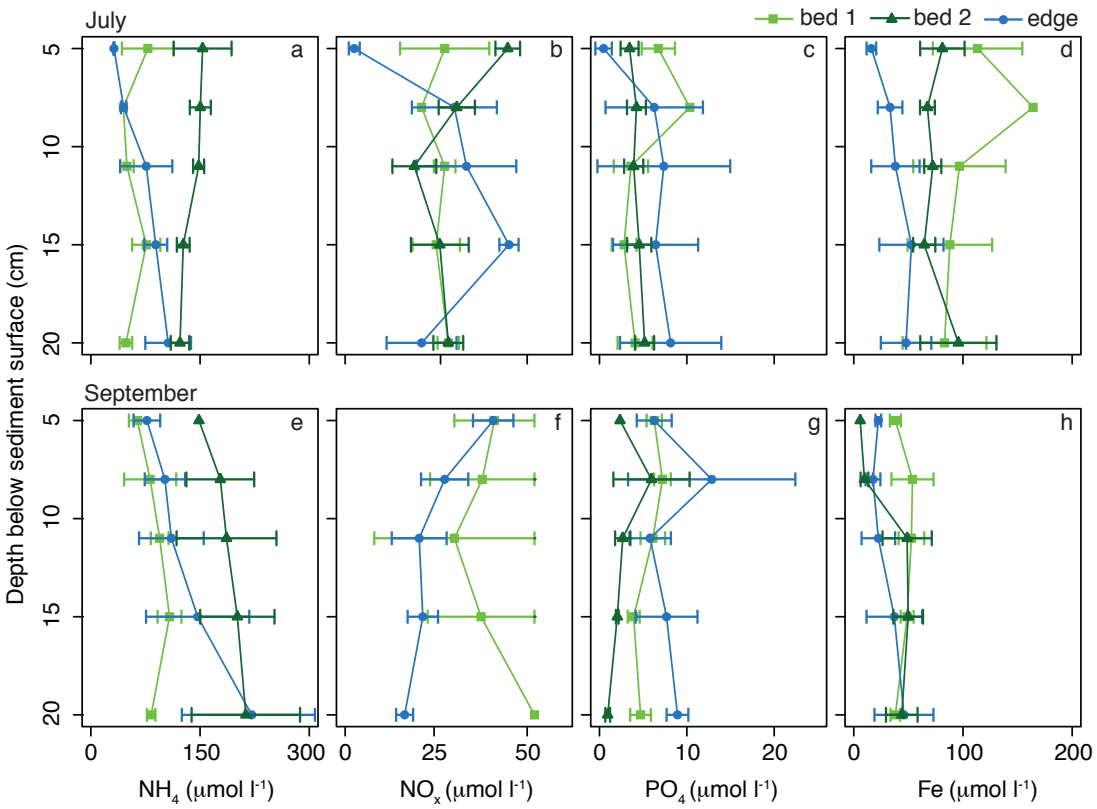
July
September
bed 1
bed 2
edge
a
b
c
d
e
f
g
h
Depth below sediment surface (cm)
5
10
15
20
0
150
300
25
50
10
20
100
200
NH4 (µmol l-1)
NOx (µmol l-1)
PO4 (µmol l-1)
Fe (µmol l-1)

References

Alcoverro, T., R. C. Zimmerman, D. G. Kohrs, and R. S. Alberte. 1999. Resource allocation and sucrose mobilization in light-limited eelgrass Zostera marina. Mar. Ecol. Prog. Ser. **187**: 121–131. doi:10.3354/meps187121.

Aspila, K. I., H. Agemian, and A.S.Y. Chau. 1976. Semi-automated method for determination of inorganic, organic, and total phosphate in sediments. Analyst **101**: 187–197, doi:10.1039/an9760100187

Allen, J. R. L. 1985. Principles of physical sedimentology. London: George Allen & Unwin Ltd

An, S., and S. B. Joye. 2001. Enhancement of coupled nitrification-denitrification by benthic photosynthesis in shallow estuarine sediments. Limnol. Oceanogr. **46**: 62–74.

Barbier, E. B., S. D. Hacker, C. Kennedy, E. W. Koch, A. C. Stier, and B. R. Silliman. 2011. The value of estuarine and coastal ecosystem services. Ecol. Monogr. **81**: 169–193. doi:10.1890/10-1510.1.

Barko, J. W., and M. R. Smart. 1981. Comparative influences of light and temperature on the growth and metabolism of selected submersed freshwater macrophytes. Ecol. Monogr. **51**: 219–236.

Bartoli, M., D. Nizzoli, G. Castaldelli, and P. Viaroli. 2008. Community metabolism and buffering capacity of nitrogen in a *Ruppia cirrhosa* meadow. Journal of Experimental Mar. Biol. and Ecol. **360**: 21–30. doi:10.1016/j.jembe.2008.03.005.

Bayley, S., V. D. Stotts, P. F. Springer, and J. Steenis. 1978. Changes in submerged aquatic macrophyte populations at the head of Chesapeake Bay, 1958-1975. Estuaries **1**: 73–84.

Blackburn, R. D., J. M. Lawrence, and D. E. Davis. 1961. Effects of light intensity and quality on the growth of *Elodea densa* and *Heteranthera dubia*. Weeds **9**: 251–257.

Bouma, T. J., L. A. van Duren, S. Temmerman, T. Claverie, A. Blanco-Garcia, T. Ysebaert, and P. M. J. Herman. 2007. Spatial flow and sedimentation patterns within patches of epibenthic structures: Combining field, flume and modelling experiments. Cont. Shelf Res. **27**: 1020–1045.

Bulthuis, D.A., G.W. Brand and M.C. Mobley 1984. Suspended and sediments and nutrients in water ebbing from seagrass-covered and denuded tidal mudflats in a southern Australian embayment. Aquat Bot **20**: 257-266.

Burkholder, J. M., D. A. Tomasko, and B. W. Touchette. 2007. Seagrasses and eutrophication. J. Exp. Mar. Biol. Ecol. **350**: 46–72.

Burris, J. E. 1981. Effects of Oxygen and Inorganic Carbon Concentrations on the Photosynthetic Quotients of Marine-Algae. Mar. Biol. **65**: 215–219.

Cabaço, S., R. Santos, and C. M Duarte. 2008. The impact of sediment burial and erosion on seagrasses : A review. Estuar., Coast. and Shelf Sci. **79**: 354–366. doi:10.1016/j.ecss.2008.04.021.

Cabello-Pasini, A., C. Lara-Turrent, and R. C. Zimmerman. 2002. Effect of storms on photosynthesis, carbohydrate content and survival of eelgrass populations from a coastal lagoon and the adjacent open ocean. Aquat. Bot. **74**: 149–164. doi:10.1016/S0304-3770(02)00076-1.

Caffrey, J. M. and W. M. Kemp. 1990. Nitrogen cycling in sediments with estuarine populations of *Potamogeton perfoliatus* and *Zostera marina*. Mar. Ecol. Prog. Ser. **66**: 147–160.

Caffrey, J. M., and W. M. Kemp. 1992. Influence of the submersed plant, Potamogeton perfoliatus, on nitrogen cycling in estuarine sediments. Limnol. Oceanogr. **37**: 1483-1495.

Caffrey, J. M., M. C. Murrell, K. S. Amacker, J. W. Harper, S. Phipps, and M. S. Woodrey. 2014. Seasonal and inter-annual patterns in primary production, respiration, and net ecosystem metabolism in three estuaries in the northeast Gulf of Mexico. Estuar. Coasts **37**(51): 222-241

Campbell, S. and L. J. McKenzie. 2004. Flood related loss and recovery of intertidal seagrass meadows in southern Queensland, Australia. Estuar., Coast. Shelf Sci. **60**: 477–490. doi:10.1016/j.ecss.2004.02.007.

Cardoso, P., M. Pardal, A. Lillebø, S. Ferreira, D. Raffaelli, and J. Marques. 2004. Dynamic changes in seagrass assemblages under eutrophication and implications for recovery. J. Exp. Mar. Biol. Ecol. **302**: 233–248.

Cardoso, P. G., D. Rafaelli, A. I. Lillebø, T. Verdelhos, and M. A. Pardal. 2008. The impact of extreme flooding events and anthropogenic stressors on the macrobenthic communities' dynamics. Estuar., Coast. Shelf Sci. **76**: 353-365.

Cardoso, P. G., S. Leston, T. F. Grilo, M. D. Bordalo, D. Crespo, D. Raffaelli, and M. A. Pardal. 2010. Implications of nutrient decline in the seagrass ecosystem

success. Mar. Pollut. Bull. **60**: 601–8.

Carpenter, S. R., N. F. Caraco, D. L. Correll, R. W. Howarth, V. H. Sharpley, and V. H Smith. 1998. Nonpoint pollution of surface waters with phosphorous and nitrogen. Ecol. Appl. **8**: 559–568.

Carpenter, S. R., J. J. Cole, J. R. Hodgeon, J. F. Kitchell, M. L. Pace, D. Bade, K. L. Cottingham, T. E. Essington, J. N. Houser, and D. E. Schindler. 2001. Trophic cascades, nutrients, and lake productivity: whole-lake experiments. Ecol. Monogr. **71**: 163–186.

Carpenter, S. R., J. J. Cole, J. R. Hodgeon, J. F. Kitchell, M. L. Pace, D. Bade, K. L. Cottingham, T. E. Essington, J. N. Houser, and D. E. Schindler. 2001. Trophic cascades, nutrients, and lake productivity: whole-lake experiments. Ecol. Monogr. **71**: 163–186.

Carpenter, S. R., E. V. Armbrust, P. W. Arzerberger, S. F. Chapin III, J. J. Elser, E. J. Hackett, A. R. Ives, P. M. Kareiva, M. A. Leibold, P. Lundberg, , M. Mangel, N. Merchant, W. W. Murdoch, M. A. Palmer, D. P. C. Peters, S. T. A. Pickett, K. K. Smith, D. H. Wall, and A. S. Zimmerman, 2009. Accelerate synthesis in ecology and environmental sciences. BioScience **59**(8): 699-701.

Carr, J., P. D'Odorico, K. McGlathery, and P. Wiberg. 2010. Stability and bistability of seagrass ecosystems in shallow coastal lagoons: Role of feedbacks with sediment resuspension and light attenuation. J. Geophys. Res. **115**: G03011, doi:10.1029/2009JG001103

Carter, V., J. E. J. Paschal, and N. Bartow. 1985. Distribution and abundance of submersed aquatic vegetation in the tidal Potomac River and Estuary, Maryland and Virginia, May 1978-November 1981. USGS Water Supply Paper 2234-A. pubs.er.usgs.gov/publication/wsp2234A

Cerco, C. F. 2000. Phytoplankton Kinetics in the Chesapeake Bay Eutrophication Model. Water Qual. Ecosyst. Model. **1**: 5–49.

Cerco, C. F., and K. Moore. 2001. System-Wide Submerged Aquatic Vegetation Model for Chesapeake Bay. Estuaries **24**: 522–534.

Chen, S., L. P. Sanford, E. W. Koch, F. Shi, and E. W. North. 2007. A nearshore model to investigate the effects of seagrass bed geometry on wave attenuation and suspended sediment transport. Estuar. Coast. **30**: 296–310.

Cloern, J. E. 2001. Our evolving conceptual model of the coastal eutrophication problem. Mar. Ecol. Prog. Ser. **210**: 223–253. doi:10.3354/meps210223.

Cornelisen, C. and F. Thomas. 2006. Water flow enhances ammonium and nitrate uptake in a seagrass community. Mar. Ecol. Prog. Ser. **312**: 1–13. doi:10.3354/meps312001.

Cornwell, J. C., W. M. Kemp, and T. M. Kana. 1999. Denitrification in coastal ecosystems: Methods, environmental controls, and ecosystem level controls, a review. Aquat. Ecol. **33**: 41–54.

Costanza, R., R. D'Arge, R. DeGroot, S. Farber, M. Grasso, B. Hannon, K. Limbrug, S. Naeem, R. V. O'Neil, J. Paruelo, R. G. Raskin, P. Sutton, and M. van den Belt. 1997. The value of the world's ecosystem services and natural capital. Nature **387**: 253–260.

Crawley, M. J. 2007. The R book, 1st ed. Wiley.

De Boer, W. F. 2007. Seagrass–sediment interactions, positive feedbacks and critical thresholds for occurrence: a review. Hydrobiologia **591**: 5–24. doi:10.1007/s10750-007-0780-9.

Dennison, W. C. 1987. Effects of light on seagrass photosynthesis, growth and depth distribution. Aquat. Bot. **27**: 15–26.

Dennison, W. C., R. J. Orth, K. A. Moore, J. C. Stevenson, V. Carter, S. Kouar, P. W. Bergstrom, and R. A. Batiuk. 1993. Assessing water quality with submersed aquatic vegetation: Habitat requirements as barometers of Chesapeake Bay health. BioScience **43**: 86–94.

Dettmann, E. H. 2001. Effect of Water Residence Time on Annual Export and Denitrification of Nitrogen in Estuaries: A Model Analysis. Estuaries **24**: 481.

Diaz, R. J., and R. Rosenberg. 2008. Spreading dead zones and consequences for marine ecosystems. Science **321**: 926–929. doi:10.1126/science.1156401.

Duarte, C. M. and J. Cebrian. 1996. The fate of marine autotrophic production. Limnol. Oceanogr. **41**(8): 1758-1766.

Duarte, C. M. 2012. Nutrient concentration of aquatic plants: Across species Patterns. Limnol. Oceanogr. **37**: 882–889.

Duffy, J. E., P. L. Reynolds, C. Bostrom, J. A. Coyer, M. Cusson, S. Donadi, J. G. Douglass, J. S. Eklof, A. H. Engelen, B. K. Eriksson, S. Fredriksen, L. Gamfeldt, C. Gustafsson, G. Hoarau, M. Hori, K. Hovel, K. Iken, J. S. Lefcheck, P. Moksnes, M. Nakaoka, M. I. O'Connor, J. Olsen, J. P. Richardson, J. L. Ruesink, E. E. Sotka, J. Thormar, M. A. Whalen, and J. J. Stachowicz. 2015. Biodiversity mediates top-down control in eelgrass

ecosystems: A global comparative-experimental approach. Ecol. Letters **19**(7): 696-705. doi: 10.1111/ele.12448

Efron, B. 1987. Better bootstrap confidence intervals. Jour. Amer. Stat. Assoc. **82**(397): 171-185.

Eyre, B. D., A. J. P. Ferguson, A. Webb, D. Maher, and J. M. Oakes. 2010. Denitrification, N-fixation and nitrogen and phosphorus fluxes in different benthic habitats and their contribution to the nitrogen and phosphorus budgets of a shallow oligotrophic sub-tropical coastal system (southern Moreton Bay, Australia). Biogeochemistry **102**: 111–133.

Fagherazzi, S., P. L. Wiberg, and A. D. Howard. 2003. Tidal flow field in a small basin. Jour. Geophys. Res. **108**: 1–10. doi:10.1029/2002JC001340.

Flindt, M.R. 1994. Measurements of nutrient fluxes and mass balances by on-line in situ dialysis in a Zostera marina bed culture. Int Limnol Theor Appl **25**:2259–2264

Flindt, M. R., M. Â. Pardal, A. I. Lillebø, I. Martins, and J. C. Marques. 1999. Nutrient cycling and plant dynamics in estuaries: A brief review. Acta Oecologica **20**: 237–248.

Folke, C. 2006. Resilience: The emergence of a perspective for social–ecological systems analyses. Glob. Environ. Change **16**: 253–267. doi:10.1016/j.gloenvcha.2006.04.002.

Fonseca, M. S., J. S. Fisher, J. C. Zieman, and G. W. Thayer. 1982. Influence of the seagrass, *Zostera marina L*., on current flow. Estuar., Coast. Shelf Sci. **15**: 351–364. doi:10.1016/0272-7714(82)90046-4.

Fonseca, M. S., and J. S. Fisher. 1986. A comparison of canopy friction and sediment movement between four species of seagrass with reference to their ecology and restoration. Mar. Ecol. Prog. Ser. **29**: 15–22.

Fonseca, M. S., and S. S. Bell. 1998. Influence of physical setting on seagrass landscapes. Mar. Ecol. Prog. Ser. **171**: 109–121.

Fraser, M. W., G. A. Kendrick, J. Statton, R. K. Hovey, A. Zavala-Perez, and D. I Walker. 2014. Extreme climate events lower resilience of foundation seagrass at edge of biogeographical range. Journ. Ecol. **102**: 1528-1536. doi:10.1111/1365-2745.12300.

Froelich, P. N. 1988. Kinetic control of dissolved phosphate in natural rivers and estuaries: A primer on the phosphate buffer mechanism. Limnol. Oceanogr. **33**: 649–668.

Gacia, E., T. . Granata, and C. . Duarte. 1999. An approach to measurement of particle flux and sediment retention within seagrass (Posidonia oceanica) meadows. Aquat. Bot. **65**: 255–268.

Gambi, M. C., A. R. M. Nowell, and P. A. Jumars. 1990. Flume observations on flow dynamics in *Zostera marina* (eelgrass) beds. Mar. Ecol. Prog. Ser. **61**: 159–169. doi:10.3354/meps061159.

Gao, Y., J. C. Cornwell, D. K. Stoecker, and M. S. Owens. 2012. Effects of cyanobacterial-driven pH increases on sediment nutrient fluxes and coupled nitrification-denitrification in a shallow fresh water estuary. Biogeosciences **9**: 2697–2710.

García, R., D. van Oevelen, K. Soetaert, L. Thomsen, H. C. De Stigter, and E. Epping. 2008. Deposition rates, mixing intensity and organic content in two contrasting submarine canyons. Prog. Oceanogr. **76**: 192–215.

Geyer, W. R., and R. P. Signell. 1992. A Reassessment of the Role of Tidal Dispersion in Estuaries and Bays. Estuaries **15**: 97.

Granata, T., T. Serra, J. Colomer, X. Casamitjana, C. M. Duarte, and E. Gacia. 2001. Flow and particle distributions in a nearshore seagrass meadow before and after a storm. Mar. Ecol. Prog. Ser. **218**: 95–106. doi:10.3354/meps218095.

Grilo, T. F., P. G. Cardoso, M. Dolbeth, M. D. Bordalo, and M. A. Pardal. 2011. Effects of extreme climate events on the macrobenthic communities' structure and functioning of a temperate estuary. Mar. Poll. Bull. **62**(2): 303-311. 10.1016/j.marpolbul.2010.10.010.

Gruber, R. K., and W. M. Kemp. 2010. Feedback effects in a coastal canopy-forming submersed plant bed. Limnol. Oceanogr. **55**: 2285–2298.

Gruber, R. K., D. C. Hinkle, and W. M. Kemp. 2011. Spatial patterns in water quality associated with submersed plant beds. Estuar. Coasts **34**: 961–972. doi:10.1007/s12237-010-9368-0.

Gurbisz, C., and W. M. Kemp. 2014. Unexpected resurgence of a large submersed plant bed in Chesapeake Bay: Analysis of time series data. Limnol. Oceanogr. **59**: 482–494. doi:10.4319/lo.2014.59.2.0482.

Gurbisz, C., W. M. Kemp, L. P. Sanford, and R. J. Orth. 2016. Mechanisms of Storm-Related Loss and Resilience in a Large Submersed Plant Bed. Estuar. Coasts, doi:10.1007/s12237-016-0074-4

Hagy, J. D., W. R. Boynton, C. W. Keefe, and K. V. Wood. 2004. Hypoxia in Chesapeake Bay, 1950-2001: Long-term change in relation to nutrient loading and river flow. Estuaries **27**: 634–658.

Haller, W. T., D. L. Sutton, and W. C. Barlowe, W. C. 1974. Effects of salinity on growth of several aquatic macrophtyes. Ecology **55**: 891-894.

Hanington, P., K. Hunnam, and R. Johnstone. 2014. Widespread loss of the seagrass Syringodium isoetifolium after a major flood event in Moreton Bay, Australia: Implications for benthic processes. Aquat. Bot. **120**: 244–250.

Harley, M. T., and S. Findlay. 1994. Photosynthesis-irradiance relationships for three species of submersed macrophytes in the tidal freshwater Hudson River. Estuar. **17**: 200–205.

Havens, K. E., J. Hauxwell, A. C. Tyler, S. Thomas, K. J. McGlathery, J. Cebrian, I. Valiela, A. D. Steinman, and S. J. Hwang. 2001. Complex interactions between autotrophs in shallow marine and freshwater ecosystems: implications for community responses to nutrient stress. Environ. Pollut. **113**: 95–107.

Hemminga, M. A., P. G. Harrison, and F. van Lent. 1991. The balance of nutrient losses and gains in seagrass meadows. Mar. Ecol. Prog. Ser. **71**: 85–96.

Hesslein, R. H. 1976. An in situ sampler for close interval pore water studies. Limnol. Oceanogr. **21**: 912–914.

Hirsch, R. M., J. R. Slack, and R. A. Smith. 1982. Techniques of trend analysis for monthly water quality data. Water Resour. Res. **18**: 107-121.

Hirsch, R. M., D. L. Moyer, and S. A. Archfield. 2010. Weighted regressions on time, discharge, and season (WRTDS), with an application to Chesapeake Bay river inputs. J. Amer. Water Resour. Assoc. **46**: 857–880.

Hofmann, a. F., K. Soetaert, and J. J. Middelburg. 2008. Present nitrogen and carbon dynamics in the Scheldt estuary using a novel 1-D model. Biogeosciences **5**: 981–1006.

Holling, C. S. 1973. Resilience and stability of ecological systems. Annu. Rev. Ecol. Syst. **4**: 1–23.

Hosmer, D. W. and Lemeshow, S. 2000. Applied logistic regression. New York: John Wiley & Sons, Inc.

Howarth, R. W., M. Hayn, R. M. Marino, N. Ganju, K. Foreman, K. McGlathery, A. E. Giblin, P. Berg, and J. D. Walker. 2013. Metabolism of a nitrogen-enriched coastal marine lagoon during the summertime. Biogeochem. **118**: 1–20. doi:10.1007/s10533-013-9901-x.

Infantes, E., a Orfila, G. Simarro, J. Terrados, M. Luhar, and H. Nepf. 2012. Effect

of a seagrass (*Posidonia oceanica*) meadow on wave propagation. Mar. Ecol. Prog. Ser. **456**: 63–72.

Intergovernmental Panel on Climate Change (IPCC), 2014. Climate Change 2014: Impacts, Adaptation, and Vulnerability. Part A: Global and Sectoral Aspects. Contribution of Working Group II to the Fifth Assessment Report of the Intergovernmental Panel on Climate Change [Field, C.B., V.R. Barros, D.J. Dokken, K.J. Mach, M.D. Mastrandrea, T.E. Bilir, M. Chatterjee, K.L. Ebi, Y.O. Estrada, R.C. Genova, B. Girma, E.S. Kissel, A.N. Levy, S. MacCracken, P.R. Mastrandrea, and L.L. White (eds.)]. Cambridge University Press, Cambridge, United Kingdom and New York, NY, USA, 1132 pp.

Jackson, J. B., M. X. Kirby, W H Berger, K. A. Bjorndal, L. W. Botsford, B. J. Bourque, R. H. Bradbury, R. Cooke, J. Erlandson, J. A. Estes, T. Pl Hughes, S. Kidwell, C. B. Lange, H. S. Lenihan, J. M. Pandolfi, C. H. Peterson, R. S. Steneck, M. J. Tegner, and R. R. Warner. 2001. Historical overfishing and the recent collapse of coastal ecosystems. Science **293**: 629–637. doi:10.1126/science.1059199.

Jordan, T. E., J. C. Cornwell, W. R. Boynton, and J.T. Anderson. Changes in phosphorous biogeochemistry along an estuarine salinity gradient: The iron conveyer belt. Limnol. Oceanogr. 53(1): 172-184.

Kana, T. M., C. Darkangelo, M. D. Hunt, J. B. Oldham, G. E. Bennett, and J. C. Cornwell. 1994. Membrane lnlet Mass Spectrometer for Rapid Environmental Water Samples. **66**: 4166–4170.

Karjalainen, H., G. Stefansdottir, L. Tuominen, and T. Kairesalo. 2001. Do submersed plants enhance microbial activity in sediment? Aquat. Bot. **69**: 1–13.

Kemp, W. M., R. R. Twilly, J. C. Stevenson, W. R. Boynton, and J. C. Means. 1983. The decline of submerged vascular plants in upper Chesapeake Bay: Summary of results concerning possible causes. Mar. Technol. Soc. **17**: 78–89.

Kemp, W. M., W. R. Boynton, and R. R. Twilley. 1984. Influences of submersed vascular plants on ecological processes in upper Chesapeake Bay, p. 367–394. *In* V.S. Kennedy [ed.], The Estuary as a Filter. Academic Press, Inc.

Kemp, W. M., M. R. Lewis, and T. W. Jones. 1986. Comparison of methods for measuring production by the submersed macrophyte. Potamogeton perfoliatus L. Limnol. Oceanogr. **31**: 1322–1334.

Kemp, W. M., P. Sampou, J. Caffrey, M. Mayer, K. Henriksen, and W. R. Boynton. 1990. Ammonium recycling versus denitrification in Chesapeake Bay sediments. Limnol. Oceanogr. **35**: 1545–1563.

Kemp, W. M., R. Batiuk, R. Bartleson, P. Bergstrom, V. Carter, C. L. Gallegos, W. Hunley, L. Karrh, E. W. Koch, J. M. Landwehr, K. A. Moore, L. Murray, M. Naylor, N. B. Rybicki, J. C. Stevenson, and D. J. Wilcox. 2004. Habitat requirements for submerged aquatic vegetation in Chesapeake Bay: Water quality, light regime, and physical-chemical factors. Estuaries **27**: 363–377.

Kemp, W., W. Boynton, J. Adolf, D. Boesch, W. Boicourt, G. Brush, J. Cornwell, T. Fisher, P. Glibert, J. Hagy, L. Harding, E. Houde, D. Kimmel, W. Miller, R. Newell, M. Roman, E. Smith, and J. Stevenson. 2005. Eutrophication of Chesapeake Bay: Historical trends and ecological interactions. Mar. Ecol. Prog. Ser. **303**: 1–29.

Kemp, W. M., and W. R. Boynton 2011. Synthesis in estuarine and coastal ecological research: What is it, why is it important, and how do we teach it? Estuar. Coasts **35**(1): 1-22.

Koch, E. W. 1999. Preliminary evidence on the interdependent effect of currents and porewater geochemistry on Thalassia testudinum Banks ex Konig seedlins. Aquat. Bot. **63**: 95–102.

Koch, E. W. 2001. Beyond light: Physical, geological, and geochemical parameters as possible submersed aquatic vegetation habitat requirements. Estuar. **24**: 1–17.

Kollar, S. A. 1989. Submerged macrophyte survival and water quality monitroing results in upper Chesapeake Bay. Final report to the Maryland Department of Natural Resources Coastal Resources Division, Grant #C-105-89-102. http://www.dnr.state.md.us/irc/docs/00002042.pdf

Laird, N. M. and J. H. Ware (1982) Random-Effects Models for Longitudinal Data. Biometrics **38**: 963–974.

Lande, R., and S. Shannon. 1996. The role of genetic variation in adaptation and population persistence in a changing environment. Evolution **50**: 434–437.

Lara, M., G. Peralta, J. J. Alonso, E. P. Morris, V. González-Ortiz, J. J. Rueda-Márquez, and J. L. Pérez-Lloréns. 2012. Effects of intertidal seagrass habitat fragmentation on turbulent diffusion and retention time of solutes. Mar. Poll. Bull. **64**: 2471–2479. doi:10.1016/j.marpolbul.2012.07.044.

Lawson, S. E., K. J. McGlathery, and P. L. Wiberg. 2012. Enhancement of sediment suspension and nutrient flux by benthic macrophytes at low biomass. Mar. Ecol. Prog. Ser. **448**: 259–270.

Lightbody, A. F., and H. M. Nepf. 2006. Prediction of velocity profiles and longitudinal dispersion in emergent salt marsh vegetation. Limnol. Oceanogr. **51**: 218–228.

Longstaff, B. J., and W. C Dennison. 1999. Seagrass survival during pulsed turbidity events: the effects of light deprivation on the seagrasses *Halodule pinifolia* and *Halophila ovalis*. Aquatic Botany **65**: 105–121. doi:10.1016/S0304-3770(99)00035-2.

Lotze, H., H. S. Lenihan, B. J. Borque, R. H. Bradbury, R. G. Cooke, M. C. Kay, S. M. Kidwell, M. X. Kirby, C. H. Peterson, and J. B. C. Jackson. 2006. Depletion, degradation, and recovery potential of estuaries and coastal seas. Science **312** (5781): 1806-1809.

Lubbers, L., W. R. Boynton, and W. M. Kemp. 1990. Variations in structure of estuarine fish communities in relation to abundance of submersed vascular plants. Mar. Ecol. Prog. Ser. **65**: 1–14.

Luhar, M., J. Rominger, and H. Nepf. 2008. Interaction between flow, transport and vegetation spatial structure. Environ. Fluid Mech. **8**: 423–439. doi:10.1007/s10652-008-9080-9.

Luhar, M., and H. M. Nepf. 2013. From the blade scale to the reach scale: A characterization of aquatic vegetative drag. Adv. Water Resourc. **51**: 305–316. doi:10.1016/j.advwatres.2012.02.002.

Lyubchic, V., B. R. Gray, Y. R. Gel. 2015. Multilevel random slope approach and nonparametric inference for river temperature, under haphazard sampling. In: V. Lakashmanan et al. (eds) Machine Learning and Data Mining Approaches to Climate Science. Springer International Publishing: Switzerland.

Madsen, J. D., P. A. Chambers, W. F. James, E. W. Koch, and D. F. Westlake. 2001. The interaction between water movement, sediment dynamics and submersed macrophytes. Hydrobiologia **444**: 71–84.

Malone, T. C., D. J. Conley, T. R. Fisher, P. M. Glibert, L. W. Harding, and K. G. Sellner. 1996. Scales of nutrient-limited phytoplankton productivity in Chesapeake Bay. Estuar. Coasts **19**(2b): 371-385

Marino, R., and R. W. Howarth. 1993. Atmospheric oxygen exchange in the Hudson River: Dome measurements and comparison with other natural waters. Estuar. **16**(3A): 433-455.

Mariotti, G. and S. Fagherazzi. 2013. A two-point dynamic model for the coupled evolution of channels and tidal flats. Journal of Geophys. Res.: Earth Surf. **118**: 1387-1399. doi: 10.1002/jgrf.20070

May, R. M. 1977. Thresholds and breakpoints in ecosystems with a multiplicity of stable states. Nature **269**: 471–477.

Maxwell, P. S., K. A. Pitt, D. D. Burfeind, A. D. Olds, R. C. Babcock, and R. M. Connolly. 2014. Phenotypic plasticity promotes persistence following severe events: Physiological and morphological responses of seagrass to flooding. Jour. Ecol. **102**: 54–64. doi:10.1111/1365-2745.12167.

McBride, G. B. 1993. What do significance tests really tell us about the environment? Environ. Manage. **17**: 423–432.

McFarland, D. G., and D. J. Shafer. 2008. Factors influencing reproduction in American wild celery: A synthesis. Jour. Aquat. Plant Manage. **46**: 129–144.

McGlathery, K. J., N. Risgaard-Petersen, and P. B. Christiansen. 1998. Temporal and spatial variation in nitrogen fixation activity in the eelgrass Zostera marina rhizosphere. Mar. Ecol. Prog. Ser. **168**: 245–258.

McGlathery, K. J., K. Sundbäck, and I. C. Anderson. 2007. Eutrophication in shallow coastal bays and lagoons: The role of plants in the coastal filter. Mar. Ecol. Prog. Ser. **348**: 1–18. doi:10.3354/meps07132.

Middelboe, A. L. and S. Markager. 1997. Depth limits and minimum light requirements of freshwater macrophytes. Freshwater Biol. **37**: 553-568.

Moore, K. A., Richard L. Wetzel, and Robert J. Orth. 1997. Seasonal pulses of turbidity and their relations to eelgrass (*Zostera marina L.*) survival in an estuary. Jour. Exper. Mar. Biol. and Ecol. **215**: 115–134. doi:10.1016/S0022-0981(96)02774-8.

Moore, K. A., D. J. Wilcox, and R. J. Orth. 2000. Analysis of the abundance of submersed aquatic vegetation communities in the Chesapeake Bay. Estuar. **23**: 115–127.

Moore, K. A. 2004. Influence of seagrasses on water quality in shallow regions of the lower Chesapeake Bay. J. Coast. Res. **45**: 162–178.

Murphy, E., M. Ghisalberti, and H. Nepf. 2007. Model and laboratory study of dispersion in flows with submerged vegetation. Water Resour. Res. **43**: 1–12.

Muggeo, V. M. R. 2008. segmented : An R package to fit regression models with broken-line relationships. R News **8**: 20-25.

Najjar, R. G., C. R. Pyke, M. B. Adams, D. Breitburg, C. Hershner, W. M. Kemp, R. Howarth, M. R. Mulholland, M. Paolisso, D. Secor, K. Sellner, D. Wardrop, and R. Wood. 2010. Potential climate-change impacts on the Chesapeake Bay. Estuar., Coast. Shelf Sci. **86**: 1–20. doi:10.1016/j.ecss.2009.09.026.

Nixon, S. W., J. W. Ammerman, L.P. Atkinson, V. M. Berounsky, G. Billen, W. C. Boicourt, W. R. Boynton, T. M. Church, D. M. Ditoro, R. Elmgren, H. J. Garber, A. E. Giblin, R. A. Jahnke, N. J. P. Owens, M. E. Q. Pilson, and S. P. Seitzinger. 1996. The fate of nitrogen and phosphorus at the land-sea margin of the North Atlantic Ocean. Biogeochem. **35**: 141–180.

Nejrup, L. B., and Pedersen, M. F. 2008. Effects of salinity and water temperature on the ecological performance of *Zostera marina*. Aquat. Bot. **88**: 239-246.

Nepf, H., M. Ghisalberti, B. White, and E. Murphy. 2007. Retention time and dispersion associated with submerged aquatic canopies. Water Resour. Res. **43**: 1–10.

Nepf, H. M., C. G. Mugnier, and R. a Zavistoski. 1997. The Effects of Vegetation on Longitudinal Dispersion. Estuar. Coast. Shelf Sci. **44**: 675–684.

Odum, H.T. 1956. Primary production in flowing waters. Limnol. and Oceanogr. **1**(2): 102-117.

Orth, R. J., and K. A. Moore. 1983. Chesapeake Bay: An unprecedented decline in submerged aquatic vegetation. Science **222**: 51–53.

Orth, R. J., M. Luckenback, S. Marion, K. A. Moore, D. J. Wilcox. 2006. Seagrass recovery in the Delmarva Coastal Bays, USA. Aquat. Bot. **84**: 26-36.

Orth, R. J., M. R. Williams, S. R. Marion, D. J. Wilcox, T. J. B. Carruthers, K. A. Moore, W. M. Kemp, W. C. Dennison, N. Rybicki, P. Bergstrom, and R. A. Batiuk. 2010. Long-term trends in submersed aquatic vegetation (SAV) in Chesapeake Bay, USA, related to water quality. Estuar. Coasts **33**: 1144–1163.

Orth, R. J., K. A. Moore, S. R. Marion, D. J. Wilcox, and D. B. Parrish. 2012. Seed addition facilitates eelgrass recovery in a coastal bay system. Mar. Ecol. Prog. Ser. **448**: 177-195.

Palinkas, C. M., J. P. Halka, M. Li, L. P. Sanford, and P. Cheng. 2013. Sediment deposition from tropical storms in the upper Chesapeake Bay: Field observations and model simulations. Cont. Shelf Res. **86**: 6–16. doi:10.1016/j.csr.2013.09.012.

Parsons, T. R., Y. Maita, and C. M. Lalli. 1984. A manual of chemical and biological methods for seawater analysis. Oxford: Pergamon Press.

Peterson, C. H., R. A. Luettich Jr., F. Micheli, and G. A. Skilleter. 2004. Attenuation of water flow inside seagrass canopies of differing structure. Mar. Ecol. Prog. Ser. **268**: 81–92.

Pinheiro, J. C. and D. M. Bates. 2000. Mixed effects models in S and S-Plus. New York: Springer-Verlag.

Preen, A. R., W. J. Lee Long, and R. G. Coles. 1995. Flood and cyclone related loss, and partial recovery, of more than 1000 km^2 of seagrass in Hervey Bay, Queensland, Australia. Aquat. Bot. **52**: 3–17.

Ralph, G. M., R. D. Seitz, R. J. Orth, K. E. Knick, and R. N. Lipcius. 2013. Broad-scale association between seagrass cover and juvenile blue crab density in Chesapeake Bay. Mar. Ecol. Prog. Ser. **488**: 51–63. doi:10.3354/meps10417.

Rappaport, D. J., and W. G. Whitford. 1999. How ecosystems respond to stress. Bioscience **49**: 193–203. doi:10.2307/1313509.

Rasheed, M., and R. Unsworth. 2011. Long-term climate-associated dynamics of a tropical seagrass meadow: implications for the future. Mar. Ecol. Prog. Ser. **422**: 93–103.

Reise, K., and J. Kohlus. 2007. Seagrass recovery in the Northern Wadden Sea? Helgol. Mar. Res. **62**: 77–84.

Reusch, T. B. H., A. Ehlers, A. Hämmerli, and B. Worm. 2005. Ecosystem recovery after climatic extremes enhanced by genotypic diversity. Proc. Nat. Acad. Sci. U. S. A. **102**: 2826–31. doi:10.1073/pnas.0500008102.

Risgaard-Petersen, N., L. Ditlev, and M. Ottosen. 2000. Nitrogen cycling in two temperate Zostera marina beds: seasonal variation. Mar. Ecol. Prog. Ser. **198**: 93–107.

Risgaard-Petersen N. 2004. Denitrification. In: Nielsen SL, Banta GT, Pedersen MF (eds) Estuarine nutrient cycling: the influence of primary producers. Kluwer Academic, Dordrecht, p 263–280 Risgaard-Petersen

Romero, J., K. S. Lee, M. Perez, M. A. Mateo, and T. Alcoverro. 2006. Nutrient dynamics in seagrass ecosystems. In Seagrasses: biology, ecology, and conservation, ed. Larkum, A. W. D., R. J. Orth, C. M. Duarte, 227-254. The Netherlands: Springer.

Rominger, J. T., and H. M. Nepf. 2011. Flow adjustment and interior flow associated with a rectangular porous obstruction. J. Fluid Mech. **680**: 636–659.

Ruhl, H. A., and N. B. Rybicki. 2010. Long-term reductions in anthropogenic nutrients link to improvements in Chesapeake Bay habitat. Proc. Natl. Acad. Sci. U. S. A. **107**: 16566–16570.

Rybicki, N. B., H. L. Jenter, V. Carter, R. a. Baltzer, and M. Turtora. 1997. Observations of tidal flux between a submersed aquatic plant stand and the

adjacent channel in the Potomac River near Washington, D.C. Limnol. Oceanogr. **42**: 307–317.

Rybicki, N., and J. M. Landwehr. 2007. Long-term changes in abundance and diversity of macrophyte and waterfowl populations in an estuary with exotic macrophytes and inproving water quality. Limnol. Oceanogr. **52**: 1195–1207.

Rysgaard, S., N. Risgaard-Petersen, and N. P. Sloth. 1996. Nitrification, denitrification, and nitrate ammonification in sediments of two coastal lagoons in Southern France. Hydrobiologia **329**: 133–141.

Sanford, L. P. 1994. Wave-forced resuspension of upper Chesapeake Bay muds. Estuaries **17**: 148–165. doi:10.1007/BF02694911.

Sanford, L. P. 1997. Turbulent mixing in experimental ecosystem studies. Mar. Ecol. Prog. Ser. **161**: 265–293.

Sanford, L. P. 2008. Modeling a dynamically varying mixed sediment bed with erosion, deposition, bioturbation, consolidation, and armoring. Comp. Geosci. **34**: 1263-1283.

Sand-Jensen, K., and J. Borum. 1991. Interactions among phytoplankton, periphyton, and macrophytes in temperate freshwaters and estuaries. Aquat. Bot. **41**: 137–176.

Scheffer, M. 1990. Multiplicity of stable states in freshwater systems. Hydrobiologia **200-201**: 475–486.

Scheffer, M., S. H. Hosper, M. L. Meijer, B. Moss, and E. Jeppesen. 1993. Alternative equilibria in shallow lakes. Trends Ecol. Evol. **8**: 275–279.

Scheffer, M., S. Carpenter, J. A. Foley, C. Folke, and B. Walker. 2001. Catastrophic shifts in ecosystems. Nature **413**: 591–596.

Scheffer, M., S. R. Carpenter, T. M. Lenton, J. Bascompte, W. Brock, V. Dakos, J. van de Koppel, I. a. van de Leemput, S. a. Levin, E. H. van Nes, M. Pascual, and J. Vandermeer. 2012. Anticipating Critical Transitions. Science **338**: 344–348.

Schubel, J. R., and D. W. Pritchard. 1986. Responses of Upper Chesapeake Bay to variations in discharge of the Susquehanna River. Estuaries **9**: 236–249.

Schutten, J., J. Dainty, and A. J. Davy. 2005. Root anchorage and its significance for submerged plants in shallow lakes. Jour. Ecol. **93**: 556–571. doi:10.1111/j.1365-2745.2005.00980.x.

Sculthorpe, C. D. 1967. The biology of aquatic vascular plants. London: Edward Arnold.

Seitzinger, S., J. Harrison, J. Bohlke, A. Bouwman, R. Lowrance, B. Peterson, C. Tobias, and G. Van Drecht. 2006. Denitrification across landscaes and waterscapes: A synthesis. Ecol. Appl. **16**: 2064–2090.

Soetaert, K., and F. Meysman. 2012. Reactive transport in aquatic ecosystems: Rapid model prototyping in the open source software R. Environ. Model. Softw. **32**: 49–60.

Ståhlberg, C., D. Bastviken, B. H. Svensson, and L. Rahm. 2006. Mineralisation of organic matter in coastal sediments at different frequency and duration of resuspension. Estuar. Coast. Shelf Sci. **70**: 317–325. doi:10.1016/j.ecss.2006.06.022.

Tengberg, A., E. Almroth, and P. Hall. 2003. Resuspension and its effects on organic carbon recycling and nutrient exchange in coastal sediments: In situ measurements using new experimental technology. Jour. Exper. Mar. Biol. Ecol. **285-286**: 119–142. doi:10.1016/S0022-0981(02)00523-3.

Tomasko, D. A., C. A. Corbett, H. S. Greening, and G. E. Raulerson. 2005. Spatial and temporal variation in seagrass coverage in Southwest Florida: assessing the relative effects of anthropogenic nutrient load reductions and rainfall in four contiguous estuaries. Mar. Poll. Bull. **50**: 797–805. doi:10.1016/j.marpolbul.2005.02.010.

Twilley, R. R., W. M. Kemp, K. W. Staver, J. C. Stevenson, and W. R. Boynton. 1983. Nutrient enrichment of estuarine submersed vascular plant communities. 1. Algal growth and effects on production of plants and associated communities. Mar. Ecol. Prog. Ser. **23**: 179-191.

Valiela, I., J. Mcclelland, J. Hauxwell, P. J. Behr, D. Hersh, and K. Foreman. 1997. Macroalgal blooms in shallow estuaries: Controls and ecophysiological and ecosystem consequences. Limnol. Oceanogr. **42**: 1105–1118.

Van, T. K., W. T. Haller, and G. Bowes. 1976. Comparison of photosynthetic characteristics of 3 submersed aquatic plants. Plant Phys. **58**: 761-768.

van der Heide, T., E. H. van Nes, G. W. Geerling, A. J. P. Smolders, T. J. Bouma, and M. M. van Katwijk. 2007. Positive feedbacks in seagrass ecosystems: Implications for success in conservation and restoration. Ecosystems **10**: 1311–1322.

van der Heide, T., E. T. H. M. Peeters, D. C. R. Hermus, M. M. van Katwijk, J. G. M. Roelofs, and A. J. P. Smolders. 2009. Predicting habitat suitability in temperate seagrass ecosystems. Limnol. Oceanogr. **54**: 2018–2024.

Van der Heide, T., E. H. van Nes, M. M. van Katwijk, H. Olff, and A. J. P. Smolders. 2011. Positive feedbacks in seagrass ecosystems--evidence from large-scale empirical data. PloS one **6**: e16504. doi:10.1371/journal.pone.0016504.

Viaroli, P., M. Bartoli, G. Giordani, M. Naldi, S. Orfanidis, and J. M. Zaldivar. 2008. Community shifts, alternative stable states, biogeochemical controls and feedbacks in eutrophic coastal lagoons: A brief overview. Aquatic Conserv: Mar. Frewshw. Ecosyst. **18**: S105-S117.

Walker, B., C. S. Holling, S. R. Carpenter, and A. Kinzig. 2004. Resilience, adaptability and transformability in social–ecological systems. Ecol. Soc. **9**: 5 http://www.ecologyandsociety.org/vol9/iss2/art5/

Wang, P., and L. C. Linker. 2005. Effect of timing of extreme storms on Chesapeake Bay submerged aquatic vegetation, p. 177-184. *In* K. G. Sellner [ed.], Hurricane Isabel in perspective. Chesapeake Research Consortium Publication 05-160

.

Ward, L. G., W. M. Kemp, and W. R. Boynton. 1984. The influence of waves and seagrass communities on suspended particulates in an estuarine embayment. Mar. Geol. **59**: 85–103.

Walker, D. I., Kendrick, G. A., and McComb, A. J. 2006. Decline and recovery of seagrass ecosystems--the dynamics of change. In Seagrasses: Biology, ecology, and conservation, ed. Larkum, A., R. J. Orth, and C. Duarte, 551-565. The Netherdlands: Springer.

Waycott, M., C. M. Duarte, T. J. B. Carruthers, R. J. Orth, W. C. Dennison, S. Olyarnik, A. Calladine, J. W. Fourqurean, K. L. Heck, A. R. Hughes, G. a Kendrick, W. J. Kenworthy, F. T. Short, and S. L. Williams. 2009. Accelerating loss of seagrasses across the globe threatens coastal ecosystems. Proc. Natl. Acad. Sci. U. S. A. **106**: 12377–81.

Welsh, D., M. Bartoli, D. Nizzoli, G. Castaldelli, S. Riou, and P. Viaroli. 2000. Denitrification, nitrogen fixation, community primary productivity and inorganic-N and oxygen fluxes in an intertidal Zostera noltii meadow. Mar. Ecol. Prog. Ser. **208**: 65–77.

Yaakub, S. M., E. Chen, T. J. Bouma, P. L. A. Erftemeijer, and P. A. Todd. 2014. Chronic light reduction reduces overall resilience to additional shading stress in the seagrass *Halophila ovalis*. Mar. Poll. Bull. **83**: 467–474. doi:10.1016/j.marpolbul.2013.11.030.

Zimmerman, J. T. F. 1976. Mixing and Flushing of Tidal Embayments in the western Dutch Wadden Sea, Part II: Analysis of mixing processes. Netherlands J. Sea Res. **10**: 397–439.

Zhang, Q., D. C. Brady, and W. P. Ball. 2013. Long-term seasonal trends of nitrogen, phosphorus, and suspended sediment load from the non-tidal Susquehanna River Basin to Chesapeake Bay. Sci. Total Environ. **452-453C**: 208–221.